UNIVERSIDADE ESTADUAL PAULISTA
"JÚLIO DE MESQUITA FILHO"
Faculdade de Ciências Farmacêuticas
Campus de Araraquara
Programa de Pós-graduação em Ciências Farmacêuticas

Desenvolvimento de sistemas multifuncionais nanoestruturados para a liberação de fármacos administrados por via nasal no tratamento de glioblastoma

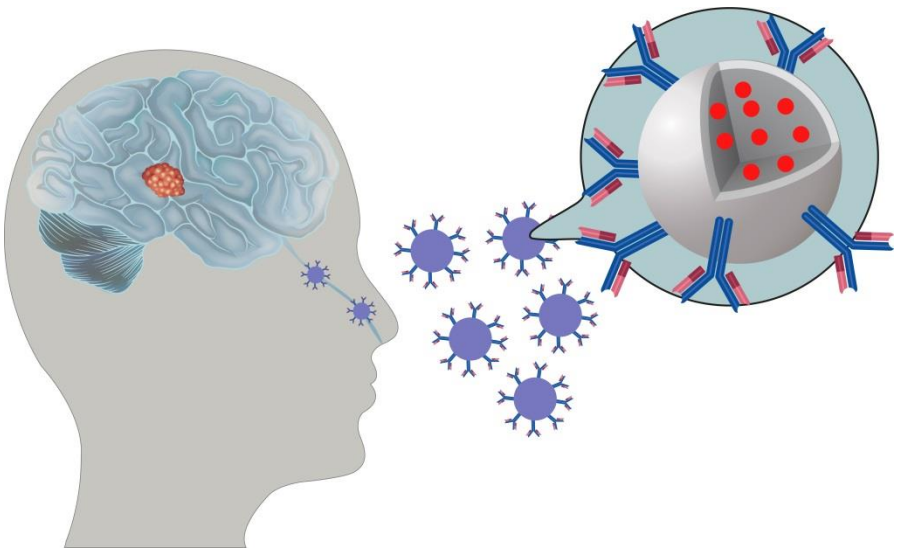

Natália Noronha Ferreira Naddeo

Orientadora: Profª. Drª. Maria Palmira Daflon Gremião

Coorientadora: Profª. Drª. Maria de Fátima Monginho Baltazar

Araraquara-SP

2020

UNIVERSIDADE ESTADUAL PAULISTA
"JÚLIO DE MESQUITA FILHO"
Faculdade de Ciências Farmacêuticas
Campus de Araraquara
Programa de Pós-graduação em Ciências Farmacêuticas

Desenvolvimento de sistemas multifuncionais nanoestruturados para a liberação de fármacos administrados por via nasal no tratamento de glioblastoma

Nanostructured multifunctional systems for drug release through the nasal route applied on glioblastoma treatment

Natália Noronha Ferreira Naddeo

Tese apresentada ao programa de Pós Graduação em Ciências Farmacêuticas, área de Pesquisa e Desenvolvimento de Fármacos e Medicamentos, da Faculdade de Ciências Farmacêuticas, Universidade Estadual Paulista "Júlio de Mesquita Filho"-UNESP, para obtenção do titulo de doutora em Ciências Farmacêuticas.

Orientadora: Profª. Drª. Maria Palmira Daflon Gremião
Coorientadora: Profª. Drª. Maria de Fátima Monginho Baltazar

Araraquara- SP
2020

Naddeo, Natália Noronha Ferreira.
N134d Desenvolvimento de sistemas multifuncionais nanoestruturados para a liberação de fármacos administrados por via nasal no tratamento de glioblastoma = Nanostructured multifunctional systems for drug release through the nasal route applied on glioblastoma treatment / Natália Noronha Ferreira Naddeo. – Araraquara: [S.n.], 2020.
130 f. : il.

Tese (Doutorado) – Universidade Estadual Paulista. "Júlio de Mesquita Filho". Faculdade de Ciências Farmacêuticas. Programa de Pós Graduação em Ciências Farmacêuticas. Área de Pesquisa e Desenvolvimento de Fármacos e Medicamentos.

Orientadora: Maria Palmira Daflon Gremião.
Coorientadora: Maria de Fátima Monginho Baltazar.

1. Glioblastoma. 2. Administração nasal. 3. Ácido α-ciano-4-hidroxicinâmico. 4. Cetuximabe. 5. Nova estratégia terapêutica. 6. Efeito combinatório. 6. Nanotecnologia. I. Gremião, Maria Palmira Daflon, orient. II. Baltazar, Maria de Fátima Monginho, coorient. III. Título.

Diretoria do Serviço Técnico de Biblioteca e Documentação - Faculdade de Ciências Farmacêuticas
UNESP - Campus de Araraquara

CAPES: 33004030078P6
Esta ficha não pode ser modificada

CERTIFICADO DE APROVAÇÃO

TÍTULO DA TESE: DESENVOLVIMENTO DE SISTEMAS MULTIFUNCIONAIS NANOESTRUTURADOS PARA A LIBERAÇÃO DE FÁRMACOS ADMINISTRADOS POR VIA NASAL NO TRATAMENTO DE GLIOBLASTOMA

AUTORA: NATÁLIA NORONHA FERREIRA NADDEO

ORIENTADORA: MARIA PALMIRA DAFLON GREMIÃO

COORIENTADORA: MARIA DE FATIMA MONGINHO BALTAZAR

Aprovada como parte das exigências para obtenção do Título de Doutora em CIÊNCIAS FARMACÊUTICAS, área de conhecimento: Sem Área de Conhecimento pela Comissão Examinadora:

Profa. Dra. MARIA PALMIRA DAFLON GREMIÃO
Departamento de Fármacos e Medicamentos / Faculdade de Ciências Farmacêuticas - UNESP - Araraquara

Profa. Dra. SILVIA STANISÇUASKI GUTERRES
Departamento de Produção e Controle de Medicamentos da Faculdade de Farmácia / UNIVERSIDADE FEDERAL DO RIO GRANDE DO SUL

Prof. Dr. HERNANE DA SILVA BARUD
Núcleo de Pesquisa em Biotecnologia / Universidade de Araraquara-UNIARA

Prof. Dr. MARCELO BISPO DE JESUS
Departamento de Bioquímica e Biologia Tecidual / Instituto de Biologia da Universidade Estadual de Campinas

Profa. Dra. FLÁVIA CHIVA CARVALHO
Departamento de Alimentos e Medicamentos / Universidade Federal de Alfenas

Araraquara, 30 de março de 2020

DEDICATION

This study is wholeheartedly dedicated to my beloved parents, who have been my source of inspiration and gave me strength when I thought of giving up, giving me also moral, spiritual, emotional and financial support;

I also dedicate all efforts and achievements reported here to my lovely husband and daughter, Bruno and Helena, whose are, and will always be, my inspiration.

Mommy loves you.

ACKNOWLEDGMENTS

First of all, I would like to thank God for always guiding me.

My sincere gratitude to Prof. Dr. Maria Palmira Gremião and Fátima Baltazar, my supervisors, to incentive, trust, dedication, knowledge transmitted, constant support, friendship and above all for the patience. It was a real privilege and an honor for me to share their exceptional scientific knowledge and also their extraordinary human qualities.

A special thanks to Bruno Naddeo, my husband, by his emotional support, lovely company, motivation, knowledge, help, good humor, love and affection. Thank you for making my thesis illustrations so exceptional using his talent.

To all my family, especially my parents Rosângela , José Antônio and my brother Rafael by their love and encouragement, always my gratitude.

To my special friend Vanessa Felix de Lima who has cared my daughter, with so much love.

To my colleagues and friends from Pharmacotechnical laboratory, especially for Fernanda, Jéssica, Camila, Leonardo, Mariana, Leda , Karen, Natália, Cintia and Valeria for their great collaboration.

To Prof. Dr. Eliana Martins Lima and Edilson Ribeiro de Oliveira Junior from Universidade Federal de Goiás - UFG by their partnerships to the execution of *in vivo* experiments to investigate nose-to-brain delivery.

To Prof. Dr. Beatriz S. Ferreira Cury my gratitude for knowledge transmitted and friendship.

All friendships of Life and Health Sciences Research Institute (ICVS), School of Medicine, University of Minho, especially to Sara Granja, Marta Costa, Olga Martinho, Diana Carneiro and Andreia Pereira that were essential to this scientific investigation.

To Dr. Rui Manuel Reis, from the Molecular Oncology Research Center, Barretos Cancer Hospital, I want to thank his collaboration.

To Dr. Edenir Pereira Filho from Departamento de Química, Universidade Federal de São Carlos, and Ovidio from The Chemical Institute of UNESP/Araraquara, I want to thank for their collaboration.

To the Advanced Microscopy Laboratory (LMA) – IQ that made available the scanning electron microscope used to acquired nanoparticle images.

I would like to thank the University of São Paulo State – UNESP, School of Pharmaceutical Science and Graduate Program in Pharmaceutical Sciences for providing logistical conditions for the thesis execution.

I acknowledge the financial support provided from Fundação de Amparo Pesquisa do Estado de São Paulo (FAPESP) / São Paulo Research Foundation grants 2016/09671-3 and 2018/04546-1. I would like to thank Coordenação de Aperfeiçoamento de Pessoal de Nível Superior (CAPES).

To all those who directly or indirectly contributed to the realization of this thesis, thank you very much.

“Nothing in life is to be feared,
it is only to be understood.
Now is the time to understand more,
so that we may fear less”.

MARIE CURIE

RESUMO

Glioblastomas (GBM) representam 77% dos tumores malignos do sistema nervoso central (SNC) e ainda hoje, apesar de todos os avanços na terapia, continua com prognóstico limitado. A existência de barreiras fisiológicas como a barreira hematoencefálica (BHE) representa o principal obstáculo que impede que concentrações adequadas do fármaco atinjam o local de ação. Por suas vantagens anatômicas, uma estratégia proposta para a administração de fármacos destinados ao SNC consiste no uso da via nasal. Além disso, o uso de terapias combinadas utilizando fármacos capazes de agir em diferentes alvos moleculares deve ser considerada para o tratamento de doenças complexas como GBM. O candidato a fármaco ácido alfa-ciano-4-hidroxicinâmico (CHC) e o anticorpo monoclonal cetuximab (CTX) já são explorados devido à capacidade de agir em diferentes alvos moleculares nas células tumorais e aplicados em conjunto, como uma nova abordagem combinada, podem melhorar os resultados terapêuticos. De forma complementar, a utilização de sistemas de liberação baseados em nanotecnologia trará inevitavelmente ganhos terapêuticos à combinação proposta, permitindo que atributos específicos sejam agregados ao sistema e possibilite não somente a administração nasal, como também a associação de diferentes fármacos em um único carreador. Assim, o presente estudo propõe o desenvolvimento de diferentes plataformas poliméricas baseadas em poli(ácido láctico-co-glicólico) (PLGA) e quitosana trimetilada (TMC) ou quitosana oligomérica (OCS) para encapsulação do CHC. Ambos os sistemas desenvolvidos contendo CHC encapsulado exibiram tamanho de aproximadamente 300 a 400 nm contendo quitosana em sua superfície mais externa (potencial zeta positivo) e uma alta porcentagem de CHC encapsulado (± 85%). A caracterização físico-química dos sistemas mostrou sua estabilidade coloidal, principalmente na presença do fármaco CHC. Dados de DRX sugerem que a interação entre CHC e as nanopartículas (NPs) de PLGA/OCS apresentam padrões diferentes das NPs de PLGA/TMC. A conjugação entre CTX e NPs foi realizada através de ligações supramoleculares e covalente resultando em 85 e 58% de eficiência, respectivamente. A análise da eficácia terapêutica utilizando protocolos *in vitro* empregando linhas celulares de glioma U251 e SW1088, estabeleceu que, comparando ambos os sistemas conjugados, o PLGA/OCS parece ter uma capacidade terapêutica mais relevante. Por esse motivo, esse sistema foi selecionado para as futuras investigações. Análise de imunoblot confirmou que o CTX associado às NPs continua a exercer sua eficácia terapêutica. A análise da atividade antiangiogênica, desenvolvimento e progressão do tumor usando modelo de membrana corioalantóica de embrião de galinha (CAM) revelaram uma tendência de redução do tumor quando NPs conjugadas foram utilizadas. Além disso, elas também exibiram uma atividade antiangiogênica. O perfil de liberação *in vitro* mostrou que a liberação de CHC foi sustentada e

retardada pelo seu encapsulamento nas NPs. Estudos de permeação *ex vivo* utilizando mucosa nasal suína mostraram que a permeação de CHC foi modificada pela sua inclusão nos sistemas. A avaliação da capacidade de NPs administradas pela via nasal em atingir o SNC utilizando tomografia de fluorescência forneceu evidências de independentemente do procedimento de conjugação, NPs foram eficazes em realizar o transporte direto para o cérebro pela rota nasal. Portanto, considerando todos os resultados mencionados, o sistema desenvolvido exibiu um conjunto de atributos favoráveis que as tornam alternativas promissoras a serem futuramente consideradas no tratamento de GBM.

PALAVRAS CHAVE: glioblastoma; administração nasal; ácido α-ciano-4-hidroxicinâmico; cetuximabe; nova estratégia terapêutica; efeito combinatório; nanotecnologia.

ABSTRACT

Glioblastomas (GBM) account for 77% of malignant tumors in the central nervous system (SNC), and today, despite all advances in therapy, remains with a limited prognosis. The existence of physiological barriers as the blood brain barrier (BBB) represents the main obstacle that limits appropriate concentrations of drugs designed to therapy. Due to their anatomical advantages, a strategy proposed for direct delivery to SNC involves the use of the nose-to-brain route. Besides, combination therapy that uses multiple drugs against different molecular targets should be considered for complex diseases such as GBM. Drugs like alpha-cyano-4-hydroxycinnamic acid (CHC) and the monoclonal antibody cetuximab (CTX) are already explored for their capacity to act against different hallmarks of cancer and applied together, as a novel combining approach, might improve therapeutic outcomes. Therefore, advances in nanotechnology-based delivery systems will inevitably bring therapeutic gains to the proposed combination since they enable acquisition of important characteristics desired and also the association of different drugs into a single carrier. Thus, the current study proposes the development of different polymeric platforms based on poly(lactic-co-glycolic acid) (PLGA) and trimethyl chitosan (TMC) /chitosan oligosaccharide (OCS) for CHC encapsulation. Both CHC-loaded developed systems (PLGA/TMC and PLGA/OCS) exhibited nanostructure organization of about 300 to 400 nm, containing chitosan on their outermost surface (positive zeta potential) and a high percentage of CHC encapsulation (±85%). Physicochemical characteristics have shown great colloidal stability, especially in the presence of CHC drug. DRX data suggest that interaction between CHC and PLGA/OCS NPs follows patterns different than PLGA/TMC NPs. Conjugation between CTX and developed CHC-loaded NPs was optimally obtained by supramolecular forces and covalent bonds, resulting in 85 and 58% of efficacy, respectively. Analysis of therapeutic efficacy using *in vitro* protocols employing U251 and SW1088 glioma cell lines, established that, comparing both conjugated systems, PLGA/OCS seems to have greatly therapeutic capacity. Therefore, this system was chosen to further investigations. Blot analysis confirmed that CTX associated with NPs continues to exert its therapeutic efficacy. Analysis of antiangiogenic activity, tumor development, and progression using the chicken chorioallantoic membrane disclosed a trend of tumor reduction when conjugated NPs were employed. In addition, this system also exhibited antiangiogenic activity. *In vitro* release profile showed that CHC release was sustained and retarded by drug encapsulation into NPs. The *ex vivo* permeation study applying nasal porcine mucosal showed that CHC permeation was delayed by the inclusion of system complexity. Analysis of NPs delivery using fluorescence tomography provides evidence that the developed PLGA/OCS NPs, independently of conjugation procedure,

were effective in providing nose-to-brain transport. Taking into consideration all of the aforementioned results, we anticipate that the developed system exhibited a set of favorable attributes that make them promising alternatives to be further considered in GBM treatment.

KEY WORKS: glioblastoma; nose-to-brain delivery; α-cyano-4-hydroxycinnamic acid; cetuximab; novel therapeutic strategy; combinatory effect; nanotechnology.

LIST OF ABBREVIATION

ANOVA- Analysis of variance

ANVISA- Brazilian National Agency for Sanitary Surveillance

BBB - Blood brain barrier

CAM - Chicken Chorioallantoic Membrane

CED - Convection-enhanced delivery

CHC - α-cyano-4-hydroxycinnamic acid

CNS - Central nervous system

CS - Chitosan

CTX – Cetuximab

DDS - drug delivery systems

DFT - Density functional theory

DLS: Dynamic light scattering

DMEM - Dulbecco's Modified Eagle's Medium

DMF- N,N-Dimethylformamide

DMSO - dimethyl sulphoxide

EE% - Entrapment efficiency

EGFR - Epidermal growth factor receptor

EMA - European Medicines Agency

ERK - Extracellular signal-regulated kinase

FBS - Fetal bovine serum

FDA - Food and Drug Administration

FEG-SEM - Field emission scanning electron microscopy

FTIR - Fourier transform infrared

GBM – Glioblastoma

HIF-1α - Hypoxia-inducible factor-1 alpha

HNSCC - Head and neck squamous cell carcinoma

HPLC - High performance liquid chromatography

IC_{50} - Half maximal inhibitory concentration

IR-ATR - Attenuated total reflectance infrared spectroscopy

LDHA - Lactate dehydrogenase A

MAbs - Monoclonal antibodies

Mal-PEG-NHS - N-Hydroxysuccinimide-PEGmaleimide

MCTs - Monocarboxylate transporters

MTIC - 5-(3-methyltriazen-1-yl) imidazole-4-carboxamide

NPs - Nanoparticles

OCS - Chitosan oligosaccharide

P-AKT – Phosphorylated protein kinase B

PARP- poly (ADP-ribose) polymerase

PDI - polydispersity index

P-EGFR – Phosphorylated epidermal grow factor receptor

P-ERK1/2 - Phosphorylated extracellular signal-regulated kinases

Pen-Strep - Penicillin/streptomycin

PKM2 - Pyruvate kinase M2

PLGA – Poly (d,l-lactide-*co*glycolide

RSD - Relative standard deviation

RTK - Tyrosine kinase receptors

SATA - N-succinimidyl S-acetylthioacetate

SD – Standard deviation

SRB - Sulforhodamine B

TBS-T - Tris-Buffered Saline/0.1% Tween 20

TCA- trichloroacetic acid

TEM - Transmission electron microscopy

TFA - Trifluoroacetic acid

TMC - N,N,N-trimethyl chitosan

TMZ - Temozolomide

WHO -World Health Organization

XRD - X-ray diffraction

ZP- Zeta potential

LIST OF TABLES

LIST OF FIGURES

SUMMARY

1. INTRODUÇÃO

Entre os tumores cerebrais, o glioblastoma (GBM) representa a forma mais maligna e letal, sendo uma das principais causas de morte relacionadas ao câncer (Colen *et al.*, 2011). Extremamente agressivo altamente invasivo e neurologicamente destrutivo, em sua manifestação, a sobrevida média é de 12 a 16 meses, dados estatísticos que permanecem inalterados nos últimos anos, apesar da descoberta de novos fármacos e avanços tecnológicos (Maher *et al.*, 2001; Karsy, Michael *et al.*, 2018).

Alguns fármacos tem demonstrado potencial atividade no tratamento de GBM. Entretanto, poucos agentes quimioterápicos possuem aprovação pela Food and Drug Adminitration (FDA). Embora novas vias moleculares sejam publicadas todos os dias, aprimorando nosso conhecimento sobre a capacidade biológica e invasiva das células de GBM, a transposição da ciência básica para prática clínica não segue a mesma tendência (Veliz et al., 2015). Tratamentos eficazes que visam atingir o sistema nervoso central (SNC) ainda representam um grande desafio para a comunidade científica, levando em consideração a incapacidade de muitos fármacos em acessar o cérebro (Begley, 2004). A presença de barreiras fisiológicas, principalmente a barreira hematoencefálica (BHE), limita acessibilidade do fármaco, dificultando a eficácia de terapias medicamentosas (Portnow et al., 2009; Alexander et al., 2019). Assim, muitos candidatos a fármacos que provaram ser eficazes em seus locais de ação, falharam e foram descartados durante os ensaios clínicos (Begley, 2004).

Até o momento, o protocolo de tratamento padrão para GBM se inicia com intervenção cirúrgica seguida de radioterapia combinada com a administração oral de temozolomida (TMZ) que provou ser um dos agentes antineoplásicos mais eficazes (Lee; Ooi , 2016). No entanto, embora esse agente alquilante possua a capacidade de atravessar o BHE, sua meia-vida curta requer altas doses que devem ser administradas pela via oral para garantir níveis terapêuticos no cérebro, o que, por sua vez, traz vários efeitos colaterais (Portnow et al. 2009). Apesar disso, poucas mudanças e melhorias na sobrevida foram relatadas (Gately et al., 2018).

A ativação anormal do receptor do fator de crescimento epidérmico (EGFR) ocorre em aproximadamente 40% dos casos de GBM (Roskoski, 2014; Hicks *et al.*, 2016). Assim muitos ensaios clínicos em andamento exploram a utilização de fármacos direcionados para este alvo (Roskoski, 2014). O Cetuximabe (CTX) é um anticorpo monoclonal IgG1 quimérico que liga-se ao segmento extracelular do domínio III ligado ao EGFR, inibindo a ativação de várias vias de transdução de sinal que estão associadas ao desenvolvimento tumoral, progressão, disseminação

metastática e diminuição da sobrevida. Além disso, o CTX também regula a expressão do fator de crescimento endothelial vascular (VEGF), o que pode dificultar o processo de angiogênese (Roskoski, 2014).

Adicionalmente, uma característica importante das células tumorais consiste na ocorrência de uma reprogramação no seu metabolismo energético. A intensa proliferação celular requer um ajuste capaz de fornecer a energia necessária ao crescimento e divisão celular. Como este suprimento energético deve ser rapidamente produzido, as células tumorais substituem a respiração aeróbica pela glicólise anaeróbica, mesmo na presença de oxigênio, um fenômeno registrado pela primeira vez por Otto Warburg (Warburg, 1930; Warburg, 1956; Hanahan; Weinberg, 2011). Como consequência do designado "efeito Warburg", as células cancerígenas secretam lactato / H^+ (ácido lático) que deve ser exportado para o ambiente externo para manutenção do pH intracelular (Gillies *et al.*, 2008; Hanahan; Weinberg, 2011; Miranda-Goncalves *et al.*, 2013; Amorim *et al.*, 2015). Os gliomas malignos são altamente glicolíticos, produzindo altos níveis de ácido lático que devem ser externalizados para o meio extracelular através de transportadores específicos evitando a morte das células por acidose.

As proteínas transportadoras de monocarboxilato (MCTs) compreendem uma família de 14 membros em que 4 isoformas estão relacionadas ao transporte transmembrana de prótons (Izumi *et al.*, 2003). A inibição da atividade dos MCTs, que interrompe o estado de homeostasia por alterações de pH, vem sendo apontada como um dos novos alvos a ser explorado no tratamento de tumores cerebrais, como GBM. O ácido α-ciano-4-hidroxicinâmico (CHC), um monocarboxilato aromático de 189,2 $g.mol^{-1}$ promove uma inibição competitiva da atividade de MCTs em mamíferos sem apresentar citotoxicidade aparente *in vivo* (Colen *et al.*, 2006; Colen *et al.*, 2011).

Estudos anteriores demonstraram que o uso de CHC contra diferentes células de glioma diminuiu o metabolismo glicolítico, a migração e a invasão, induzindo a morte celular (Miranda-Goncalves et al., 2013). A avaliação do CHC como estratégia terapêutica em tumores cerebrais usando entrega por convecção (CED) demonstrou inibição *in vivo* do crescimento do tumor e a ocorrência de necrose completa do tecido tumoral em modelo animal (Colen et al., 2011).

Embora esses resultados sejam bastante encorajadores, a molécula CHC apresenta uma solubilidade bastante limitada o que deve comprometer seu efeito terapêutico quando administrada por vias de administração convencionais como a oral. Na tentativa de superar essas limitações, o CHC já foi incorporado em estruturas de zeólitos, sólidos cristalinos com estruturas microporosas muito regulares nas quais substâncias químicas ativas podem ser incluídos, para o desenvolvimento de sistemas de liberação aplicados ao tratamento do câncer. Como resultado, o encapsulamento de

CHC nestes sistemas também forneceu um aumento significativo de sua capacidade terapêutica (Vilaça *et al.*, 2011). Por outro lado, a administração sistêmica de CTX reduz a proliferação celular em uma série de células tumorais (Van Den Eynde *et al.*, 2011) e, embora essa realidade possa ser estendida ao GBM, a terapia anti-EGFR usando CTX é limitada pela incapacidade deste fármaco em atingir o sítio de ação em concentrações adequadas para que se tenha sua eficácia terapêutica (Eller *et al.*, 2005; Hicks *et al.*, 2016).

A expansão do conhecimento e a compreensão sobre as características moleculares do GBM demonstra um comportamento altamente agressivo e adaptativo, sugerindo que um único agente terapêutico não trará avanços significativos na sua terapia. Assim, a abordagem de múltiplos alvos através de fármacos capazes de agir em diferentes vias de sinalização, de maneira simultânea, pode fornecer um cenário mais favorável no tratamento. Uma série de protocolos de terapia utilizando fármacos associados já foi testada, no entanto, uma associação destinada a inibir o EGFR juntamente com MCTs ainda não foi estudada para GBM.

Muitas vezes, compreender um efeito terapêutico, unicamente, não determina o êxito de uma terapia, especialmente para GBM. Diferentes ensaios clínicos empregando novas substâncias terapêuticas únicas não têm mostrado resultados encorajadores. O principal fator associado à falha terapêutica está associado à BHE, que torna o cérebro praticamente inacessível a grandes moléculas polares (Benoit et al., 2000; Lalatsa; Barbu, 2016). Por outro lado, a via nasal de administração oferece uma alternativa não invasiva interessante para uma conexão direta com o cérebro. Devido a suas características tais como fácil administração, rápida absorção e automedicação, essa nova abordagem está se intensificando (Romeo et al., 1998; Alex et al., 2015).

A administração de fármacos pela via nasal para atingir o cérebro é possível pela localização anatômica da cavidade nasal que contem uma região onde o neuroepitélio está exposto ao ambiente externo possibilitando o rápido transporte do fármaco para o cérebro (Haque *et al.*, 2014). Entretanto, é necessário pontuar que esta via de administração apresenta alguns desafios como a permeabilidade deste epitélio e o tempo de residência da formulação na cavidade nasal. Assim, esforços consideráveis têm sido explorados para o desenvolvimento de sistemas projetados para administração nasal (Alex *et al.*, 2015).

Na área da tecnologia farmacêutica, a proposta de reformulação de um antigo fármaco como uma nova estratégia terapêutica e atividade biológica aprimorada tem sido o foco principal de muitos pesquisadores. Como os resultados desejados a uma terapia não se baseiam apenas no perfil farmacocinético e farmacodinâmico do fármaco, mas também em sua biodisponibilidade no sítio de ação, nas respostas biológicas e nos resultados terapêuticos esperados relacionados à abordagem da

entrega, especialmente para doenças complexas como GBM. Plataformas tecnológicas baseadas em polímeros permitem o desenvolvimento de sistemas inovadores com uma ampla gama de propriedades físico-químicas e estruturais, que podem ser delineadas para atingir características específicas e desejadas para a administração de fármacos. A compartimentalização do fármaco em um ambiente restrito também é uma estratégia promissora para modular propriedades biofarmacêuticas em que atributos críticos, como proteção contra degradação e interação biológica, podem ser projetados de acordo com as necessidades específicas. Para esta finalidade, uma variedade de biomateriais vem sendo proposta. Entre eles, polímeros naturais e sintéticos têm atraído cada vez mais atenção devido à sua grande variedade de estruturas. Sua versatilidade também permite a associação de diferentes fármacos produzindo um carreador único com propriedades desejáveis à via de administração pretendida.

Nano ou microestruturas baseadas em PLGA e quitosana provaram melhorar significativamente a interação do fármaco com as células tumorais, promovendo o aumento de sua citotoxicidade (Chakravarthi; Robinson, 2011). Além disso, estas plataformas já foram destacadas por proporcionarem o transporte de diferentes fármacos ao cérebro através da via nasal uma vez que podem modular a interação desses sistemas com a mucosa interferindo na permeabilidade de diferentes fármacos (Tong et al., 2017; Meng et al., 2018).

Levando em consideração todos os desafios apresentados acima para o tratamento com GBM e tentando estimular o desenvolvimento de novas estratégias terapêuticas que possam melhorar desempenho terapêutico, primeiro levantamos a hipótese de que dois fármacos já estudados (CHC e CTX) poderiam fornecer efeitos aditivos ou sinérgicos contra o GBM. Adicionalmente, os sistemas nanoestruturados para a liberação de fármacos foram introduzidos para fornecer ganhos terapêuticos uma vez que permitem a modulação de propriedades específicas estruturais e biofarmacêuticas para melhorar a resposta biológica desejada. Além disso, devido a sua versatilidade, carreadores baseados em polímeros podem proporcionar a associação de diferentes substancias em um único sistema.

Assim o presente estudo foi desenvolvido para investigar a possibilidade de uma nova terapia combinada para GBM aliada à nanotecnologia por meio da entrega direta ao cérebro através da via nasal de administração. Nanopartículas (NPs) de PLGA e quitosana foram inicialmente desenvolvidas para o encapsulamento do fármaco CHC. Em seguida, uma completa caracterização físico-química foi realizada com o objetivo de comparar as duas plataformas. Posteriormente, CTX foi conjugado na superfície dessas nanoestruturas utilizando diferentes estratégias. A prova de conceito foi investigada pela análise do desempenho terapêutico *in vitro* utilizando cultura de

células nas linhas celulares de glioma SW1088 e U251. Para finalizar, a resposta biológica e a entrega do sistema através da via nasal foram investigadas utilizando protocolos *in vivo.*

1. INTRODUCTION

Amongst all brain tumors, glioblastoma (GBM) represent the most malignant and also the most lethal form, being one of the important causes of cancer-related death (Colen et al., 2011). Extremely aggressive, highly invasive, and neurologically destructive, in its greatest hostile manifestation, the median survival ranges from 12 to 16 months- a statistical fact that has almost nothing changed over the last years of drug discovery and technological advances (Maher *et al.*, 2001; Karsy, Michael *et al.*, 2018).

A set of drugs have shown potential activity against GBM, but only a few chemotherapeutic agents are currently FDA-approved for treatment. Although new molecular pathways are published every day, improving our knowledge about the biological and invasive ability of GBM cells, transposition of basic science into achievements applied in clinical practice has not followed this trend (Veliz *et al.*, 2015). Effective treatments aimed to reach central nervous system (CNS) still represent a big challenge to the scientific community, taking into account the inability of many drugs to access the brain (Begley, 2004). The presence of physiological barriers, primarily the blood brain barrier (BBB), limits their accessibility, hindering the efficacy of distinct drug therapies (Portnow *et al.*, 2009; Alexander *et al.*, 2019). Therefore, many potential drug candidates, which were proven to be effective in their sites of action, have failed and have been discarded during clinical trials (Begley, 2004).

To date, standard treatment for GBM begins with a maximal safe surgical resection, followed by radiotherapy combined with oral temozolomide (TMZ) administration, which has proven to be one of the most effective antineoplastic agents for high-grade glioma (Lee; Ooi, 2016). However, although this alkylating agent holds the ability to cross the BBB, its short half-life requires high doses that must be orally administered to ensure therapeutic levels in the brain, which, in turn, brings about several side effects (Portnow *et al.*, 2009). Despite this fact, little changes and survival improvements with resection thresholds have been reported (Gately *et al.*, 2018).

The abnormal activation of the epidermal grow factor receptor (EGFR) occurs in approximately 40% of the GBM cases (Roskoski, 2014; Hicks *et al.*, 2016). Thus, many clinical trials are ongoing to test the efficacy of various EGFR-targeted drugs (Roskoski, 2014). Cetuximab (CTX) is a chimeric IgG1 monoclonal antibody that binds the extracellular segment of the tethered active EGFR domain III inhibiting the activation of several signal transduction pathways downstream from EGFR, associated to tumor development, progression, metastatic spread, and

decreased survival. In addition, CTX also down-regulates vascular endothelial growth factor (VEGF) expression, what may hamper the angiogenesis process (Roskoski, 2014).

Additionally, another important hallmark of cancer consists of the occurrence of a reprogramming energy metabolism. The intensive cell proliferation in neoplastic diseases requires an adjustment to supply cell growth and division. Since the high required energy must be quickly produced, even in the presence of oxygen, cancer cells direct their glucose metabolism to anaerobic glycolysis, a phenomenon first registered by Otto Warburg (Warburg, 1930; Warburg, 1956; Hanahan; Weinberg, 2011). As a consequence of the designated "Warburg effect", cancer cells secrete lactate/H^+ (lactic acid) which must be exported to outside environment for intracellular pH maintenance (Gillies *et al.*, 2008; Hanahan; Weinberg, 2011; Miranda-Goncalves *et al.*, 2013; Amorim *et al.*, 2015).

Malignant glioma is highly glycolytic, producing high levels of lactic acid, which must be effluxed from the tumor microenvironment by specific transporters (Miranda-Goncalves *et al.*, 2013). Monocarboxylate transporters (MCTs) comprise a family of 14 members where 4 proton-linked isoforms (MCT1-MCT4) play essential role on transmembrane transport (Izumi *et al.*, 2003). MCT inhibition, which disrupt the homeostasis state by pH changes, have been pointed as an attractive novel chemotherapeutic strategy towards GBM (Miranda-Goncalves *et al.*, 2013). α-Cyano-4-hydroxycinnamic acid (CHC), an aromatic monocarboxylate of 189.2 $g.mol^{-1}$, promotes a competitive inhibition of mammalian lactate transporter activity with no apparent cytotoxicity in vivo (Colen *et al.*, 2006; Colen *et al.*, 2011) .

Previous studies demonstrated that the use of CHC against glioma cell lines decreased glycolytic metabolism, migration, invasion and induce cell death (Miranda-Goncalves *et al.*, 2013). The evaluation of CHC as therapeutic tool for metabolic targeting of brain tumors using convection-enhanced delivery (CED) have demonstrated *in vivo* inhibition of tumor growth and the occurrence of complete tumor tissue necrosis in most of the experimental animals (Colen *et al.*, 2011).

However, although these results are encouraging, the CHC molecule presents limited solubility, what should not ensure its therapeutic effect when administered by typical routes. Attempting to overcome those limitations, CHC has been already incorporated into zeolite, crystalline solids with very regular microporous structures in which active chemical interesting compounds can be included, to provide drug delivery systems for cancer treatment. Furthermore, CHC encapsulation into zeolite, also provided a significant increased cytotoxic effect against cancer cells (Vilaça *et al.*, 2011). On the other hand, systematic administration of CTX reduces abnormal cellular proliferation in a series of cancer models (Van Den Eynde *et al.*, 2011)

and although this reality can be extended to GBM, the anti-EGFR therapy using CTX is limited by the drug inability to reach the site of action in great concentrations to provide therapeutic efficacy (Eller *et al.*, 2005; Hicks *et al.*, 2016).

Expansion of knowledge and understanding about GBM molecular features demonstrates a highly aggressive and adaptive behavior, suggesting that a single therapeutic agent will not bring significant advances. Thus, the association of multiple target approach can provide a more favorable scenario. A series of therapy protocols using associated drugs have been tested, however, associations aimed at inhibiting EGFR together with MCTs have not yet been studied for GBM.

Sometimes, understanding the therapeutic effect solely, does not allow its use with considerable efficacy, especially for malignant GBM. Clinical trials of new chemical substances with previous *in vitro* studied therapy have shown no encouraging results. Facing their inherent characteristics, for instance, the main factor associated to failure, consists in the existence of the blood brain barrier (BBB), which makes the brain practically inaccessible to large polar molecules (Benoit *et al.*, 2000; Lalatsa; Barbu, 2016). Therefore, the nose-to-brain delivery offers an interesting non-invasive alternative to reach the brain. Due to its characteristics such as easy administration, fast absorption and self-medication, this novel approach is currently intensifying (Romeo *et al.*, 1998; Alex *et al.*, 2015).

Nose to brain delivery is possible based on anatomical nose location, which has a unique olfactory region where the neuroepithelium is exposed to external environment, providing drug absorption into the brain (Haque *et al.*, 2014). However, it is necessary to point out that this route of administration presents some challenges such as the epithelium permeability and the limited residence time of the formulation in the nasal cavity. Thus, considerable efforts have been exploited towards the development of systems designed for intranasal administration (Alex *et al.*, 2015).

In the field of drug designing, re-formulation of an old therapeutic drug as a novel therapeutic strategy with improved biological activities has been the primary focus of pharmacotechnical researchers. Since the desired outcomes of any therapy does not rely only on the pharmacokinetic and dynamic profile of the drug, but more importantly, on its bioavailability in the site of action, biological response and therapeutic outcomes must be related to the delivery approach, especially for complex diseases such as GBM. Technological polymeric platforms have allowed the development of innovative systems with a wide range of physicochemical and structural properties, which can be delineated to achieve specific characteristics desired for nasal administration. Drug compartmentalization is also a promising strategy to modulate biopharmaceutical properties where critical attributes, such as protection against degradation and biological interaction, may be

designed according to the therapeutic needs. To this approach, different biomaterials have been proposed. Among them, natural and synthetic polymers have drawn increasing attention because of their wide variety of structures. Their versatility also permits the association of different drugs producing a single nanostructured carrier with desired properties to the proposed route of administration.

Nano or micro structures based on PLGA and CS have proven to significantly enhance the cellular association, increasing drug cytotoxicity against cancer cells (Chakravarthi; Robinson, 2011). In addition, these structures have already been highlighted to provide effective nose to brain transport of different drugs (Tong *et al.*, 2017; Meng *et al.*, 2018).

Taking into consideration all above presented challenges for GBM treatment and attempting to stimulate the development of new therapeutic strategies that can improve patient outcomes, we firstly hypothesized that the combination of two already studied drugs (CHC and CTX) could provide additive or synergistic effects against GBM. Further, nanotechnology may be introduced to the innovation to provide nano-mediated therapeutic gains to the proposed combination since they enable modulation of the carrier to achieve the desired biological response. In addition, due to its versatility, polymeric technological platforms can allow the association of different drugs into a single carrier.

Thus, the present study was undertaken to investigate the possibility of a new combined therapy for GBM allied to nanotechnology trough nose-to-brain delivery. Thus, nanoparticles (NPs) of PLGA and chitosan (TMC and OCS) were first employed for encapsulation of CHC drug. Next, a deeper physicochemical characterization was carried out comparing both developed platforms. Then, CTX was conjugated on the nanostructure surface using different strategies. The proof of concept was investigated by the analysis of therapeutic performance *in vitro* using cell culture carried out on SW1088 and U251 glioma cell lines. Finally, the biological response and nose-to-brain delivery was investigated using *in vivo* assays.

2. TEORETICAL ASPECTS

2.1. BRAIN TUMORS AND GLIOBLASTOMA

Brain and central nervous system (CNS) tumors comprise a heterogeneous group of diseases, with more than 100 histologic types, according to the World Health Organization (WHO). These tumors can occur in the brain, cranial nerves, spinal nerves, spinal cord and the meninges, and can be broadly classified as malignant or benign based on histopathological features (Barnholtz-Sloan *et al.*, 2018).

When a brain tumor is diagnosed as malignant, as a common experience for cancer diseases, patients get an uncertainty about its aggressiveness, treatment response, prognosis and quality of life. Subtle neurologic disability is expected and, for most serious cases, progressive functional impairment and cognitive decline are most often present (Cahill *et al.*, 2012). For all those reasons, malignant brain tumors are considered the most aggressive type of cancer. Habitually, treatments are palliative. When neurosurgery cannot be considered, radiotherapy and chemotherapy are applied to prolong life, decelerate neurological impairment and alleviate symptoms (Omuro; Deangelis, 2013).

Gliomas include a very diverse group of intrinsic CNS tumors traditionally classified according to their microscopic similarities with putative cells of origin along glial precursor lineages. Among them, diffuse gliomas represent the most frequent neoplasm which can also be categorized according to its histopathological analysis as diffuse astrocytomas where glioblastoma (GBM) assume the most frequent and malignant representative (Wesseling; Capper, 2018).

GBM is highly invasive, and neurologically destructive in its most hostile manifestation, with an average life expectancy ranging from 12 to 16 months and despite the notable advance of drug discovery, molecular biology, and technological advances, this statistical fact has hardly changed over recent years (Maher *et al.*, 2001; Karsy, M. *et al.*, 2018).

Incidence and mortality of cancer are speedily growing worldwide. In the USA, 80,000 new cases of primary brain tumors were expected in 2018 of which one-third was malignant. Under this scenario, gliomas account for 75%, where more than half are GBM (Ostrom *et al.*, 2017; Bray *et al.*, 2018; Lapointe *et al.*, 2018).

Prevalence studies estimate that the average annual GBM incidence rate is variable, ranging from 0.59 to 3.69 per 100,000 people diagnosed worldwide (Barnholtz-Sloan *et al.*, 2018). Overall, GBM is uncommon in children and incidence, is most of the times, higher in male than female.

Incidence increases with age, and the rates are highest in the 75 to 84 years old age-group (Eder; Kalman, 2014; Tamimi; Juweid, 2017).

GBM proliferation and invasiveness is generally limited to CNS organs and the occurrence of metastasis or tumor cells in the blood is not usual. However, the aggressive and invasive nature, are both responsible for tumor recurrence after therapy. Despite the intensive study of the disease, applied therapies lack the ability to completely eliminate tumor cells. A small portion of cancer stem cells that escape from radiotherapy or chemotherapy doses, due to the low drug availability provided by the blood brain barrier (BBB), can quickly recovery as a new tumor mass (Basso *et al.*, 2018).

Effective treatments aimed to reach CNS still represent a big challenge to the scientific community, taking into account the inability of many drugs to access the brain (Begley, 2004). The presence of physiological barriers, primarily the BBB, limits their accessibility, hindering the efficacy of distinct drug therapies (Portnow *et al.*, 2009; Alexander *et al.*, 2019). Therefore, many potential drug candidates, which were proven to be effective in their sites of action, have failed and discarded during clinical trials (Begley, 2004).

Standard therapy protocol applied for GBM patients includes surgical resection followed by radiotherapy with oral temozolomide (TMZ) and an additional 6 monthly cycles of TMZ (Stupp *et al.*, 2001; Stupp *et al.*, 2005). TMZ is an alkylating agent that causes spontaneous cytotoxicity by converting the reactive methylating 5-(3-methyltriazen-1-yl) imidazole-4-carboxamide (MTIC), to the methyldiazonium cation which reacts with DNA to form methyl adducts, such as N3-methyladenine, N7-methylguanine, and O6-methyl-guanine. These fact results in DNA damage, that, if not repaired by RAD51-driven homologous recombination, leads to cell-cycle arrest or cell death (Friedman *et al.*, 2000).

Although this alkylating agent holds the ability to cross the BBB, its short half-life requires high doses that must be orally administered to ensure therapeutic levels in the brain, which, in turn, brings about several side effects (Portnow *et al.*, 2009). The most common toxicities include gastrointestinal side effects, such as nausea and vomiting, myelosuppression (manifested as thrombocytopenia), and neutropenia (Trinh *et al.*, 2009). Lymphopenia has also been reported as an important hematologic side effect of TMZ use, affecting initially CD4 components (Su *et al.*, 2004).

When discovered, TMZ represented a new class of second generation imidazotetrazine prodrugs able to achieve the cerebrospinal fluid and do not require hepatic metabolism for activation (Friedman *et al.*, 2000). However, different researchers have described resistance for TMZ caused by multiple mechanisms which can be related to DNA repair, chemical mediators

overexpression, abnormal signal transducers or even miRNAs (Friedman *et al.*, 2000; Zhang *et al.*, 2012; Messaoudi *et al.*, 2015).

Attempting to overcome this fact, studies are under way to evaluate combinatory effect between TMZ with other chemotherapeutic agents in the treatment of malignant GBM showing positive (Li *et al.*, 2016; Liu, Y.-J. *et al.*, 2017; Hsu *et al.*, 2018), negative (Ma *et al.*, 2015) or both perspectives (Zanotto-Filho *et al.*, 2015). Importantly, despite this breakthrough, acquired overall 5-year survival in clinical applications still remains less than 10% (Shah *et al.*, 2014).

A series of drugs have shown potential activity for GBM therapy by different mechanisms of action and consequent outcomes. However, just a few chemotherapy agents are approved for treatment. Although new molecular pathways are daily published which are crucial to understand the biology and invasive ability, translation of basic science into applied achievements for clinical practice does not usually follow this tendency (Veliz *et al.*, 2015). Indeed, the alternative of immunotherapy for GBM has provided valuable insights but sometimes also failed to generate comparable clinical results (Veliz *et al.*, 2015).

For instance, to consider molecular genetics together with biology and immunology seems to assure the best future aiming at new combinatory or even adjuvant treatments for malignant GBM patients (Fukai *et al.*, 2008). In addition, the combination of different approaches together with pharmaceutical technology should also be considered as a new promising future.

Importantly, all inconvenience aforementioned can be minimized or even circumvented when alternative routes of administration are employed for the treatment of CNS diseases. After numerous studies have been published and patents filed, the possibility of nose-to-brain delivery has gained momentum since it possesses several advantages provided over others means of brain target drug administration, reaching even the clinical stage (Da Fonseca *et al.*, 2011; Djupesland, 2013; Djupesland *et al.*, 2014; Chen; Da Fonseca, 2018; Liu; Zhang, 2019; Quintana; Westlye, 2019).

2.2. OPPORTUNITIES FOR THERAPEUTIC DEVELOPMENT

2.2.1. THE ROLE OF EPIDERMAL GROWTH FACTOR RECEPTOR (EGFR) IN GBM

The expression of multiple proteins and genes changes drastically in GBM. This fact leads to abnormal activation of different oncogenes and/or silencing of tumor-suppressor genes (Binder *et al.*, 2018). Based on deeper knowledge of expression analysis, which involves DNA sequencing

studies, different signaling pathway are highlighted to be commonly disrupted in GBM (Zahonero; Sanchez-Gomez, 2014).

One of the well-known molecular features is related to the tyrosine kinase receptors (RTK) and although a series of RTK have been reported to be overexpressed and contribute to GBM spread and aggressiveness, the aberrant activation of the epidermal growth factor receptor (EGFR) occurs in approximately 40-60% of the GBM cases and plays an important role since its deregulated expression or activity is directly associated to tumor development, progression, metastatic spread and decreased survival (Zahonero; Sanchez-Gomez, 2014; Veliz *et al.*, 2015; Zorzan *et al.*, 2015; Hicks *et al.*, 2016). A partial deletion in the extracellular domain of a DNA fragment containing exons 2–7 of the gene, known as *constitutively active* EGFRvIII mutation, represents a major mutant form of EGFR which can also be found in a high percentage of GBM patients (Halatsch *et al.*, 2006; Kamiya-Matsuoka e Gilbert, 2015).

EGFR, an RTK that binds ligands of the epidermal growth factor family consisting of four members that belong to the ErbB lineage of proteins (ErbB1–4) that share similarities in structure and function. The 170-kDa transmembrane glycoprotein exhibits three main regions: an extracellular receptor domain, a transmembrane region and an intracellular domain with tyrosine kinase activity (Zahonero; Sanchez-Gomez, 2014). Once bound to its ligand, the receptor becomes autophosphorylated, activating a series of signal transduction pathways involved in the adjustment of cell differentiation, cell proliferation and survival (Crespo *et al.*, 2015). In turn, while some researchers have found poor prognosis for GBM patients carrying EGFR gene amplification, others announce that this correlation might be used as a predictor only among older patients (Crespo *et al.*, 2015). However, from the neuropathological point of view, EGFR amplification represents strong evidence in GBM or even that it should be treated as such.

Independent of any particular characteristics, EGFR alterations entail a specific program of tumor development and, as a consequence, cells will behave differently to the other aggressive GBM (Zahonero; Sanchez-Gomez, 2014).

Three step mechanisms are related to the activation of EGFR signaling. Firstly, the contact between a specific ligand to the receptor activates dimerization of the ligand-binding domains. After that, the dimerization procedure results in auto-phosphorylation of specific tyrosine residues into the intracellular domain of EGFR Y992, Y1045, Y1068, Y1148, and the major phosphorylation site Y1173. Finally, the activated form recruits several molecules associated to phosphorylated tyrosines which will initiate important signaling cascades linked to the activated EGFR (**Figure 1**) (Downward *et al.*, 1984; Zahonero; Sanchez-Gomez, 2014).

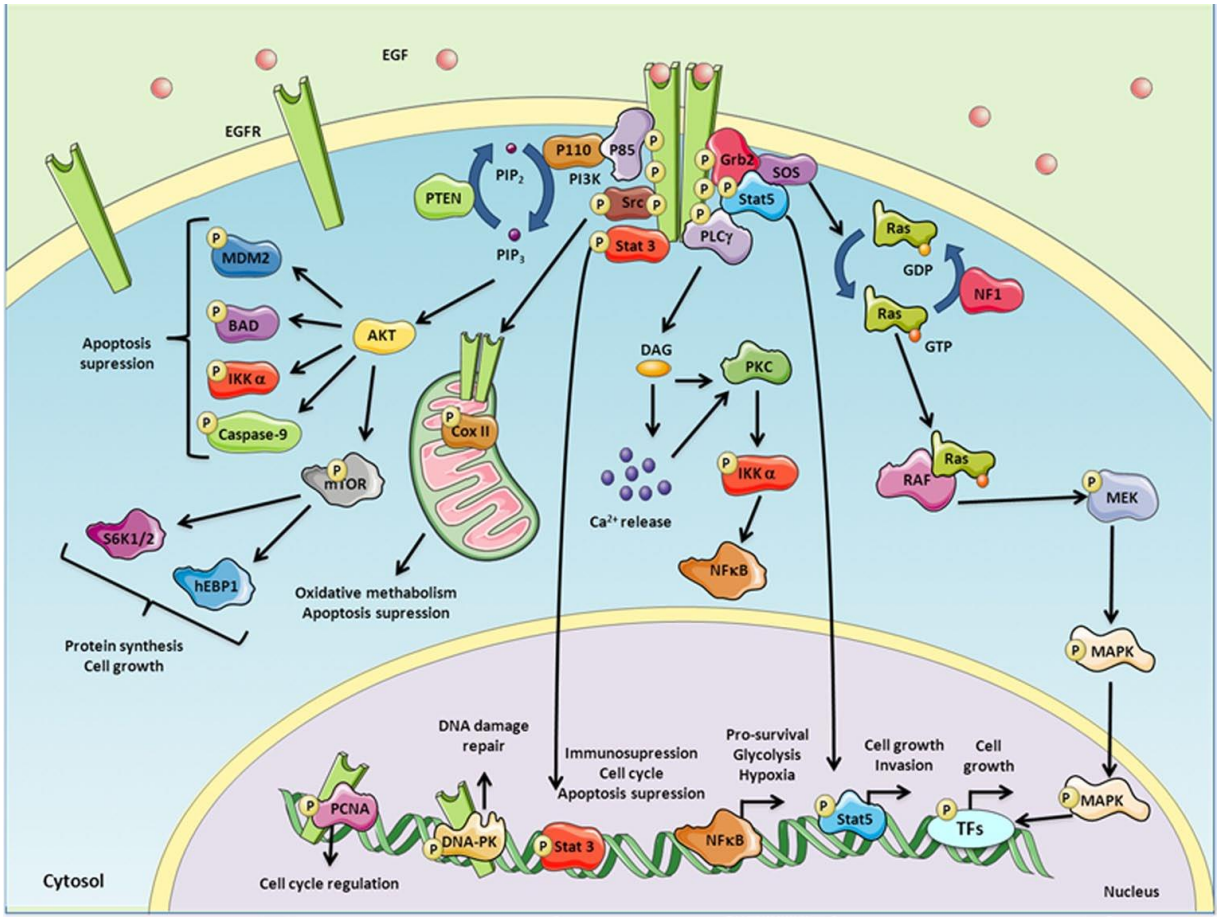

Figure 1: Schematic illustration of EGFR signaling pathways. Activation of EGFR by EGF triggers phosphorylation of several residues that will result in different associated events. Source: Zahonero & Sánchez-Gómez, 2014 (Zahonero; Sanchez-Gomez, 2014).

In fact, recently, several mono or multiple EGFR-targeted therapies have been investigated such as small-molecule inhibitors and biotechnological antibodies (Reilly *et al.*, 2015). Curiously, while EGFR kinase inhibitors have proven to be useful in treating other types of tumors; effective clinical outcomes are not so evident in GBM patients. Why this happens it still unclear and may merely reproduce a problem associated to the drug itself such as limited capacity to cross the BBB, or even by the fact that GBM cells can quickly find an alternative signaling pathway to outline the inhibition of the target molecule (Fine, 2015).

Apart from small molecule tyrosine kinase inhibitors (TKIs), various anti-HER1/EGFR monoclonal antibodies (MAbs), a new generation of promising so-called "target therapies" have been developed and analyzed as a novel strategy against GBM. Their mechanism of action is based on the impairment of ligand-dependent activation and downstream signaling by blocking the receptor extracellular domain (Halatsch *et al.*, 2006).

1.1.1.1. Cetuximab

Cetuximab (CTX) (Erbitux™, ImClone Systems Inc., New York, NY, USA; Bristol-Myers Squibb, New York, NY, USA; and Merck KGaA, Darmstadt, Germany), a recombinant chimeric human murine immunoglobulin G1 and anti-epidermal growth factor receptor MAb, has been pointed as promising targeted drug for EGFR-expressing tumors (Fukai *et al.*, 2008). Its activity impairs EGFR-mediated signal transduction by interfering with ligand binding with higher affinity than the endogenous ligands (Halatsch *et al.*, 2006; Taylor *et al.*, 2012). This event hinders receptor phosphorylation and activation, leading to its internalization or degradation (Vincenzi *et al.*, 2008). Indeed, preclinical data suggest that cetuximab also acts against EGFRvlll (Belda-Iniesta *et al.*, 2006).

The 152-kDa macromolecule is engineered by four polypeptide chains, two of them, identical heavy chains of 449 amino acids and two identical light chains of 214 amino acids connected by supramolecular and covalent bonds (Humblet, 2004). Firstly, it was approved by Food and Drug Administration (FDA) in the treatment of metastatic colorectal cancer as a single agent or in combination with chemotherapy. Moreover, the therapeutic agent is also recommended for locally/regionally advanced head and neck squamous cell carcinoma as single therapy or associated with radiotherapy (Vincenzi *et al.*, 2008).

Systemic administration of cetuximab by parenteral route promotes a reduction on cell proliferation in a variety of cancer models in addition to be well tolerated when administered intravenously in patients with GBM. However, it is important to point out that efficacy of anti-EGFR administered systemically is limited by the BBB since less than 0.5% of circulating antibodies reach the brain. Moreover, its short half-life in the serum requires repeated administration to achieve therapeutic benefits (Hicks *et al.*, 2016). However, although CTX was less effective against intra than extracranial xenografts, antitumor activity was encountered, particularly when combined with radiotherapy (Halatsch *et al.*, 2006).

The mechanisms related to CTX therapeutic activity are not completely elucidated yet. However, benefits such as inhibition of cell cycle progression, increased apoptosis, inhibition of invasion and metastases, induction of antibody-dependent cell-mediated cytotoxicity, inhibition of cell cycle progression, increase in apoptosis and also inhibition of angiogenesis, have been reported (Vincenzi *et al.*, 2008; Golay; Introna, 2012).

Belda-Iniesta and co-workers described clinical outcomes and radiological responses for different human EGFR expressing GBM patients. Their results have shown that histopathological

features of GBM were clearly modified by CTX. However, they also concluded that CTX effect remains undetermined in the absence of a clinical trial (Belda-Iniesta *et al.*, 2006). Independently of the outcome, some features, such as EGFR gene amplification without EGFRvIII mutation may identify a subpopulation with a higher sensitivity for CTX (Lv *et al.*, 2012), reinforces that each case should be analyzed taking into account particular aspects and standard protocols are not always effective.

Evidently, therapeutic efficacy acquires more prominence when CTX is combined with chemotherapy or radiotherapy. Some studies have shown that CTX inhibits DNA damage repair and increase radiosensitivity linked to specific disruption in cell cycle, angiogenesis and enhancement of apoptosis (Dittmann *et al.*, 2005; Vincenzi *et al.*, 2008). Apparently, CTX promotes the cell cycle arrest in more sensitive phases and reduction of cells in the most resistant S phase (Eller *et al.*, 2005).

Chemotherapeutics such as cisplatin, 5-fluorouracil, and paclitaxel among others, can increase EGFR phosphorylation and activation. Therefore, combination groups normally show a significant higher response and longer time to progression than the monotherapy groups (Vincenzi *et al.*, 2008). The possibility of affecting simultaneously different signaling pathways and thus enhancing the ultimate effect of tumor cell death, was demonstrated for GBM cells using CTX together with different chemotherapeutic agents. Their results evidenced a dose-dependent cytotoxicity produced from applied combinatory regimens (Eller *et al.*, 2005).

Multimodality treatments including radio-chemotherapy with EGFR inhibition demonstrate additive cytotoxic effect *in vitro* for different GBM cell lines. In two of five studied models, the combination of TMZ plus CTX resulted in significant antagonism. However, the addition of radiotherapy could overcome this fact underlining the importance of triple multimodal combinations in clinical settings (Combs *et al.*, 2007).

Regardless of benefits, increasing evidence highlights different mechanisms of CTX resistance which can include mutation in KRAS, EGFR and BRAF, and activation of other RTK that bypass the EGFR signaling. Acquired CTX therapy resistance can also be linked to defective DNA repair in tumor cells (Weinandy *et al.*, 2014).

2.2.2. OTHER MOLECULAR PATHWAYS INVOLVED IN GBM PATHOGENESIS: CELL METABOLISM REWIRING

Ungoverned proliferation is an intrinsic characteristic of different cancer cells. Thus, an important hallmark of cancer concerns the occurrence of a reprogramming energy metabolism. The

bioenergetic and biosynthetic demands of the rapid proliferation require adjustments to sustain cell growth and division. Normally and under the presence of oxygen, in most mammalian cells, mitochondria are responsible to oxidize pyruvate to CO_2 and H_2O, which are essential to the maintenance of energy production throughout a range of oxygen concentrations. However, since the high required energy must be quickly produced, cancer cells, like proliferating tissues, replace their glucose metabolism to glycolysis with lactic acid production, a phenomenon first registered by Otto Warburg in 1920s (Warburg, 1930; Warburg, 1956; Gatenby; Gillies, 2004; Hanahan; Weinberg, 2011).

Once they have identified the well-known Warburg effect, later, researchers realized that altered glucose metabolism in tumor cells is more than a simple adaptation to hypoxia. The near universal observation in invasive human cancer cells and its persistence even under normoxic conditions correlated to tumor aggressiveness, announce that this glycolytic phenotype brainstorms significant advantages during somatic evolution of cancer cells what will also contribute to the malignant phenotype. Supporting this observance, the metabolic reprogramming also certifies and supports the large-scale biosynthetic enrollment that is required for active cell proliferation (Gatenby; Gillies, 2004).

As a consequence of the Warburg effect, cancer cells secrete lactate/H^+ (lactic acid) which must be exported to the outside environment for intracellular pH maintenance (Gillies *et al.*, 2008; Hanahan; Weinberg, 2011; Miranda-Goncalves *et al.*, 2013; Amorim *et al.*, 2015). To normalize this condition, they rely on proton exchangers and transporters which export these substances to the microenvironment, allowing them to survive in the unfavorable conditions they have created. Thus, despite the high production of acidic molecules, their intracellular pH is alkaline (~7.4). On the other hand, the microenvironment acidification (pH~6.5) facilitates tumor invasion by acid-induced degradation of the extracellular matrix, destruction of adjacent and normal cell population and promotion of angiogenesis (Granja, Tavares-Valente, Queiros, *et al.*, 2017). Attempting to target this cell metabolism shift, several pH regulators including ATPases, Na+/H+ exchanges, monocarboxylate transporters (MCTs) and carbonic anhydrases are addressed as possible therapeutic targets for cancer therapy (Gonçalves *et al.*, 2015; Granja, Tavares-Valente, Queiros, *et al.*, 2017).

Malignant GBM are highly glycolytic producing high levels of lactic acid (Miranda-Goncalves *et al.*, 2013). Researchers believe that GBM remodeling metabolism increases glycolytic activity 3-fold compared to normal brain tissues (Tabatabaei *et al.*, 2008). The examination of this

molecular reprogramming provides promising new directions to be explored in the treatment gleaned from an old concept (Yuen *et al.*, 2016).

The produced lactic acid exhibits a low pKa and stands predominantly dissociated as lactate anion and proton that will be used as source of energy, metabolic substrate or even recycled for oxidative tumor cells working on metabolic symbiosis (Semenza, 2008). Considering the metabolic cooperation between healthy cells, it may come as no surprise that under pathological cancer conditions, a similar mechanism operates attempts to benefit them (Pérez-Escuredo *et al.*, 2016).

1.1.1.2. Monocarboxylate transporters (MCTs)

MCTs catalyze the proton-linked transport of molecules such as lactate, pyruvate and ketone bodies across the plasma membrane. The total family of transporters comprises 14 members and hares a common topology. However, only the first 4 proton-linked isoforms (MCT1-MCT4) play an essential role on mammal transmembrane transport with different substrate and inhibitor affinities (Halestrap; Price, 1999; Izumi *et al.*, 2003).

The importance of MCTs in cancer biology has been highlighted in different human solid tumors (Izumi *et al.*, 2003; Cheng *et al.*, 2012; Gurrapu *et al.*, 2015). They play a dual role, by facilitating the efflux of lactate upholding a glycolytic phenotype as well as co-transporting a proton along with lactate, assisting the maintenance of intracellular pH (Baltazar *et al.*, 2014). Among cancer cells, MCT1 and MCT4 are the most widely expressed isoforms. In brain rodent tissues, three MCT isoforms, MCT1, MCT2 and MCT4 have been described with distinct cellular and regional distribution. While MCT1 is homogeneously distributed in the whole brain into endothelial cells and parenchymal cells astrocytes, MCT2 is strongly expressed in the neurons, cortex, the hippocampus and the cerebellum. On the other hand, MCT4 is expressed exclusively in astrocytes (Pierre; Pellerin, 2005).

Miranda-Gonçalves and co-workers characterized the expression of MCTs and CD147, a chaperone protein for MCTs, by immunohistochemistry in glioma samples. Their results highlighted the overexpression of MCT1, MCT4 and CD147 at the plasma membrane of GBM compared to nontumoral tissues. They also hypothesized that MCT1would mediate lactate efflux as a result of the glycolytic phenotype. Furthermore, its inhibition has been pointed as an attractive novel chemotherapeutic strategy towards GBM (Miranda-Goncalves *et al.*, 2013). Thus, the lactate homeostasis is considered a critical aspect for the maintenance of malignant state once the blockade of lactate production as well as inhibition of lactate transport can affect the viability of established tumors (Bannister, 2014).

2.2.2.1.1. α-Cyano-4-hydroxycinnamic acid (CHC)

Apart from physiological competitive inhibitors, several chemical substances are known to promote the inhibition of MCT activity such as phloretin, quercetin, 4,4′-diisothiocyanatostilbene-2,2′-disulphonic acid (DIDS), pteridine and coumarin derivatives and α-cyano-4-hydroxycinnamic acid (CHC) (Amorim *et al.*, 2015; Gurrapu *et al.*, 2015; Gurrapu *et al.*, 2016). However, none of them are specific for a given MCT isoform and, indeed, most present a high affinity for other proteins (Pérez-Escuredo *et al.*, 2016). Among them, an aromatic monocarboxylate of 189.2 $g.mol^{-1}$, abbreviated as α-CCA, 4CIN, CHCA, ACCA and CHC have been extensively used as reactive compound that provides MCTs inhibition (Bannister, 2014). Researchers believe that CHC is at least 2-fold more potent as a mitochondrial pyruvate inhibitor, than MCT1. However, this substance is also considered nonspecific (Halestrap; Price, 1999).

CHC belongs to a family of organic compounds synthesized from phenylalanine known as hydroxycinnamic acid derivatives which include sinapic/sinapinic ferulic and caffeic acids (**Figure 2)**. This substance was firstly employed in protein mass spectrometry analysis as a matrix for desorption/ionization. Nevertheless, its biological importance as classical mitochondrial pyruvate transport inhibitor as well as MCT inhibitor should also be considered (Halestrap; Price, 1999; Mojica *et al.*, 2015).

As a chemical substance with proven biological activity (an experimental anticancer drug) especially against cancer cells (Mathupala *et al.*, 2004; Sonveaux *et al.*, 2008; Bannister, 2014), there is little information about CHC molecule such as its physicochemical stability, derived species, full mechanism of action or even analytical methods for quantification. An investigation of vibrational modes of solid CHC using attenuated total reflectance (ATR) infrared spectroscopy was reported by Dembereldorj and Sang-Woo (2010) (Dembereldorj; Joo, 2010). Afterwards, Mojica and co-workers presented the first vibrational study of CHC and their derivatives including density functional theory (DFT) based computer simulations and its correlation with Raman modes (Mojica *et al.*, 2015). However, none of these studies was able to correlate chemical structure with biological activity.

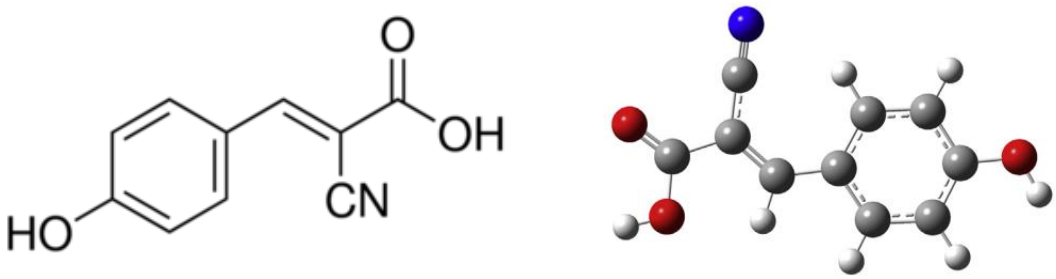

Figure 2: Simple and optimized structure of α-cyano-4-hydroxycinnamic acid. Adapted from Mojica and co-workers, 2015 (Mojica et al., 2015).

The therapeutic effect of CHC against cancer cells has already been investigated for colorectal[50], cervix carcinoma (Sonveaux *et al.*, 2008; Amorim *et al.*, 2015), breast cancer (Diers *et al.*, 2012), melanoma (Wahl *et al.*, 2002), prostate (Kim *et al.*, 2012; Pértega-Gomes; Baltazar, 2014) and brain tumors (Colen *et al.*, 2011; Miranda-Goncalves *et al.*, 2013). In general, most of the time, reported incomes highlighted that CHC disturbs cancer cell homeostasis inducing cell death, reduction of cell growth, proliferation and tumor invasion beyond other important features which may renew its use as chemotherapeutic agent.

The evaluation of CHC as a therapeutic tool for metabolic targeting of brain tumors using convection-enhanced delivery (CED) have demonstrated *in vivo* inhibition of tumor growth and the occurrence of complete tumor tissue necrosis in most of the experimental animals (Colen *et al.*, 2011). However, although these results are encouraging, CHC molecule presents limited solubility, what should not ensure its therapeutic effect when administered by typical routes. Attempting to overcome those limitations, CHC has been already incorporated into zeolite structures to provide drug delivery systems for cancer treatment. Furthermore, CHC encapsulation into zeolites, microporous, aluminosilicate minerals, also provided a significant increased potency (Vilaça *et al.*, 2011).

Recently, the AstraZeneca group was the pioneer to provide clinical studies of much more potent MCT1 inhibitors. The importance of its clinical outcomes is based on the fact that MCT1 expression is rapidly upregulated upon T-lymphocyte activation in order to supply the demand for lactate efflux resulting from an increased glycolytic rate. Thus, the developed substance promotes a metabolism cellular suppression which also provide the inability to sustain the rapid rate of cell division occurring during the early immune response (Guile *et al.*, 2006; Bannister, 2014). The compound AZD3965 is currently evaluated as an anticancer agent in Phase I clinical trials for patients with prostate cancer, gastric cancer or diffuse large B cell lymphoma (ClinicalTrials.govNCT01791595) (Pérez-Escuredo *et al.*, 2016; Afonso *et al.*, 2019).

2.2.3. Drug association approach

Sustaining proliferative signaling, metabolic reprogramming, induction of angiogenesis, activation of invasion, and the occurrence of metastasis are all well-known hallmarks of cancer, which motivate scientists to develop new drugs or new therapeutic strategies that can improve existing protocols (Hanahan; Weinberg, 2011; Agnihotri; Zadeh, 2016; Keller; Schmidt, 2017). As described above, CHC and CTX are already explored for their therapeutic benefits against the aforementioned concepts.

Accumulating evidence suggests that combining two or more drugs that exhibit different action or resistance mechanisms can provide additive or synergistic effects.

Additive or synergistic effects between CHC and other drugs have also been explored for cancer treatment (Miranda-Goncalves *et al.*, 2013; Baltazar *et al.*, 2014; Amorim *et al.*, 2015). Inhibitors of other biological targets that also facilitate the occurrence of glycolysis should also act additively, if not synergistically, with MCT inhibitors (Bannister, 2014).

The development of MCT inhibitors for cancer therapy is currently an ongoing task. While historical inhibitors for MCTs are not strongly selective, CHC in particular has shown interesting therapeutic results *in vitro* and *in vivo* (Pérez-Escuredo *et al.*, 2016). A new drug discovery or development comprises a longstanding procedure where starting an experiment for drug registration into the market takes about 15 years of a huge investment. This fact has sparked an increased interest for drug repurposing incorporated or improved with pharmaceutical technology. Besides, accumulating evidence suggests that combination of two or more drugs that exhibit different cytotoxic mechanisms or are subject to different mechanisms of resistance can provide additive or synergistic effects. Previously, the activation of EGFR in GBM has shown to increase both glucose uptake and lactate production, evidence that those targets might exhibit a self-regulation relationship. Yang and co-workers reveled that EGFR activation promotes aerobic glycolysis by pyruvate kinase M2 (PKM2)-dependent positive feedback looping in its expression or even expression of glucose transport GLUT1 and lactate dehydrogenase A (LDHA). The increased expression of different rate-limiting glycolytic genes plays a critical role in EGF-induced Warburg effect, which leads to an increased glucose uptake and higher lactate production in the presence of oxygen, enhancing brain tumor development. As a conclusion, extracellular signal-regulated kinase (ERK) phosphorylation-dependent nuclear translocation of PKM2 is required for its autoregulation and PKM2-dependent expression of glycolytic genes, which are essential for the EGFR-promoted Warburg effect and tumorigenesis (Yang *et al.*, 2012).

Besides, Velpula and colleagues proposed that the ubiquitous EGFR activation observed in GBM is associated with deregulated metabolic responses and cell proliferation. The study demonstrated a functional significance and interaction of EGFR with mitochondrial pyruvate dehydrogenase (PDK1) kinase. In fact, inhibition of PDK1 reduced EGFR phosphorylation and EGFR-induced tumor growth, suggesting that this association might play a critical role in GBM therapy.

The exploration of CTX pharmacodynamics to further understand therapy-induced changes provided in colorectal tumor cells and tumor microenvironment emphasized a deregulated tumor metabolism through glycolysis, gluconeogenesis, TCA cycle and lipid synthesis. Cetuximab inhibited tumor growth *in vivo*, and this effect was associated with selectively perturbed glucose metabolism and reduced hypoxic volumes based on PET/MRI imaging (Greening *et al.*, 2015).

Several studies suggested that CTX exerts its antitumor activity at least in part via inhibiting the Warburg effect through downregulating hypoxia-inducible factor-1 alpha (HIF-1α) (Luwor *et al.*, 2005; Lu *et al.*, 2013; Luo *et al.*, 2017). Furthermore, inhibition of metabolic key enzymes participating in the cellular glycolytic process, seem to overcome cetuximab resistance (Fu *et al.*, 2016).

Although a series of therapy protocols using drug combinations have been tested, the association aiming to inhibit EGFR together with MCTs using CTX and CHC respectively, has not yet been studied. There is an important relationship between EGFR and tumor cell metabolism which is particularly interesting in the context of GBM. Thus, associated therapy using CTX and CHC undoubtedly, must be thoroughly investigated (Bannister, 2014).

The development of new therapeutic strategies using a combined approach for GBM treatment is of great importance. Besides, the ultimate goal in GBM therapy is to achieve an effective delivery together with specific targeting to cancer cells. To become a successful clinical therapy, agents must overcome not only the difficulties of reaching the anatomical location of GBM cells but also the physiologic barriers encountered on the way. In this regard, the possibility of nose-to-brain delivery has gained attention since this alternative route can provide a direct and effective transport (Da Fonseca *et al.*, 2011; Djupesland, 2013; Djupesland *et al.*, 2014; Chen; Da Fonseca, 2018; Liu; Zhang, 2019; Quintana; Westlye, 2019).

2.1. NOSE-TO-BRAIN DELIVERY: AN AGED CONCEPT WITH A NOVEL PERSPECTIVE

One of the first reports describing the possibility of a direct passage from an extra-environment to the brain, via the nose pathway, dates from 1937 and could prove the existence of an intimate connection between the subarachnoid space and nasal cavities of rabbits by administering different coloring agents. From then on, the knowledge generated about this topic, especially in the late 90s, has raised some expectations (Faber, 1937; Sakane *et al.,* 1991). Over the last two decades, a great number of encouraging outcomes have been reported, attempting the treatment of brain diseases by the nose-to-brain approach. Such studies have ensured quick development of this alternative in terms of safety, efficiency, and convenience (Wu, H. *et al.,* 2008).

Intranasal administration has long been used in Chinese traditional medicine. This route stands out as a non-invasive passageway to transport drugs directly to the central nervous system bypassing the BBB (Gartziandia *et al.,* 2016). The biggest advantages of nasal delivery, when compared to the oral route, are the possibility of avoiding elimination by the liver, gastrointestinal tract, serum degradation, and kidney filtration, which aids the drug in bypassing the processes of degradation. Compared to other routes of administration, it is undeniable that nose-to-brain delivery provides many advantages to treat CNS diseases, since it works promptly and reduces the dose and frequency of administration, enhancing patient compliance (Mittal *et al.*, 2014; Chu *et al.*, 2018). Furthermore, the nasal mucosa offers numerous benefits as a target tissue, exhibiting large surface area that affords a rapid onset of therapeutic effect which results in higher bioavailability, thus allowing the use of lower doses of the drug (Costantino *et al.*, 2007).

The nasal cavity is a complex organ which is divided by the nasal septum into two cavities covered with mucosa (Wu, H. *et al.,* 2008). They are also composed of vestibular, respiratory, and olfactory regions. Any drug or formulation, when administered into the nasal cavity, can be primary absorbed into the systemic circulation. However, this region also contains trigeminal neurons that enable direct access to the brain via trigeminal nerves (Alexander *et al.*, 2019). The human olfactory mucosa, located on the top of the nasal cavity, encloses olfactory cells, which are dual neurons that are in contact with the external environment and the lamina propria, assembling olfactory nerves (Wu, H. *et al.,* 2008). Different drugs can access the CNS through a "shortcut" that follows the trigeminal or olfactory nerves, located at the upper part of the nasal cavity (Samaridou e Alonso, 2018). Starting at the olfactory region, drugs primarily follow to the olfactory bulb via trigeminal and olfactory neurons and are than absorbed into the lamina propria and cerebrospinal fluid,

reaching different brain regions (Alexander *et al.*, 2019). Transport may occur either through the axonal pathway after neuron internalization, through paracellular transport across cell spaces, through channels next to olfactory nerves, or through transcellular transport across the basal epithelial cells. The first being considered the dominant mechanism based on previous animal studies (Djupesland *et al.*, 2014; Samaridou; Alonso, 2018). Most importantly, mechanistic studies have shown that nose-to-brain transport takes place by either extracellular or transcellular mechanisms (Crowe *et al.*, 2018; Samaridou; Alonso, 2018).

However, it is important to consider that the proposed strategy also presents certain limitations since significant challenges are associated to this modality of administration. According to anatomical features and the small volume of the nasal cavity, large doses cannot be administered through this route (maximal dosing volume in humans is 0.4 mL). Another important factor is the presence of metabolic enzymes in the mammalian olfactory mucosa (Djupesland *et al.*, 2014). Proteolytic enzymes and mucosa secretases from the mucosal secretions compose an 'enzyme barrier into the nasal cavity, which produces a 'pseudo-first pass effect' and decreases delivery amounts and therapeutic efficacy (Wu, H. *et al.*, 2008). Additionally, drug permeability is an issue, especially for hydrophilic drugs. It is also important to consider the short drug residence time and the insufficient drug absorption across the nasal epithelium due to the mucociliar clearance (Nigam *et al.*, 2019).

Not all drug substances can gain access to the brain via the nose. The transport possibility is affected by factors such as nasal physiology, physicochemical drug properties and, most importantly, drug formulation (Wu, H. *et al.*, 2008). The analyses of the nose-to-brain field addressed in several publications, have shown that about 85% of conducted research refer to the administration of different drugs as a single solution or even after a co-administration of permeation enhancers able to facilitate the drugs' transport across the olfactory epithelium. Therefore, lately, a new frontier has emerged in this field, which includes innovative nanostructured-based drug delivery systems (Samaridou; Alonso, 2018).

Innovative pharmaceutical technology provides different strategies that are able to overcome such limitations. Furthermore, they also enable the modulation of drug transportation through mucosal surfaces, which provides mucus/nanocarrier interactions and improves mucoadhesion or penetration, opening opportunities for more effective treatments. Another advantage of the aforementioned tools is their structural versatility, which allows the association of different drugs into a single carrier (Tzeng; Green, 2013; Pourgholi *et al.*, 2016; Ferreira *et al.*, 2018).

2.2. DRUG DELIVERY SYSTEMS

Daily, a series of novel and powerful chemical substances for therapeutic purposes continue to be developed and synthetized by the pharmaceutical industry, an investment that exceeds billions USD per annum. Over the past decades, technological advances on new drug production and pharmaceutical technology have overcome the basic organic synthesis strengthening the development of a new and revolutionary market which includes improvements of drugs already available as conventional medicines.

When traditional pharmaceutical dosages are administered, after a period of time, drug concentration in the blood peaks and then declines. The therapeutic effect should achieve when plasma levels are below their toxic dosage and above their ineffective dose. However, the maintenance of plasmatic concentration depends on patient compliance against the drug dosage. Especially from the need for prolonged drug release and better control on drug administration, drug delivery systems (DSS) were engineered as a strategy to maintain the therapeutic range with just a single dose, local delivery to a particular body compartment, which can lower systemic drug levels, preserve medications that are rapidly metabolized by the body, improve patient compliance and comfort (Kost; Langer, 2012).

Historically, the first controlled release formulation was introduced by Smith Kline & French in 1952 when dextroamphetamine was delivered for 12-hours (Helfand; Cowen, 1983). Afterwards, in the mid-1960s at Harvard University, Judah Folkman mentioned a drug delivery device when studied sealed segments of Silastic® (silicone rubber) that could contain a therapeutic substance providing a constant drug release rate. A report that later became the original concept of an implanted zero-order reservoir drug delivery device (Hoffman, 2008).

Controlled drug delivery technology represents one of the most fascinating frontier areas of science. Although an old concept, the field came into maturity in the early 1980s due to the wonderful interaction among pharmaceutical scientists, engineers, chemists, physicists and medical practitioners (Peppas, 2013). New solutions to deliver old drugs is not a contemporary issue, but remains as a crucial biomedical aspect (Mainardes; Silva, 2004).

Development of a new DDS faces several challenges. However, the necessity of reaching the target site stands out, which is often far away from the administration one, remaining at the target site to deliver the drug, preferably in a time-controlled manner, limiting the drug's adverse side effects and ensuring biocompatibility. Formulation represents an important aspect of product

development being often a critical path to guarantee the clinical outcomes. So far, technological alternatives might be considered in an attempt to improve efficacy (Gaumet *et al.*, 2008).

Researchers believe that different generations can be considered regarding the evolution of DDS. According to this concept, the first generation (from 1950 to 1980) includes basic aspects and fundamental understanding especially focused in oral delivery, transdermal delivery and drug release mechanisms (Yun *et al.*, 2015). Second generation may be summarized as smart delivery systems (from 1980 to 2010) when concepts such as zero order release *versus* first-order has emerged. At this moment, nanotechnology was introduced as well as smart polymers and hydrogels, self-regulated release, biodegradable devices, peptide and protein delivery, tumor target and gene delivery. The third generation that we are now experiencing, comprises the predicted concepts of modulated systems that includes glucose-sensitive on-off insulin devices, target delivery of anticancer drugs, long term delivery systems (6 to 12 months) with minimal initial burst effect, *in vivo/in vitro* correlation and prediction profile from *in vitro* studies (Park, 2014).

From the technical point of view, while the first generation was effective in controling physicochemical properties of delivery systems the second generation was marked by the inability of these systems to transpose biological barriers. Therefore, this new prospective generation is expected to overcome both physicochemical and biological obstacles (Yun *et al.*, 2015).

The first clinically available drug delivery devices were macroscopic in scale. One of them, widely reported, was developed by the Alza Corporation, a company founded in the late 1960s focused on the concept of controlled drug delivery. The ophthalmic insert called the Ocusert® released the anti-glaucoma drug pilocarpine at a constant rate in the eye. An intrauterine device was also developed to release the contraceptive progesterone at a constant rate into the uterine cavity. For different applications, both proposed systems were based on polymer technology (Hoffman, 2008).

From the beginning of DDS concepts, polymers always play a central role in the control of drug release and fabrication of different devices since their properties can be manipulated in order to improve efficiency. Thus, polymer technology has expanded side by side with delivery concepts (Mainardes; Silva, 2004; Coelho *et al.*, 2010).

The strategy of drug association or even compartmentalization into polymeric technological devices may allow an effective protection, modulation of physicochemical and drug release properties. Furthermore, patterns of biological interaction become strongly influenced by the developed system characteristics and not solely determined by the drug.

A series of both natural and synthetic biodegradable polymers have been investigated for drug release or drug targeting purposes. However, few of them are considered biocompatible, that is, in vivo enzymatically or non-enzymatically degraded to produce biocompatible and safe products that will be future removed by metabolic pathways (Mainardes; Silva, 2004). Until now, a wide range of different polymer-based platforms have been proposed as DDS. However, undoubtedly, nanotechnology conceptualization provided a new emerged trend in dealing with delivery systems (Park, 2014).

2.2.1. NANOTECHNOLOGY

The terminology "nanotechnology" was first mentioned to the scientific world by N. Taniguchi at the international conference on industrial production in Tokyo, 1974 to describe processed materials with nanosized accuracy and creation of nanosized mechanisms (Tolochko, 2009). This concept has appeared as the realm of DDS on the last decade of second generation. At this time, scientists believed that nanosized materials would have different properties that were unachievable by microsized systems. This assumption was thought to be reasonable and "nano" emerged as essential (Park, 2013). Thus, in the mid to late 1970s, the idea of polymer-drug conjugates or nanostructured therapeutics, arose independently around the world (Hoffman, 2008).

Nanothecnology-based DDS is a rapidly developing multidisciplinary science that ensures the fabrication of the polymers at the nanometer scale for various medical applications (Jacob *et al.*, 2018). As a result of intensive support from the governmental funding agencies on nanotechnology since the year 2000, for more than the last 10 years, nanoparticles have been the most popular topic into the drug delivery field (Park, 2014).

Nanoformulations display an indisputable potential as drug carriers. Different nanostructures that exhibit unique physiochemical and biological properties yields from different size reduction methods and technologies that makes them suitable, especially, for pharmaceutical application. Pharmaceutical technology is an emerging branch among nanotechnology sciences covering the applications of nano-concept to pharmacy and biomedical field providing devices for drug delivery, diagnostic, imaging, and biosensors. Accordingly, a more fine-tuned diagnosis and focused treatment of disease at a molecular level were achieved (Rana; Sharma, 2019).

The nanotechnology connected with drug delivery today represents a powerful tool mainly by their nanosized properties. These systems show, most of the times, size ranging from 1 to 100 nm and, therefore, great similarity to different biological entities. While DDS efficiency is directly affected by their dimensions, their properties enable the penetration through biological and

physiological barriers that are normally impermeable for larger systems. Since therapeutic values of different promising drugs is sometimes diminished due to the presence of biological barriers, nanotechnology gives a solution to effectively deliver drug entities to these sites of action by altering and tuning pharmacokinetic or pharmacodynamic properties of encapsulated drugs (Rana; Sharma, 2019).

Evidence that nanotechnology can enhance the direct transport to CNS are noticeable and crucial, since it not only allows drug protection, but most importantly, it improves the uptake by the olfactory mucosa and access to CNS (Gao *et al.*, 2007; Migliore *et al.*, 2010; Xia *et al.*, 2011; Mittal *et al.*, 2014; Samaridou; Alonso, 2018). Thus, encapsulation of the drug in a nanostructured delivery vehicle can serve as a very powerful strategic approach for nose-to brain transport (Yadav *et al.*, 2015). To date, tumor-specific delivery vehicles have mostly been made within nanoscale dimensions, because of the benefits provided in regard to therapeutic performance on tumor tissues (Zhu *et al.*, 2016).

Among all nanostructured platforms described so far for nose-to-brain delivery, polymeric nanoparticles are under intense investigation as potential carriers, because of their unique surface properties. These structures have shown preferential accumulation into the tumor microregion, as well as an ability to encapsulate and deliver distinct molecules in a "Trojan Horse" fashion (Sukumar *et al.*, 2019). Thus, polymeric nanoformulations offer a potentially exciting new avenue to improve treatment outcomes.

Importantly, the residence time of nanoparticles in the nasal cavity may be limited because of mucociliar clearance, which makes the choice of bioadhesive polymers with enhanced permeability an attractive alternative to the proposed strategy (Gao *et al.*, 2007). For instance, improved permeability of drugs was provided by nanostructured delivery systems, supporting a feasible approach for the nose-to-brain pathway (Nigam *et al.*, 2019). Besides that, bioadhesiveness can be supplied by means of surface modification of drug carriers with biological ligands that are able to recognize and adhere to specific chemical structures on the cell surface, improving system absorption (Gao *et al.*, 2007).

1.1.1.3. Polymeric nanoparticles

Polymeric nanoparticles (NPs) are prepared from biocompatible and biodegradable polymers where the drug can be dissolved, entrapped, encapsulated or even attached to the matrix (Nagavarma *et al.*, 2012). These systems have attracted great interest during the last decades especially due to a wide range of applications. Their submicron size offers a number of distinct

advantages over the other systems, including relatively higher intracellular uptake (Pinto Reis *et al.*, 2006). Furthermore, intrinsic properties can be modulated and deeper explored depending on the intended performance (Rao; Geckeler, 2011).

In general, polymeric NPs are defined as colloidal systems in the range of 10-1000nm (Couvreur, 1988). The collective term can be related to nanospheres and nanocapsules. While nanospheres consist of particles where the entire mass is solid and drug might be adsorbed or encapsulated within the particle, that is, a matrix systems which contain the drug physically and uniformly dispersed, nanocapsules are vesicular systems where the entrapped substance is confined inside a cavity surrounded by a solid polymeric material (Wise, 2000).

The uptake of NPs into the cells usually involves endocytosis processes. However, this performance depends primarily on their size and surface characteristics (Crucho; Barros, 2017).

Among all advantages provided by polymeric NPs, the possibility of improved drug stability, the possibility of provide desired characteristics intend alternatives routes of administration, the possibility of delivering a higher concentration of the drug to the target site, the acquisition of modified drug release are constantly mentioned and explored (Nagavarma *et al.*, 2012). In terms of bioavailability, they show a remarkable enhancement over different administration routes (El-Say; El-Sawy, 2017).

The design of new polymeric NPs can be elaborated through many materials and components that are selected according to the desired features and specifications. Regardless, the main constituent utilized is a polymer that can be classified as natural or synthetic according to source of origin with no preferred category as the choice step. Importantly, selected material must show a proven biocompatibility and biodegradability (El-Say e El-Sawy, 2017).

Some natural polymers are very attractive materials; besides the relatively low cost, they are biodegradable and with excellent biocompatibility. However, their use has been limited due to batch-to-batch variations. On the other hand, some synthetic polymers offer a wide variety of composition with adjustable properties what creates the possibility of projecting a delivery system with specific chemical, interfacial, mechanical or biological characteristics by the choice of building blocks or preparation techniques. Considering advantages, design of polymeric NPs containing natural and synthetic blocks may represent a rational strategy. The final purpose is to gather in the system properties of the natural polymer (biodegradability and biocompatibility) and the synthetic one (intrinsic and unalterable properties) (Coelho *et al.*, 2010).

From all natural polymers employed, polysaccharides are high molecular weight structures composed by monosaccharide repeating units that show a wide range of properties since they

exhibit reactive functional groups that allow structural modifications and further possibilities of applications.

Chitosan (CS), a natural cationic polysaccharide that exhibits a pKa of 6.1–7.3, obtained by the alkaline deacetylation of chitin, main constituent of marine crustacean shells, is considered one of the most explored material for drug delivery due to their intrinsic and valuable properties (Safdar *et al.*, 2019). Their positive charges can enhance their permeation and structural rearrangement that allows the opening of tight junction. This characteristic also provides mucoadhesive properties since the amino groups of CS interact with the anionic counterpart present in the mucous layers, mainly sialic acid, which are useful to improve drug bioavailability or even formulation retention in the nasal cavity (Casettari; Illum, 2014).

CS positive charges provided by the reactive amino groups must also be considered for conjugation with different macromolecules. The presence of amino groups renders to the polymer an efficient transfection agent. Importantly, the conjugation between two cationic moieties may also be possible by the use of a heterobifunctional PEG (Malhotra *et al.*, 2013).

Solubility is an important issue in the pharmaceutical application of chitosan. At neutral and alkaline pH conditions, the non-protonation of chitosan result in its immiscibility in water (Liu, J. *et al.*, 2017). Their semi-crystalline structure shows strong inter- and intra-molecular hydrogen bunds. Thus, the polymer can be dissolved in various organic acids since solubilization occurs by protonation of the $–NH_2$ function on the C2 position of the D-glucosamine repeat unit (**Figure 3**) (Rinaudo, 2008). Due to the reactive groups present in CS, chemical modification is possible and widely explored. These groups can be readily modified with different ligands, functional groups and moieties, developing a series of CS derivatives with attractive physicochemical properties (Naskar *et al.*, 2019).

A polyelectrolyte with good intestinal absorption is the derivative N,N,N-trimethyl chitosan (TMC). It is one of the most successfully developed quaternized CS acquired by extensive methylation. Due to the greater number of hydrophilic amino groups on the main chain, TMC is soluble in neutral water and alkaline media (**Figure 3**) (De Britto; Assis, 2007).

Physicochemically, TMC bears cationic charge, and because of that, is mucoadhesive in nature. Due to the presence of both hydrophilic (N-(CH3)3) and the hydrophobic groups (N-(CH3)2), TMC is amphiphilic and can be self-assembled to vesicles, suitable for NP processing (De Britto *et al.*, 2012).

Researchers believe that compared with CS, TMC derivative exhibits increased antibacterial activity because of the availability of positive charges after quaternization (Wu *et al.*, 2016). The

permeation enhancing effects of TMC have also been confirmed for macromolecular drugs (Thanou *et al.*, 1999). In fact, TMC has already astonished scientists through its improved characteristics, when applied for nano-structured systems (Kulkarni *et al.*, 2017).

Also a CS derivative, chitosan oligosaccharide (OCS) is essentially the chitin/chitosan degraded product which can occur by acid hydrolysis, enzymatic degradation or both, characterized by a degree of deacetylation (DD) of more than 90%. In relation to chitosan, OCS is hydrolyzed with better solubility and lower viscosity under physiological conditions due to its shorter chain lengths, in addition to possessing attributes of the parent polymer like biodegradability, mucoadhesion, biocompatibility and low toxicity what make them an interesting material for NP development. Furthermore, innumerable reports have revealed a series of potentially promising biomedical and pharmaceutical applications of OCS, highlighting their immunostimulant property, antitumoral, antioxidant, antimicrobial and anti-inflammatory activities (Wu, Haige *et al.*, 2008; Shen *et al.*, 2009; Zou *et al.*, 2016; Naveed *et al.*, 2019).

Among them, antitumoral activity of OCS is of particular interest when engineering a delivery system intended for cancer therapy. Several investigations have demonstrated that OCS treatment can interrupt cancer progression at multiple steps including growth, invasion, and metastasis (Gumińska *et al.*, 1996; Muanprasat; Chatsudthipong, 2017). However, molecular weight and DD of OCS are important factors for suppressing cancer cell growth. In spite of that, they may provide valuable material for the further development of antitumor agents deriving from chitosan (Park *et al.*, 2011).

Importantly, no single type of CS exhibits all related biological activities. It is important to know that different derivatives exert distinct biological activities and also the same derivative that shows divergent acetylation degree, molecular weight, polymerization or any physicochemical characteristic, can behave differently. So far, no detailed molecular mechanisms of biological activities are described in the literature. Thus, independent of the chosen CS species for future investigations, experimental approaches should cover their molecular-level detailed as well as insights into biochemical functions (Zou *et al.*, 2016).

Currently, chitosan has also been largely explored as surface modifier conjugated to several polymers offering some advantages to the engineered technological platform. The main purpose of its incorporation into these systems has the function of awarding greater bioadhesiveness, potentiating the transport through mucous membranes granted by supramolecular interactions between developed nanocarriers and the mucosa surface (Des Rieux *et al.*, 2006). Their use as

surface modifier is almost always associated with other synthetic polymers selected according to the desired biological response.

Regarding the use of synthetic polymers for nanoparticle development, there are a large number of research groups, worldwide, using poly(lactic-co-glycolic) acids (PLA/PLGA) for controlled drug delivery systems (Brannon-Peppas, 1995). PLGA is one of the most successful materials to formulate polymeric NPs due to its alluring properties such as biocompatibility and United States Food and Drug Administration (FDA) and European Medicine Agency (EMA) approval for parenteral use.

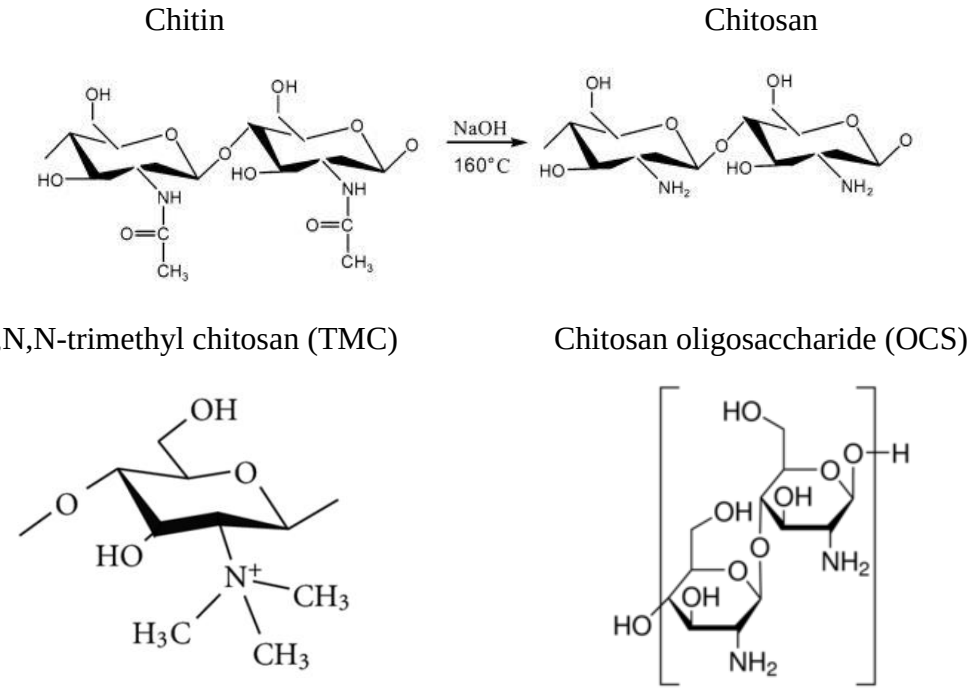

Figure 3: Preparation of chitosan by the alkaline deacetylation of chitin and chemical structures of chitosan derivatives TMC and OCS. Adapted from Rinaudo, 2006 (Rinaudo, 2006).

Well described formulation methodologies to develop NPs using PLGA applied for hydrophilic or hydrophobic drugs can be easily found. In addition, reports have shown the PLGA capacity for drug protection from degradation, possibility to provide modified release, target to specific organs or cells or even to provide better interaction with the biological materials (Danhier *et al.*, 2012).

The polymer is commercially available with different molecular weights and copolymer composition which will directly influence the degradation time. Identification is usually done by monomer ratio used. As an example, PLGA 15:85 identifies a copolymer which composition is 15% of lactic acid and 85% of glycolic acid (Danhier *et al.*, 2012). PLGA polymers are miscible in

a variety of volatile organic solvents as acetone, dichloromethane, chloroform and ethyl acetate which somewhat limits techniques of preparation for NPs production. Physical properties like molecular weight, polydispersity index, and degree of crystallinity have shown to affect NP degradation, swelling behavior and mechanical strength (Sharma *et al.*, 2016). PLGA has been successfully used to develop nanostructure-based drug DDS for different applications. Extensive *in-vitro* and *in-vivo* testing has proven the concept of potential advantage to use this polymer in the treatment of various complex diseases as cancer (Mir *et al.*, 2017).

Nano- or micro-structures based on PLGA and CS have proven to significantly enhance the cellular association, increasing drug cytotoxicity against cancer cells (Chakravarthi; Robinson, 2011). In addition, these structures have already been highlighted to provide effective nose to brain transport of different drugs (Tong *et al.*, 2017; Meng *et al.*, 2018).

In the field of drug design, re-formulation of an old therapeutic drug as a novel therapeutic strategy with improved biological activities has been the primary focus of pharmacotechnical researchers. Since the desired outcomes of any therapy does not rely only on the pharmacokinetic and dynamic profile of the drug, but more importantly, on its bioavailability in the site of action, biological response and therapeutic outcomes must be related to the delivery approach, especially for complex diseases such as GBM.

3. AIM

The present study was undertaken to investigate the use of a new combined therapy applying different drugs (α-cyano-4-hydroxycinnamic acid and cetuximab) which acts in different signaling pathways in tumor cells. In this regard, firstly, nanotechnology was remployed trough the rational development of poly(lactic-co-glycolic) acid/chitosan nanoparticles for α-cyano-4-hydroxycinnamic acid encapsulation, considering their limited solubility. Chosen excipients were selected to provide mucoadhesive and permeation features to the proposed systems. Subsequently, cetuximab was conjugated on the nanostructures surface using different strategies creating a single delivery system with desirable properties for nasal administration.

4. MATERIALS AND METHODS

4.1. DETERMINATION OF CHC AND CTX IC_{50} AGAINST GLIOMA CELL LINES

4.1.1. Cell lines and cell culture

Glioma cell lines U251 and SW1088, known to express MCT1 and MCT4 and overexpress the EGFR protein, were used for these studies (Miranda-Goncalves *et al.*, 2013; Mortensen *et al.*, 2013). Cell line SW1088 was obtained from the American Type Culture Collection and U251 was provided by Professor Joseph Costello, California University, Neurosurgery department, San Francisco. Authentication was performed at IdentiCell Laboratories (Department of Molecular Medicine at Aarhus University Hospital Skejby, Arhus, Denmark). The cells were maintained in Dulbecco's Modified Eagle's Medium (DMEM 1×, High Glucose; Gibco, Invitrogen), supplemented with 10% fetal bovine serum (FBS; Gibco, Invitrogen) and 1% antibiotic penicillin/streptomycin (Pen-Strep; Gibco, Invitrogen) in a humidified atmosphere at 37 ºC and 5% CO_2.

4.1.2. Chemicals

Stock solutions of α-cyano-4-hydroxycinnamic acid (CHC) (Sigma-Aldrich, St. Louis, USA), and Erbitux® (Merck KGaA, Darmstad, Germany), which contains the active substance cetuximab (CTX), were prepared by solubilizing them in dimethyl sulphoxide (DMSO, Sigma-Aldrich, St. Louis, USA) and DMEM, supplemented with 0.5% FBS and 1% Pen-Strep solution. The final concentration of DMSO was maintained at a maximum of 1%. All negative controls were performed using DMSO and DMEM.

4.1.3. Cell viability

Cell viability was assessed through the sulforhodamine B colorimetric assay (SRB) 72 hours after treatment, according to the manufacturer's recommendations. Firstly, cells were plated into 96-well plates at densities of $2x10^3$ for U251 and $3x10^3$ for SW1088 using DMEM 10% and left to adhere overnight. Afterwards, cells were treated with increased concentrations of CHC (0.5 to 7 for U251 and 0.5 to 15 mM for SW1088) and CTX (50 to 1000 ug/mL) in DMEM 0.5% FBS. Evaluated concentration of CHC for U251 and SW1088 was chosen based on results previously published by Miranda-Gonçalves and co-workers. They also highlighted the greater sensitivity of

U251 to CHC treatment compared with SW1088 (Miranda-Goncalves *et al.*, 2013). Absorbance was measured using the Varioskan Flash multimode reader (Thermo Scientific, Finland), at 490 nm. The IC_{50} (value that inhibits cell growth in 50%) was calculated from at least 3 independent experiments (n=3) by nonlinear regression using GraphPad Prism Software. Experiments were conducted at Life and Health Sciences Research Institute (ICVS), School of Medicine, University of Minho, Braga, Portugal.

4.2. COMBINED EFFECT OF CHC AND CTX AGAINST GLIOMA CELL LINES

The combined effect of CTX and CHC against U251 and SW1088 was assessed by using the cell viability assay as described above. For this purpose, the treatments used in the present study consisted of: the amount of CHC previously determined to induce 50% of cell death; the amount of CTX previously determined to induce 50% of cell death; and both dosages applied simultaneously as a single solution.

4.3. NANOPARTICLE (NP) DEVELOPMENT

4.3.1. Materials

TMC was kindly synthetized and donated by Brazilian Agricultural Research Corporation – EMBRAPA (São Carlos, Brazil). 50:50 Poly(d,l-lactide-*co*glycolide) (PLGA) and chitosan oligosaccharide lactate (OCS) (Mn 5,000; > 90% deacetylated) were purchased from Sigma-Aldrich (São Paulo, Brazil). All other chemicals including sodium chloride, hydrochloric acid, sodium hydroxide were analytic reagent grade purchased from Sigma-Aldrich (São Paulo, Brazil).

4.3.2. Methods

1.1.1.4. Development of PLGA-trimethyl chitosan (PLGA/TMC) NPs using nanoprecipitation technique

PLGA-TMC nanoparticles (NPs) were prepared using a previously described nanoprecipitation method with modifications (Sanna *et al.*, 2012; Bonaccorso *et al.*, 2017). First, the PLGA polymer and CHC were dissolved in 2 mL acetone. The solution was then added into 5mL aqueous solution containing Pluronic® 188 50mg and TMC 5mg, using a 5mL syringe coupled with a 0.45x13 26G1/2 BD® needle and magnetic stirring. The resultant milky colloidal suspension was left in magnetic stirring to remove the acetone solvent. NPs were collected after 20

minutes of centrifugation at 16,000 rpm, using a Spectrafuge 16M, Labnet, Brazil, and washed with purified water to remove the unencapsulated CHC drug. For comparative purposes, empty NPs (absent of CHC drug) were obtained following the same procedure described above. These systems will be referred as PLGA/TMC NPs throughout this PhD thesis.

1.1.1.5. Development of PLGA-oligomeric chitosan NPs (PLGA/OCS) by one-step oil in water emulsion, solvent evaporation technique

PLGA-OCS nanoparticles were produced by the single emulsion method previously described with modifications (Win *et al.*, 2015). In summary, CHC was dissolved in acetone while PLGA in dichloromethane solution composing a homogeneous organic solvent system. The organic phase was added into the aqueous solution containing Pluronic 127 and 1mg of OCS using a 5mL syringe coupled to 0.70x30mm BD® needle. Emulsification was carried out by 3 min sonication (pulse mode of 1.5 min on and 30 s off) in an ice bath (QSonica, Sonicators, USA). The resulting milky colloidal emulsion was left in magnetic stirring to remove organic solvents. Afterwards, 1mL of NPs was added to Amicon® 100kDa cut off, centrifuged at 3000rpm using Excelsa® II Centrifuge (Fanem®, Brazil) for 10 minutes, washed and stored for further characterization. These system will be referred as PLGA/OCS NPs throughout this PhD thesis.

4.3.2.1.1. Full factorial design (2^n) to optimize the NPs PLGA/OCS production

NPs development was optimized using a full factorial design to evaluate the effects of selected variables (v): ratio between different organic (O) and water (AQ) (v1), Pluronic 127 concentration (v2), sonication time (v3) and PLGA concentration (v4) on the responses: size (S), zeta potential (ZP), polydispersity index (PDI) and drug-entrapment efficiency (EE%). A total of 16 formulation runs were generated and levels of dependent and independent variables are shown in **Table 1**. Matlab software was used to perform regression analyses as well as to calculate the interaction among independent factors. Statistical significance was set at $p < 0.05$ (95% of confidence level).

Table 1: Codified variable composition and results of experimental plan using complete factorial design (2^4) for PLGA/OCS NPs development by one-step oil in water emulsion and solvent evaporation method.

Run order	V1	V2	V3	V4	Size (nm)	PDI	Zeta Potential (Mv)	Entrapment efficiency (%)
	O:AQ (Ratio)	Pluronic 127 oncentration	Sonication time	PLGA concentration				
1	-1	-1	-1	-1	252.7	0.366	54.3	86.79
2	1	-1	-1	-1	500.8	0.572	55.7	88.44
3	-1	1	-1	-1	213	0.372	33.2	86.28
4	1	1	-1	-1	870.5	0.645	43.1	85.65
5	-1	-1	1	-1	343.4	0.442	51.9	91.18
6	1	-1	1	-1	648.4	0.533	58.9	89.20
7	-1	1	1	-1	258.3	0.446	37.1	88.83
8	1	1	1	-1	564.8	0.536	45.7	87.08
9	-1	-1	-1	1	240.8	0.385	38.0	93.23
10	1	-1	-1	1	863.5	0.701	45.4	92.42
11	-1	1	-1	1	383.3	0.539	44.2	75.69
12	1	1	-1	1	553.2	0.598	44.7	89.91
13	-1	-1	1	1	284.2	0.267	40.5	92.64
14	1	-1	1	1	541.6	0.576	57.6	91.22
15	-1	1	1	1	299.6	0.396	39.2	91.13
16	1	1	1	1	860.2	0.678	43.2	88.94

	Organic (O): Aqueous (AQ) ratio	Pluronic 127 concentration (%)	Sonication time	[PLGA] ($mg.mL^{-1}$)
1	1:5	3.0	2 cycles	10
-1	2:1	1.3	1 cycle	5

4.4. CHC-LOADED NP CHARACTERIZATION

4.4.1. Particle size and polydispersity index

The particle size and polydispersity index (PDI) were measured using photon correlation spectroscopy / dynamic light scattering (DLS) on Zetasizer NanoZS (Malvern Instruments, Malvern, UK). DLS measurements were done with a wavelength of 532 nm at 25 ºC with an angle detection of 173º. The analysis was conducted using 10µL of NPs samples diluted in 1mL of purified water (according to the selected attenuator and count rate (Kcps) pointed by the equipment). Results were described as mean of tree independent determinations (n=3) and corresponding standard deviation.

4.4.2. Zeta potential

Zeta potential values were measured at 25°C using Zetasizer NanoZS (Malvern Instruments, Malvern, UK) equipment through the electrophoretic mobility. In this technique, a voltage is applied between a pair of electrodes promoting the particle attraction by the appositely charged electrode. Thus, their velocity is measured and expressed as electrophoretic mobility(Kaszuba *et al.*, 2010). Samples were diluted as described on section 3.4.1 and data were obtained by the averaging of three measurements (n=3) and standard deviation.

4.4.3. Entrapment efficiency (EE%)

The amount of CHC encapsulated by the NPs was determined by using UV-VIS Spectroscopy Cary 60 (Agilent Technologies, USA), at 325nm, using a previously obtained standard calibration curve ($y=113.15x + 0.0016$; $r^2=0.999$), applying validated methodology. A known amount of CHC-loaded NPs were placed in Amicon® MWCO 100kDa Ultra-15 Centrifugal Filter Units and centrifuged at 3000rpm using Excelsa® II Centrifuge (Fanem®, Brazil) for 10 minutes. Quantification of CHC was carried out by measuring the amount of free particles deposited on the bottom of the Amicon® filter. Results are exhibited here as the mean of three independent determinations (n=3) and standard deviations.

4.4.4. NP colloidal stability

After preparation, NPs were stored in a refrigerator (8ºC) and periodically (at least once a week) analyzed for size, PDI, and zeta potential using the Zetasizer NanoZS (Malvern Instruments,

Malvern, UK). Samples were diluted using ultra-purified water (1:100) and data was obtained by calculating the average of all three measurements (n=3) and standard deviation.

4.4.5. Attenuated total reflectance-Fourier transform infrared (ATR-FTIR) spectroscopy

Infrared spectroscopy of TMC, OCS, PLGA, empty NPs, and CHC-loaded NPs was performed using Fourier transform infrared (FTIR) spectrometer Vertex 70 (Bruker, Massachusetts-USA) equipped with a Golden Gate single reflection ATR accessory and a DLaTGS detector to investigate polymer-CHC interactions. Powdered samples were scanned over a wave region of 400-4000cm^{-1}. Experiment was conducted at Instituto de Química, Universidade Estadual Paulista (UNESP), Araraquara.

4.4.6. X-ray diffraction (XRD)

XRD analysis of TMC, OCS, PLGA, empty NPs and CHC-loaded NPs were conducted using a D5000-DIFFRAC PLUS XRD Commander (Siemens®, Germany) with monochromatic Cu-Kα radiation (λ = 1,5406 Å), operating at 40 kV and 30 mA. Samples were analysed with a detector resolution in 2θ (diffraction angle) with scan step time of 0.05/min in the range between 4-70º, at room temperature. Experiment was conducted at Instituto de Química, Universidade Estadual Paulista (UNESP), Araraquara.

4.4.7. Field emission scanning electron microscopy (FEG-SEM)

FEG-SEM was performed on empty NPs and CHC-loaded NPs to analyze size and morphology. Samples were diluted (1:100 v/v), placed on a metallic holder, and left to dry at room temperature. Afterwards, samples were covered with carbon, and photomicrographs at different magnifications were taken using a JOEL-JSM-7500F coupled to the Joel Pc-100 ver.2.1.0.3. Software. Experiment was conducted at Instituto de Química, Universidade Estadual Paulista (UNESP), Araraquara.

4.4.8. Transmission electron microscopy (TEM)

Transmission electron microscopy measurement was carried out using TEM Phillips CM200 Super Twin Model. Firstly, NPs were diluted (1:20, v/v) using Milli-Q water and samples were prepared by dropping 10µL into a carbon-coated copper grid and allowed to dry at room

temperature. The grid was then scanned using operating voltage 200 kV and 2.4 Å resolution. Experiment was conducted at Instituto de Química, Universidade Estadual Paulista (UNESP), Araraquara.

4.5. NP CONJUGATION WITH CTX BY SUPRAMOLECULAR FORCES AND COVALENT BONDS

PLGA/TMC and PLGA/OCS NPs which exhibit a similar composition (PLGA and chitosan) were conjugated with the mAb cetuximab using different strategies (**Table 2**).

Table 2: Nanoparticle (NP) composition used for conjugation with CTX and further biologic assays.

Sample	Composition	CHC concentration
NPs PLGA/TMC	PLGA 1.4 $mg.mL^{-1}$ Trimethyl chitosan (TMC)1 $mg.mL^{-1}$ Pluronic 188 10 $mg.mL^{-1}$	1.6 $mg.mL^{-1}$
NPs PLGA/OCS	PLGA 10 $mg.mL^{-1}$ Oligomeric chitosan (OCS) 1 $mg.mL^{-1}$ Pluronic 127 30 $mg.mL^{-1}$	1.4 $mg.mL^{-1}$

PLGA/TMC NPs was combined with CTX by supramolecular bonds. For this purpose, 500µL of NPs were added to 250µL of CTX (5 $mg.mL^{-1}$), pH was adjusted to 6.5 and left under magnetic stirring for 12 hours. After this time period, the system was placed into Amicon® MWCO 100kDa Filter and centrifuged at 9000 rpm using Heraeus Multifuge 3L-R Centrifuge (Thermo Electron Corporation, Germany) for 10 minutes. The amount of free CTX was collected from the bottom part and quantified using HPLC to calculate the conjugation efficiency (%).

PLGA/OCS NPs was conjugated with CTX by covalent bonds. The conjugation was possible using a heterobifunctional PEG (N-Hydroxysuccinimide-PEGmaleimide) as a cross linker agent which promotes, in one of their two ends, the reaction through its N-hydroxysuccinimide (NHS) group and primary amines from OCS (Malhotra *et al.*, 2013). At the other end of PEG, conjugation between CTX and NPs surface was possible using the maleimide chemistry (link between maleimide and cysteine-modified CTX). Briefly, 1 mL of NPs was added to a previously prepared Maleimide-PEG-NHS solution (48µg into 100µL of N,N-Dimethylformamide - DMF). The mixture was left under circular rotation at 4ºC for 4 hours. Separately, 500 µL of CTX was added to 10 µL N-succinimidyl S-acetylthioacetate (SATA) solution (5 mg into 250 µL purified water) which was left under circular rotation at 4ºC for 2 hours. After this time, 20 µL of prepared deprotection buffer was added; pH was adjusted to 8.0 and left under circular motion at 4ºC for 2 hours

according to the manufacturer's instructions. Finally, NPs conjugated with Mal-PEG-NHS was added to activate CTX and left under circular motion at 4ºC overnight.

For quantification purposes, a known amount of NPs was placed into an Amicon® MWCO 100kDa filter and centrifuged for 10 minutes at 9000 rpm using a Heraeus Multifuge 3L-R Centrifuge (Thermo Electron Corporation, Germany). The free CTX was collected from the bottom part and quantified to calculate conjugation efficiency (%) by the indirect method, applying previous developed and validated methodology.

4.6. *IN VITRO* BIOLOGICAL PERFORMANCE

4.6.1. Evaluation of NP biocompatibility and therapeutic efficacy

To evaluate therapeutic efficacy, cells were plated into 96-well plates at densities of $2x10^3$ and $3x10^3$ for U251 and SW1088, respectively, using DMEM 10% and left to adhere overnight. Thereafter, different treatments were applied using DMEM 0.5% FBS as the negative control in order to compare functionalized NPs (containing 4mM of CHC and 8.3 µg of CTX) to CHC-loaded NPs, and the respective concentrations as free drug. Cell viability was assessed 72 hours after treatment by the sulphorhodamine B (SRB) assay. All results were normalized using their respective controls and all necessary dilutions were carried out using DMEM 0.5% of FBS. All *in vitro* experiments were conducted at Life and Health Sciences Research Institute (ICVS), School of Medicine, University of Minho, Braga, Portugal.

4.6.2. Metabolism assay (extracellular glucose and lactate)

Quantification of extracellular glucose and lactate was carried out to evaluate the effect of the NPs on U251 and SW1088 cell metabolism. To do so, cells were plated and allowed to adhere overnight in 48-well plates at a density of 2 to $3x10^4$ cells per well. After 24 hours, cells were incubated with DMEM without glucose for 30 minutes for glucose starvation. Then, different treatments were applied (DMEM as negative control, NPs, CHC-loaded NPs, associated NPs, free CHC, and free CTX). After 24 and 48 hours, lactate and glucose contents were analyzed in the cell culture medium using commercial kits (Spinreact, respectively), as previously described (Miranda-Goncalves *et al.*, 2013; Martinho *et al.*, 2017; Miranda-Goncalves *et al.*, 2017). Total protein, expressed as total biomass, was assessed using the SRB assay for the aforementioned time points. Results are expressed as total µg/ total biomass.

4.6.3. Western blot analysis

Inhibition of EGFR and its intracellular signaling pathway were analyzed by Western blot. Cells were first plated in 6 well plates at a density of $3x10^4$ cells per well and allowed to adhere for 24 hours. After this time, cells received different treatments: DMEM (negative control), conjugated PLGA/OCS NPs and equivalent concentration of free CTX for 3 hours. Cells were also stimulated with 10ng/mL with EGF for 15 minutes before the end time point as previously described (Martinho *et al.*, 2017; Silva-Oliveira *et al.*, 2017). After that, cells were rinsed in cold PBS, scraped and lysed using a lysis buffer containing 50mM Tris pH7.6–8, 150mM, NaCl, 5mM EDTA, 1mM Na_3VO_4, 10mM NaF, 10mM sodium pyrophosphate, 1% NP-40 with protease cocktail inhibitors and then, centrifuged at 13,000 rotations per minute for 15 min at 4ºC. Protein content was measured using the Bradford colorimetric assay (Sigma-Aldrich) and a previously prepared calibration curve. Thereabout, 20µL of total protein were resolved by 10% SDS-PAGE (gel for protein separation) and transferred to nitrocellulose membranes using TransBlot Turbo transfer (Bio-Rad). After that, membranes were blocked with 5% milk in Tris-Buffered Saline/0.1% Tween 20 (TBS-T) for 1 hour at room temperature and incubated overnight with the primary antibodies at 4ºC (**Table 3**). After a wash in TBS-T, membranes were incubated with the respective secondary antibody coupled to horseradish peroxidase (1:2500, Cell signalling). Tubulin was used as loading control. Blot visualization was done by chemiluminescence (Thermo Scientific Pierce ECL Western Blotting) using the ChemiDoc™ XRS+ System (Bio-Rad).

Table 3: Primary antibodies and their respective secondary antibody used for Western blot analysis.

PROTEIN TARGET	DILUTION (SECONDARY ANTIBODIES)	SUPPLIER
P-EGFR (TYR1068)	1:1000 (Mouse)	#4060 cell signaling
EGFR	1:500 (Rabbit)	#4267 cell signaling
P-ERK1/2 (TRH202/TYR204)	1:2000 (Rabbit)	#4370 cell signaling
P-AKT (SER473)	1:2000 (Rabbit)	#4060 cell signaling
ALPHA-TUBULIN	1:5000 (Mouse)	ab6046 Abcam
PARP	1:1000 (Rabbit)	#9546 cell signaling

4.7. Evaluation of NP concentration and size distribution using nanoparticle tracking analysis (NTA)

Analysis was carried out with a NanoSight NS300 (Malvern Instruments, Worcestershire, UK) equipped with a sample chamber and a 532 nm laser. The developed NPs were diluted 400x (5µL / 2000 µL) using purified water. Systems were injected into the sample chamber with sterile

syringes and automatic pump. Software used to capture and analyze data was NTA 2.3. Video was captured by an EMCCD 215S camera, with manual adjustments to improve the image. The average size and DP values obtained correspond to the arithmetic mean of values calculated through the sizes of all particles analyzed by the software. All measurements were performed in triplicate (n=3) and room temperature following previous published work(De Morais Ribeiro *et al.*, 2018).

4.8. BIOLOGICAL PERFORMANCE *IN VIVO*

4.8.1. Analysis of tumor development, progression and antiangiogenic activity using the Chicken Chorioallantoic Membrane (CAM) assay

To evaluate antiangiogenic activity, tumor development and progression, fertilized chicken eggs (n=90), acquired from Pintobar, Portugal, were initially incubated (Laboratory Incubator Series 8000; Termaks) horizontally at 37±1 ºC with 70% humidity. Posteriorly, on the day 3 of development, a small window was made on the top of the egg shells by thoroughly removing shell fragments. The windows were then covered with invisible tape to avoid egg dehydration and, incubated at initial conditions (Martinho *et al.*, 2012; Silva-Correia *et al.*, 2012; Martinho *et al.*, 2013). On day 9 of development, U251 cells ($2x10^6$ cells in 20 µL DMEM medium) were implanted into the CAM using a matrigel support. After 3 days, pictures were taken to evaluate tumor area and perimeter using the Image J Softwere®. Eggs were then separated into different experimental groups for treatments (Ferreira, N. N. *et al.*, 2017). On day 15 of development, pictures were taken *in ovo* for area and perimeter measurements and CAMs with tumors were excised, photographed for blood vessel quantification purposes and transferred to histological cassettes embedded in paraffin. Three independent CAM assays were performed. Experiment was conducted at Life and Health Sciences Research Institute (ICVS), School of Medicine, University of Minho, Braga, Portugal.

4.9. *IN VITRO* RELEASE STUDY

Release studies of free CHC and CTX drug, CHC-loaded NPs and conjugated NPs were performed using Microette (Hanson, Chatsworth, USA) equipment consisting of Franz diffusion cells, a cellulose membrane, D9402-100FT (avg. flat width 76 mm; (3.0 in.), Sigma Aldrich, USA) and receptor solution composed of phosphate buffer pH 6.5 with 0.75 % sodium lauryl sulfate, at 37 ± 0.5 °C under stirring at 300 rpm, according to previous published methodologies with

modifications (Vaz *et al.*, 2017; Rodero *et al.*, 2018). A known amount of drug solution or NPs was transferred to the donor ring arranged in the donor compartment of the Franz diffusion cell. Solubility of the CHC and CTX drug into the receptor solution was tested to assure sink conditions. Afterwards, aliquots were collected from the recipient compartment at predetermined times (0.083, 0.166, 0.25, 0.5, 1, 2, 4, 6, 8 hours). Quantification of CHC and CTX released was performed using high-performance liquid chromatography (HPLC, Agilent, Japan), under the following conditions: 300SB-C18 column with mobile phase composed by water-0.1% (v/v) TFA and acetonitrile-0.1% TFA on gradient mode at a flow rate of 0.6 mL/min monitored by dual UV and fluorescence absorption, using 345 nm for CHC detection and $\lambda_{excitation}$ = 280 nm / $\lambda_{emission}$ = 360 nm for CTX quantification The standard analytical curve was determined using CHC (3 -75µg/mL) and CTX (25 - 250 µg/mL) into phosphate buffer pH 6.5 with 0.75 % sodium lauryl sulfate by the equations $y=54.736x + 48.88$ ($r^2 = 0.99$) and $y= 2.017x + 3.065$ ($r^2 = 0.999$), respectively.

4.9.1. Kinetic mechanisms of drug release

Mathematical models were applied to evaluate the drug release mechanisms. Release was analyzed by fitting (SigmaPlot 10.0 software) to different mathematical models (Korsmeyer - Peppas, Higuchi, First order, Hixson - Crowell, Baker - Lonsdale and Weibull) through the highest adjusted determination coefficient (r^2).

4.10. *EX VIVO* PERMEATION STUDY APPLYING NASAL PORCINE MUCOSA

The *ex vivo* permeation study was performed using porcine nasal mucosa obtained from the local slaughterhouse. The heads were separated from the animal and divided by an incision along the nasal septum. Afterwards, respiratory mucosa was carefully removed from the nasal turbinates and immediately frozen. Before the experiments, the collected mucosa was kept in freshly phosphate buffer pH 6.5 30 min for tissue stabilization (Barbi *et al.*, 2015; Qureshi *et al.*, 2019). Following this procedure, the mucosa was cut to an appropriated size (±1.8 cm^2) and placed between the donor and receiver compartments with the mucosal surface facing the donor compartment of the Franz diffusion cell (Microette Plus, Hanson Research, Chatsworth, EUA). Schematic illustration of the device employed for release and permeation studies can be seen in **Figure 4**. The receptor chamber (7 ml) was filled with phosphate buffer pH 6.5, 37ºC and stirred at 300 rpm. A known amount of drug solution or NPs was transferred to the donor ring. At predetermined times (0.5, 1, 2, 4, 6, 8, 10 and 12 hours) 2 ml of the receptor fluid was collected and

replaced by an equal volume of fresh receptor solution. By the end of 12 hours, membranes were cut into small pieces and put into Falcon tubes with 3 mL of acetonitrile. Ultra-turrax was employed for membrane digestion. Samples were filtered and injected in the HPLC system. The assay was performed with 6 replicates for each sample.

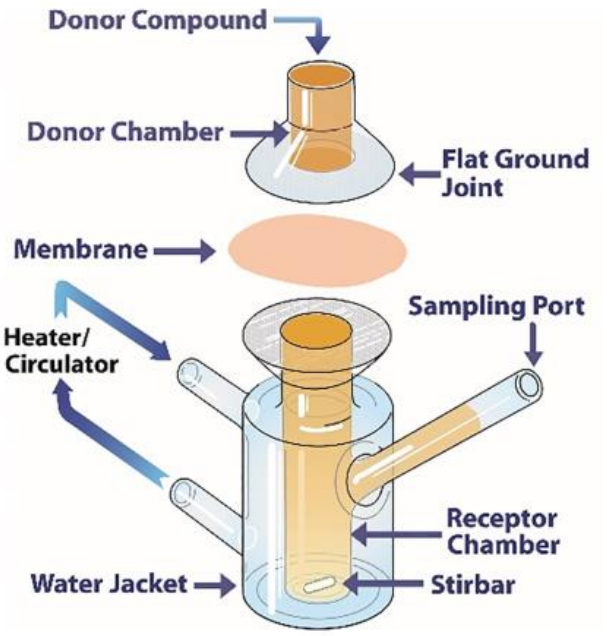

Figure 4: Schematic illustration of Franz cell diffusion device employed for release and permeation studies. Source: Salade et al., 2019 (Salade et al., 2019).

4.11. ANALYSIS OF NOSE TO BRAIN DELIVERY USING FLUORESCENCE TOMOGRAPHY

4.11.1. NP loaded IR-780

CHC-loaded PLGA/OCS NPs and conjugated PLGA/OCS NPs were produced according to the procedure previously described on sections 3.3 and 3.5. Herein, 1 mg of IR-780 was added to the organic phase before sonication. NPs were then washed 3x using Amicon® filter prior to application for *in vivo* studies.

4.11.2. Animals

In vivo experiments were previously approved by the Federal University of Goiás (UFG) Animal Research Ethics Committee (protocol 38/18) which followed the principles for laboratory animal care and the Brazilian legislation (Law 11,794, October 8, 2008). Male Wistar rats (250–

300 g) were obtained from the Central Animal Facility at UFG. Animals were acclimatized for a week prior to the beginning of experiments and kept under 12:12 h light-dark cycles at 25°C ± 1°C with food and water ad libitum. Experiment was conducted at the Federal University of Goiás (UFG), Brasil.

4.11.3. Nasal administration

Animals were anesthetized (i.p.) with ketamine (100 mg/kg) and xylazine (10 mg/kg) and placed in a supine position before administration. Aliquots of 40 µL of IR780-loaded NPs and IR780-loaded conjugated NPs were administered in each nostril using a micropipette, inserted approximately 0.7 cm into the nasal cavity (De Oliveira Junior *et al.*, 2019). At 0.5, 1 and 3 hours, animals (n = 3) were euthanized by intracardiac perfusion using PBS solution containing 0.2% of heparin sodium. Afterwards, the brain was harvested and fluorescence was observed using a fluorescence tomography system (FMT1500, Perkin Elmer, USA).

5. STATISTICAL ANALYSIS

Statistical analysis was performed using the GraphPad Prism Software vs. 6.0 (GraphPad Software Inc.). Differences between groups were compared using one-way analysis of variance (ANOVA), followed by the Tukey post hoc test. Results are expressed as a mean ± standard deviation from a minimum of three independent experiments (n=3). Differences were considered significant at ** $p < 0.05$, *** $p < 0.01$.

6. RESULTS AND DISCUSSION

6.1. New targets to be explored for GMB treatment

When a new chemical substance is discovery, isolated or even synthetized, most of the time, its potential biological effect is screened by its capacity to act against an enzyme, promoting the stimulation or inhibition of its catalytic activity. An enzyme mediated reaction is linked to a series of biochemical processes as cell growth, cell division and viability, or even the interruption of metabolic pathways by blocking the synthesis of essential metabolites (Sandler, 1980).

Extensively used in the pharmaceutical world to measure the effectiveness in inhibiting biological or biochemical functions, a primary chosen assay concerns the concept of the half maximal inhibitory concentration (IC_{50}), a value which indicates the necessary concentration of chemical substance (inhibitor) required to restrict a given function by half, applied to *in vitro* or *in*

vivo assays. Particularly, high IC_{50} values announce inhibitors that interact less effectively with an enzyme and lower IC_{50} values disclose potential inhibitors (Cheng; Prusoff, 1973; Caldwell *et al.*, 2012).

Although the concept of IC_{50} appears to be simple when applied to the pharmacology field, there are some complexities and ambiguities in its application that must be fully understood for predicting the potency of a set of inhibitors (Beam; Motsinger-Reif, 2014). For instance, it is important to highlight that IC_{50} is a relative value whose magnitude clearly depends upon many experimental factors. In addition, the resultant value is related to the enzymatic mechanism of action and mathematical model used to extract this information (Caldwell *et al.*, 2012). Some scientists directly associated the IC_{50} with the drug potency. Nevertheless, this association may be controversial since the therapeutic benefit may not increase substantially as the maximum tolerated dose is approached (Dahlmann, 2013).

Cell viability could be measured by using any of several methods *in vitro*. Although a series of spectrophotometric methods are suitable to analyze large numbers of cells, few of them possess the sensitivity required by the semi-micro dimensions of 96 well plates (Skehan *et al.*, 1990). Ideally, a colorimetric assay for living cells should utilize a colorless substrate which becames modified by living cells but not by dead cells (Mosmann, 1983). For this purpose, some reagents such as 3-(4,5-dimethylthiazol-2-yl)-2,5-diphenyl tetrazolium bromide, known as MTT and sodium;4-[3-(diethylamino)-6-diethylazaniumylidenexanthen-9-yl]benzene-1,3 disulfonate, known as Sulforhodamine B are frequently employed.

The Sulforhodamine B assay (SRB) was firstly described in 1990 and nowadays constitutes the mostly often used assay employed worldwide for *in vitro* cytotoxicity screening (Skehan *et al.*, 1990; Orellana e Kasinski, 2016). The compound is able to bind cell protein components after fixation to tissue culture plates using trichloroacetic acid (TCA) in a stoichiometric way; that is, the amount of dye extracted from stained cells is directly related to cell biomass and can be then extrapolated to measure cell proliferation/viability (Orellana; Kasinski, 2016).

The SRB method appears to show important advantages over the MTT assay for large scale screening(Skehan *et al.*, 1990). However, the MTT assay is able to detect cellular metabolic activity while SRB does not distinguish viable and dead cells. Nevertheless, this fact does not compromise the SRB ability to detect cytotoxic effects of drugs (Orellana; Kasinski, 2016).

6.1.1. Effect of CHC and CTX on glioma cell viability

Cell viability analysis was used to evaluate the effectiveness of CHC and CTX cytotoxic concentrations on U251 and SW1088 glioma cell lines; the first cell line was previously described as the most sensitive to CHC treatment, and the second as the least sensitive to the same treatment (Miranda-Goncalves *et al.*, 2013). Our results show that in the range of 2.5-15 mM of CHC, total biomass decreased as dosages increased for both glioma cell lines (**Figure 5A)**. Furthermore, when analyzing cell viability while increasing concentrations of CHC (mM), results clearly demonstrate that viability reduction was more significant between 1 and 3mM of CHC in U251 cells and between 1 and 9mM for SW1088 cells. Nonetheless, it is likely that increasing CHC concentration above the highest dosage applied in this study would result in further cell viability decrease.

CHC IC_{50} results obtained in the present study are in agreement with previous publications in which U251 cells presented greater sensitivity to CHC treatment (Miranda-Goncalves *et al.*, 2013). When comparing these two cell lines, results showed that the IC_{50} of SW1088 for CHC was almost twice the value of U251 IC_{50}.

Regarding CTX treatment (**Figure 5B**), cell viability analysis, used to investigate cytotoxic concentrations, showed the highest effective total biomass decreases at concentrations of 250 and 500 µg/mL for U251 and SW1088, respectively. IC_{50} was expressed as µg/mL, following previous published studies, for comparative purposes (Park *et al.*, 2015; Silva-Oliveira *et al.*, 2017). Differing from the results observed for the CHC regimen, treatments with increased doses of CTX did not appear to reduce cell viability in a dose-dependent manner. In fact, biomass decrease seemed to reach a plateau, where increased dosages did not result in reduction. However, biomass reduction did reach 50% and IC_{50} was calculated.

The calculated IC_{50} for CTX was approximately 500 µg/mL for U251 and 640 µg/mL for SW1088, values that correspond to 3.43 and 4.36 µM, respectively. Once again, the lowest IC_{50} for CTX was observed for U251 cells, while a less significant CTX effect was noticed for SW1088.

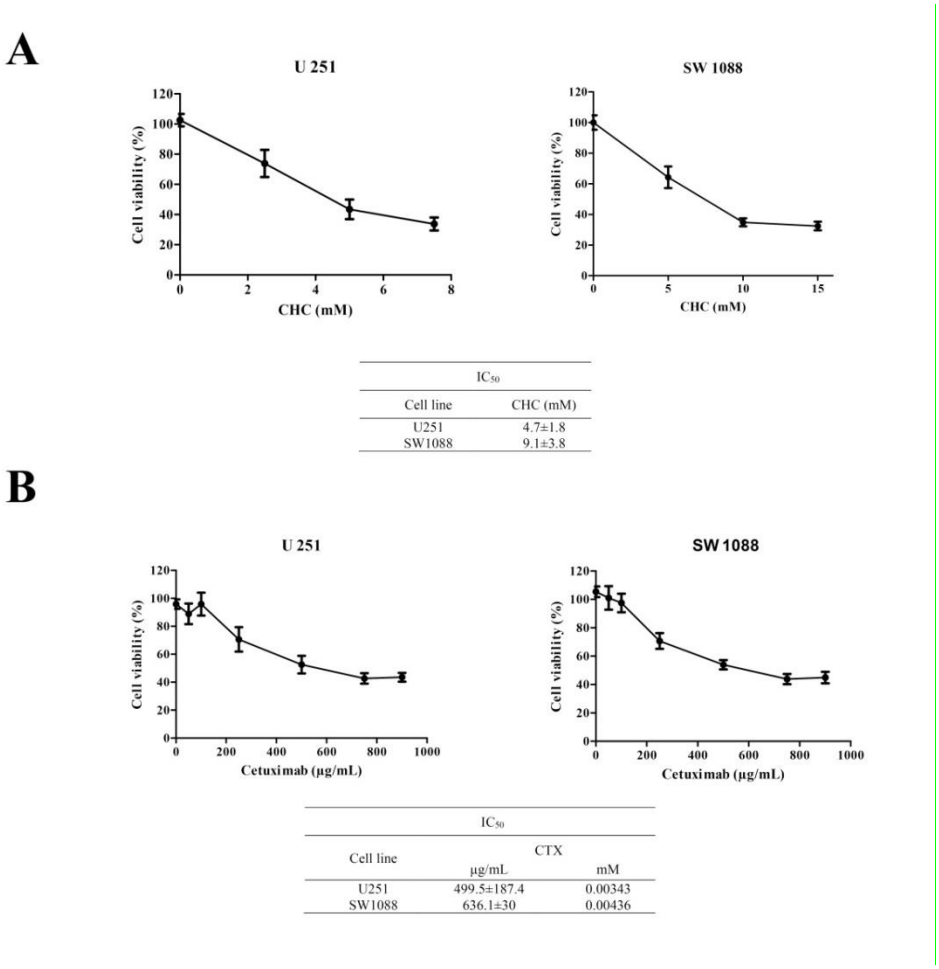

IC_{50}	
Cell line	CHC (mM)
U251	4.7±1.8
SW1088	9.1±3.8

IC_{50}		
Cell line	CTX	
	µg/mL	mM
U251	499.5±187.4	0.00343
SW1088	636.1±30	0.00436

Figure 5: **A**) Cell viability and calculated IC50 of U251 and SW1088 glioma cells in response to 72-hour treatments using different concentrations of CHC. **B**) and different concentrations of CTX. Values were calculated from 3 independent experiments (n=3) by nonlinear regression using GraphPad Prism Software.

U251 and SW1088 sensitivity levels seem to follow a different pattern for each applied treatment. For instance, Martinho and co-workers, when calculating the IC_{50} for Imatinib, Sunitinib, and Cediranib against U251 and SW1088, found that SW1088 exhibited the highest sensitivity to Imatinib. Regardless of sensitivity, the main advantage of treatment with CTX, an antibody against wild type-EGFR, is that cytotoxic effects are expected for all GBM cell lines, which amplifies EGFR, even when the EGFRvIII mutation occurs (Combs *et al.*, 2007). Therefore, the use of such treatment seems to be very promising. After establishing the individual therapeutic potential of CHC and CTX on different glioma cell lines, we investigated their combined effect by measuring total biomass using the SRB assay.

We observed that for both cell lines the treatment that combined the calculated IC_{50} for CHC and for CTX resulted in lower cell viability than the treatments with isolated drugs (± 50%) (**Figure 6***)*. In addition to the fact that the combination was effective in both cell lines, the greatest promise

of this treatment is based on the fact that, although cell line SW1088 was the least-sensitive to both CHC and CTX drugs, herein, the combination of the two appeared to be more effective.

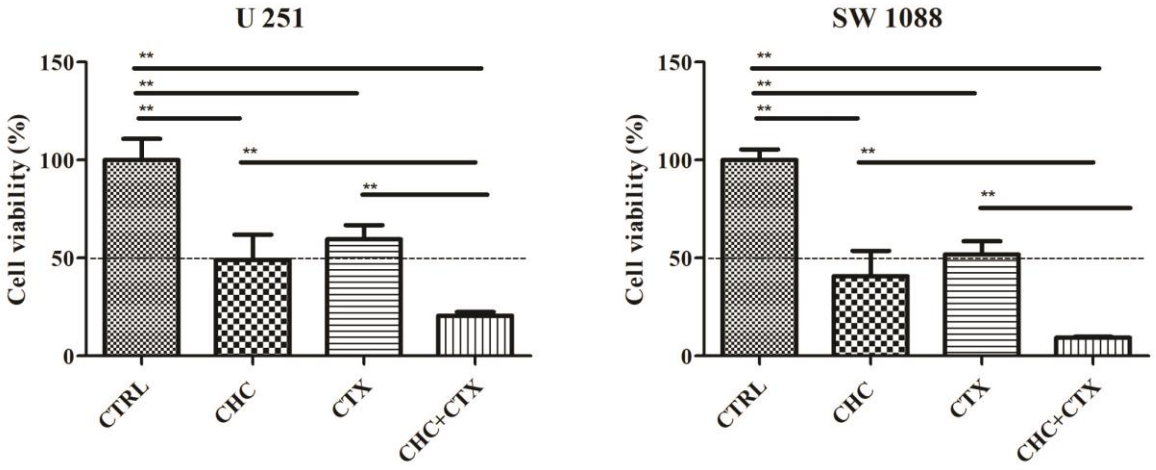

Figure 6: Combined effect of using both CHC and CTX against glioma cell lines U251 and SW1088. Results are expressed as mean –SD; n=6. CHC group received the amount of IC_{50} previously calculated; CTX group received the the amount of IC_{50} previously calculated and CHC+CTX received both dosages applied simultaneously as a single solution. One-way analysis of variance followed by Tukey's multiple comparison test were used for statistical analysis ($p<0.05$). Differences $p<0.05$ were considered statistically significant (**).

To the best of our knowledge, there are no published GBM-treatment investigations that aim to inhibit EGFR by using CTX in association with a MCT inhibitor, such as CHC. Thus, the obtained results may represent a promising alternative to be further explored.

Nevertheless, it is very important to address that GBM treatment displays peculiar challenges which need to be carefully evaluated and studied to ensure positive results. We cannot forget that, apart from the heterogeneity of GBM, the blood brain barrier and mucosal surfaces are also major hurdles for drug permeability that should not be neglected. This fact might explain why a series of new treatments are suggested daily, but few of them show promising results in clinical trials.

To overcome these obstacles, advances in material engineering and pharmaceutical technology may offer valuable tools to explore new routes for drug administration as intranasal route. When a chemical substance is included into a new carrier material, such as polymeric nanoparticles, it acquires new properties, oftentimes, distinct from the isolated drug. That said, the approach studied here can improve drug stability, solubility, absorption, and even therapeutic efficacy, due to the novel characteristics provided by the carrier platform. Given the complexity of GBM, new therapeutic protocols must be associated or improved through new insights in pharmaceutical technology to provide strongly relevant and favorable therapies.

Evidence that nanotechnology can enhance the direct transport to CNS is noticeable and crucial, since it not only allows drug protection, but most importantly, it improves the uptake by the olfactory mucosa (Gao *et al.*, 2007; Migliore *et al.*, 2010; Xia *et al.*, 2011; Mittal *et al.*, 2014; Samaridou; Alonso, 2018).

Thus, the rational design of delivery systems developed in this work was based on PLGA and chitosan (TMC and OCS) NPs that could provide an efficient CHC encapsulation and also further CTX conjugation creating a unique delivery system as a new therapeutic strategy for the GBM treatment. For that, PLGA nanoparticles containing TMC or OCS were developed using the nanoprecipitation and solvent evaporation techniques, respectively.

6.2. NP development

6.2.1. CHC-loaded PLGA-trimethyl chitosan (PLGA/TMC) NPs using nanoprecipitation technique

The main challenges in the development of new polymeric systems for drug delivery applications is the control of all critical attributes involved in obtaining these systems. Modification of some parameters cause crucial changes in characteristics such as size, drug entrapment, zeta potential, and so on (Martínez Rivas *et al.*, 2017). Thus, preliminary tests were employed to evaluate the PLGA ratio of lactide versus glycolide, CHC concentration, temperature, and stirring speed used for the production of NPs. After this screening, NPs were produced using PLGA 85:15, 60 ºC, stirring speed of 1000rpm, and CHC concentration of 2 $mg.mL^{-1}$; an experimental condition that generates stable particles (350±135 nm) with lower PDI (0.40±0.05), zeta potential values between +30 and +50mV (45±5mV), and high CHC entrapment (87±6.5)%.

6.2.2. CHC-loaded PLGA-oligomeric chitosan NPs (PLGA/OCS) by one-step oil in water emulsion, solvent evaporation technique

The encapsulation of water insoluble drugs or even polar substances into PLGA nanoparticles using the emulsion solvent evaporation technique is quite challenging (Alshamsan, 2014). The formation of stable “nano-drops” especially for hydrophobic drugs, is facilitated by the presence of stabilizers such as poly(vinyl alcohol) (PVA), poloxamer 127, poloxamer 188 and polysorbate 80 among others. However, importantly, size and shape of the NP are influenced by their nature and concentration. Indeed, size and surface charge of nanoparticulate systems is achieved when experimental variables of the preparation method employed are correctly optimized (G Nava-

Arzaluz *et al.*, 2012). Therefore, this study examined and deeper explores different variations and their respective effects on PLGA/OCS NPs development using DOE.

DLS is widely employed for size determination in solution. In this technique, a colloidal suspension is illuminated by a monochromatic laser light that is scattered into a photon detector. As a result of the Brownian motion, detected scattered light is related to the particle size assuming that all detected particles are spherical in nature (Crucho; Barros, 2017).

DLS measurements depicted PLGA/OCS NPs ranging from 213 to 870.5 nm. The organic (O): aqueous (AQ) ratio variable (v1) was the factor that exhibited the greatest influence on particle size response, representing about 75% of contribution (**Figure 7A**). In addition, this variable promoted an increase in particle size and must therefore be exploited at low levels to produce smaller particles. For particle size, none of the other analyzed variables contributed significantly to size modifications. As we can notice, smaller nanoparticles were acquired using higher concentrations of stabilizer (run order 3).

Particle size represents a key factor for nanostructured platform performance or ability to overcome mucus barriers or well-organized epithelia. However, there is no consensus about the appropriate size. Until now, whether and to what extent nanoparticles can be delivered through the nose-to-brain route is still awaiting validation by with evidence. A scientific investigation using labeled nanoparticles with different fluorescent probes has shown the translocation profile of different nanoparticle sizes along the passage from nose-to-brain. As a conclusion, results have shown that particle size, rather than surface coating using chitosan, plays an important role for transport efficiency. Indeed, ideal medium-size ranges at about 100nm. Nonetheless, larger particles can also be transported along the nose-to-brain passage but in slower pace, which apparently can be related to the faster mucociliar clearance (Ahmad *et al.*, 2017).

PDI displayed a similar behavior (**Figure 7B**) since this index is directly connected to size. The calculated t value of 0.076 (represented by dotted line) demonstrated that variable v1 (organic (O): aqueous (AQ) ratio) exhibited greater significance against the PDI value (70%). Thus, reduced values of PDI might be acquired when organic (O): aqueous (AQ) ratio of 2:1 was employed.

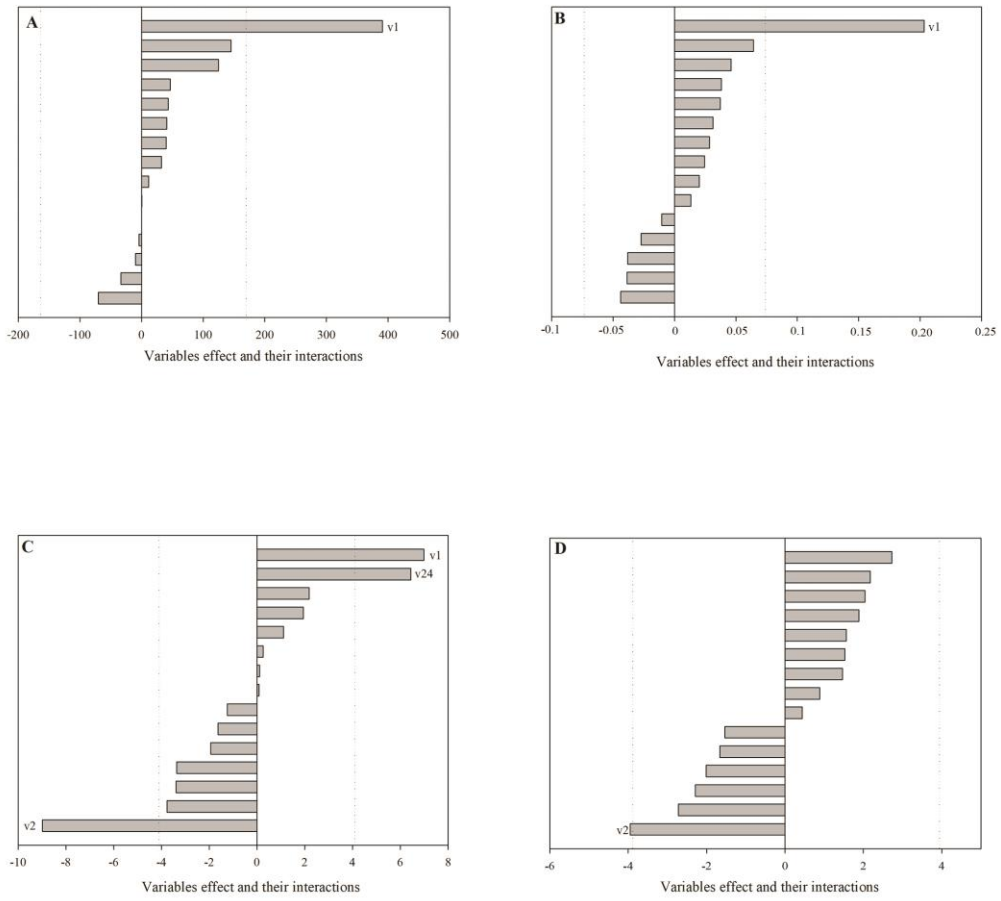

Figure 7: Analysis of different variables and their interactions on the **A**) particle size ; **B**) PDI; **C**) Zeta potential **D**) Entrapment efficiency. Dotted line represents critical t value. Non-significant variables were omitted for clarity.

The acquisition of reduced PDI value was guaranteed by the run order 13. For this system, organic (O): aqueous (AQ) ratio of 2:1, 1.3% of Pluronic 127, 2 cycles of sonication time and PLGA concentration of 5mg.mL^{-1} were used. This condition also provided a suitable size (284.2 nm). Values of PDI close to 0.4 were also acquired by the run order 1, 3, 9, 13, 15.

In addition to predict the stability of polymeric nanoparticles, ZP determinations also provide *in vivo* fate such as likely interactions with cell membranes (Crucho; Barros, 2017). Especially for the intended nasal administration, positive ZP values are interesting since they can guarantee a stronger interaction of the formulation with the nasal mucosa, improving residence time and, as a consequence, therapeutic efficacy (Barbi *et al.*, 2015).

Developed systems exhibited ZP values ranging from +33.2 to +58.9 mV (**Table 1**). **Figure 7C** shows the main factors that exhibited an influence on recorded ZP values. According to our data, organic (O): aqueous (AQ) ratio and Pluronic 127 concentration were strongly associated to ZP values, representing 22% and 36%. Nevertheless, while organic (O): aqueous (AQ) ratio contributes to the increase in ZP; Pluronic 127 concentration promotes its reduction. Moreover, the interaction between Pluronic 127 concentration and PLGA concentration also promotes a significant increase in ZP (18.35%). Taken together, although these different factors are able to modify ZP values, all acquired results of positive ZP may be interesting for the desired application.

The emulsion and solvent evaporation technique presents several advantages such as high batch-to-batch reproducibility, ease of scale-up, simplicity and narrow size distribution. Furthermore, high encapsulation efficiency is also expected (generally >70%) (Nagavarma *et al.*, 2012). Herein, entrapment efficiency (%) values range from 75.69 to 93.23. The DOE demonstrated a great influence of the variable Pluronic 127 concentration for entrapment efficiency. According to the acquired results, this variable must be explored in a high level to improve EE%.

The simultaneous optimization of PLGA/OCS NPs development depends upon a set of different variables where multiple responses on target might be achieved simultaneously, minimizing the variance. A common approach, proposed by Derringer and Suich (Derringer; Suich, 1980) for the analysis off all acquired data, together, consists on the use of desirability function in order to obtain optimal input settings, globally (Vojnovic *et al.*, 1993). Thus, we were able to calculate a global result considering the acquisition of smaller particle size with low PDI, zeta potential values between +30 to +50mV and high drug entrapment. Suitable mathematical models for response outputs were applied using the analysis of variance with significant terms and 95 % of confidence interval (main effects, two factor interactions, and pure quadratic terms).

The analysis of calculated versus desirability demonstrated that the obtained results do not follow a linear model. When a linear model was applied, the analyses of different variables taken in pairs have shown significance only for B_0 coefficient, except for organic (O): aqueous (AQ) ratio versus sonication time. For these, B_0 and B_1 coefficients were significant into the linear model and their surface response graph can be seen in **Figure 8**. According to the acquired results, the acquisition of desired characteristics must be achieved by the use of high levels of these variables. As conclusion, the optimization of PLGA/OQS NPs production must be carried out empirically, taking into account the significance found for organic (O): aqueous (AQ) ratio and sonication time.

Thus, evaluating the obtained results globally, the optimized condition for PLGA/OCS NPs production should follow an organic (O): aqueous (AQ) ratio of 2:1, higher concentration of

Pluronic 127 (3%), 2 cycles of sonication and lower concentration of PLGA (5mg.mL^{-1}). This condition is represented by run order 7 (**Table 1**) where nanoparticles of 258nm, PDI 0.44 and ZP of +37 mV and 88% of EE% were developed.

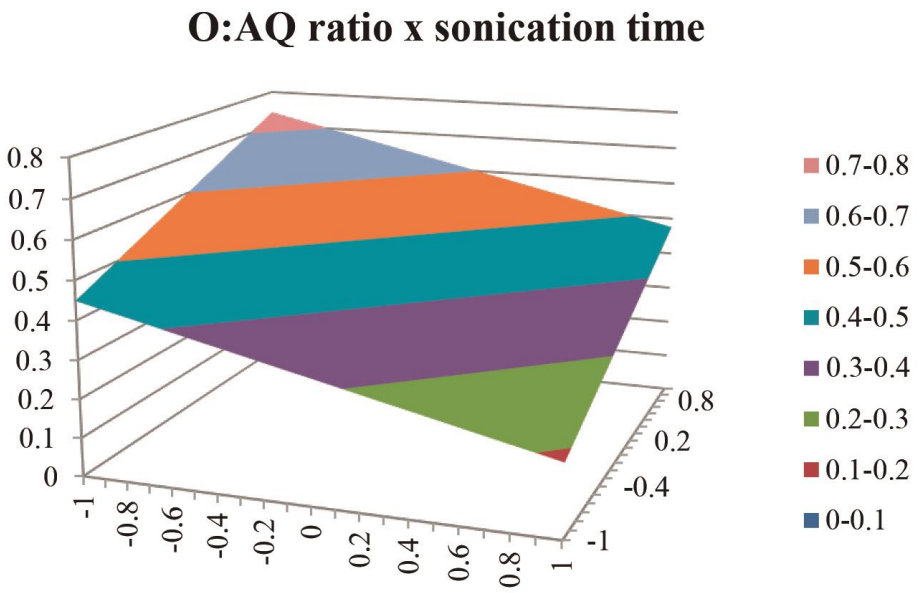

Figure 8: Surface response graph for analyses of organic (O): aqueous (AQ) ratio versus sonication time. B_0 and B_1 coefficients were significant into the linear model $p \geq 0.05$.

Overall, detailed observation and comparison between both applied methodology for NP development highlights that single emulsion technique should ensure the development of NPs with reduced size and lower PDI. Generally, nanostructured systems prepared by emulsion-solvent evaporation are larger than those obtained by nanoprecipitation (Mora-Huertas *et al.*, 2012). Nevertheless, in terms of ZP, similar values were provided by single emulsion and solvent evaporation technique. In turn, ZP values can be associated to the polymer conformation what is also related to the nature of the aqueous phase and dissociation grade of carboxylic groups (Mora-Huertas *et al.*, 2012).

Nanostructures based on biodegradable polymers are widely developed using both nanoprecipitation and solvent evaporation technique. Only few studies have focused on the relationship between process and acquired physicochemical properties of the developed systems (Mora-Huertas *et al.*, 2012). A study conducted by Bilati and co-workers investigated the interchangeability between nanoprecipitation with emulsion-based technique for hydrophilic drug encapsulation. As conclusion, the authors state that nanoprecipitation can sometimes be a good alternative to the classical and widely used double emulsion method, providing small structures

with high amount of encapsulated drug (Bilati *et al.*, 2005). Single emulsion solvent evaporation technique was evaluated against nanoprecipitation for the physical encapsulation of cucurbitacin, a hydrophobic molecule that exerts a degree of polarity. According to their results, although both applied methodology resulted in similar size range, values of loaded drug were significantly different (Alshamsan, 2014).

Summarizing, nanoprecipitation represents a simpler technique, easier to scale. However, the ability of drug entrapment was highlighted to the single emulsion, although not neglected for nanoprecipitation. Importantly, industrial production for single emulsion solvent evaporation might consider the occurrence of titanium residual from the sonication process. Thereby, physicochemical characterization and biological performance should provide evidence about particular features.

6.3. CHC-loaded NP characterization

The use of nanoparticles for pharmaceutical applications has opened a new frontier for diagnosis or even treatment of complex diseases such as cancer. Currently, there are no clearly standardized methodologies or FDA regulatory protocols for specific nanoparticle characterization, however, unquestionably, an extensive study and complete characterization is an important pre-requisite for preclinical development (Crucho; Barros, 2017).

In general, a common chemical substance, when encapsulated into nanoparticles may possess remarkable, often tunable properties, dramatically different from their bulk material (Schubert *et al.*, 2011). Regarding the new acquired features provided by the new developed system, the understanding of the physicochemical aspect changes are of outmost importance to later correlate with acquired biological performance.

6.3.1. NP colloidal stability

The application of nanostructured delivery systems into the clinical practice is encouraging with increasingly growing recognition. However, their physical stability has been a bottleneck for applications and even for scale-up product industrialization. Before or during employment, NPs are normally in nanosuspensions (aqueous solution) which depends on their surfactant content to remain physically stable (Yin *et al.*, 2017). The stability of nanoparticles can be reflected by their morphology, average size, and size distribution. Thus, periodically, over a three-month period, an aliquot of prepared NPs was pulled, diluted using MiliQ water and measured for physical stability properties by DLS (size, PDI and ZP).

Figure 9 contains measurements of size, PDI and ZP of developed PLGA/TMC NPs for stability purposes. According to the results, while empty NPs exhibited a size close to 250 nm throughout the 3-month analysis, the CHC-loaded NPs exhibited a size of 350 nm. In regard to size variability among the different weeks of analysis, size stability of empty NPs was acquired after 2 weeks and was maintained until the end of the 3-month analysis period. On the other hand, when CHC was loaded, the stabilization period was longer, only being acquired around week six of the analysis period. Furthermore, NP size appears to have had the same profile over the three-month period, regardless of CHC loading. For PDI results, significantly higher values were found in the presence of the CHC drug, which was expected once increased size was noticed along the analyzed period.

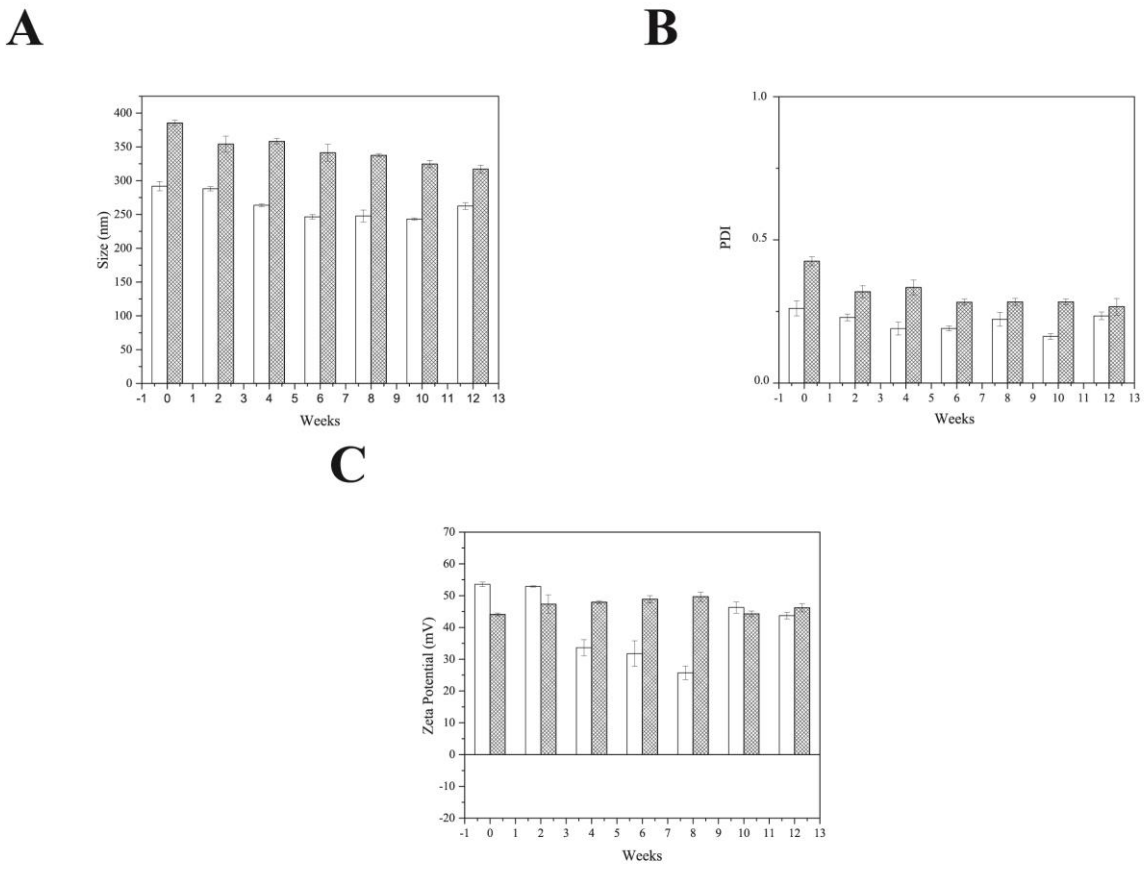

Figure 9: PLGA/TMC NP long-term stability. Periodically, an aliquot of prepared NPs was pulled, diluted using MiliQ water and assessed for physical stability properties by DLS. **A**) Size (nm); **B**) PDI and **C**) Zeta Potential (mV). White columns represent empty NPs and dotted columns represent CHC-loaded NPs.

The variability of ZP was observed from the very beginning of the analysis period (between +30 and +55mV), emphasizing system stability and presence of chitosan TMC on the outermost particle surface. Unlike previous results, empty NPs exhibited reduction in ZP between weeks 4 and

8. However, this reduction did not reach critical levels that could possibly affect stability. On the other hand, CHC-loaded NPs did not show any significant changes.

Its well-known that nanoparticulate systems may have their properties modified over time. CHC-loaded NPs appeared to show more stable values during the evaluated period than empty NPs, leading us to believe that the interaction between the CHC drug and the developed particle could provide additional stability, modifying the kinetic aspects of stabilization (Bhattacharjee, 2016).

Long-term stability analysis for PLGA/OCS NPs demonstrated that particle size was not notably different between empty nanoparticles and CHC-loaded nanoparticles during 2.5 months (around 400 nm) **Figure 10**.

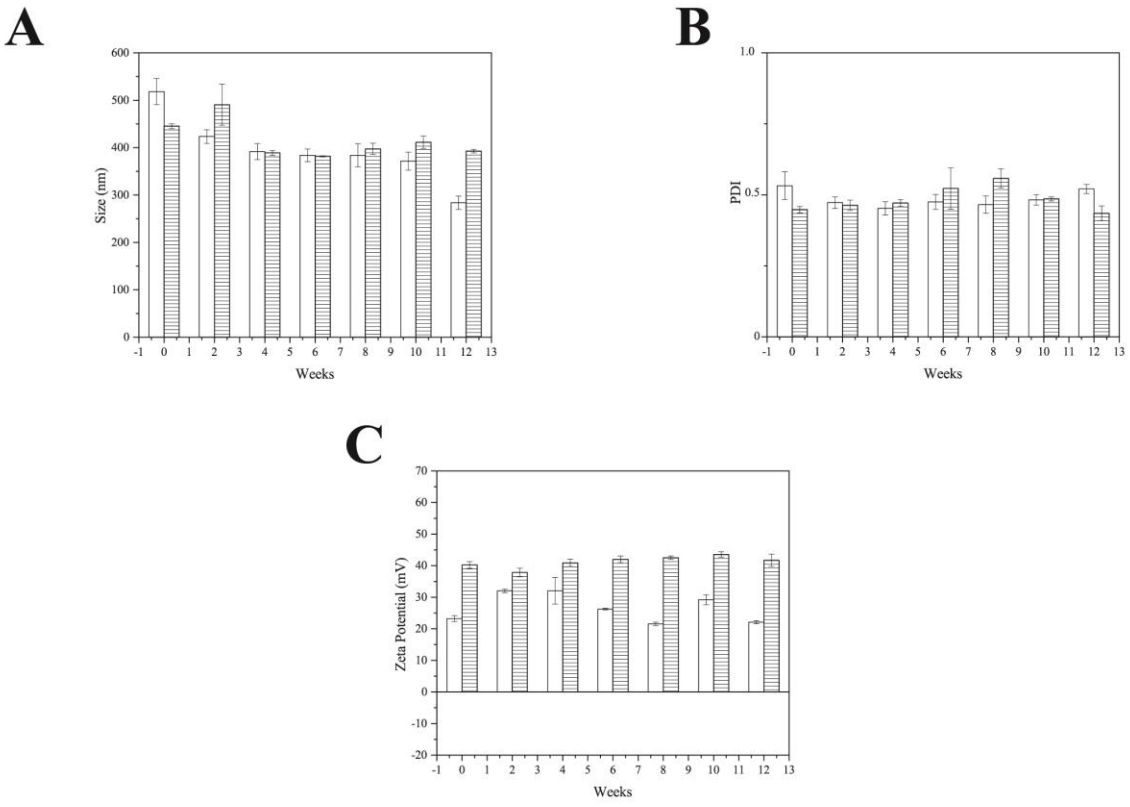

Figure 10: PLGA/OCS NP long-term stability. Periodically, an aliquot of prepared NPs was pulled, diluted using MiliQ water and assessed for physical stability properties by DLS. A) Size (nm); B) PDI and C) Zeta Potential (mV). White columns represent empty NPs and stripped columns represent CHC-loaded NPs.

However, by the end of 3 months, size appears to be changeable for empty NPs. Once again, CHC-loaded NPs appeared to show more stable values during the evaluated period than empty NPs. PDI analysis reveal values close to 0.4 with no statistical changes by the CHC loading or during the current reporting period.

ZP analysis clearly demonstrates less positive values for empty NPs (between +20 and +35mV) and improved values, when CHC was loaded into the NPs. Regardless of this fact, all acquired values reinforced the chitosan coated on the outmost particle surface. Importantly, here acquired values showed greater stability in terms of ZP variability for CHC-loaded NPs when compared to the empty NPs.

6.3.2. Attenuated total reflectance-Fourier transform infrared (ATR-FTIR) spectroscopy

FTIR analysis was conducted as a preliminary evaluation of the molecular structure of NP constituents and of the possible chemical interactions between NPs and the CHC drug. The CHC drug spectrum showed broad and strong signals of the –OH hydroxyl group, at around 3300 cm^{-1}, and it also exhibited stretching of –COOH carboxylic acid as a strong broad signal ranging between 2500 and 3300 cm^{-1} (**Figure 11A/ Figure 12A**). These signs were also overlapped by an intermediate -CH stretching of alkene (C showing sp2 hybridization). Nitrile –CN exhibited a typically weak sign, stretching at 2200 cm^{-1}. Signals assigned to C-C and C-H bands were observed between 1567–1295 cm^{-1}, corroborating with previously published CHC data (Vilaça *et al.*, 2011). From the PLGA spectrum, a C-O-C stretching peak was observed at around 1088 cm^{-1}. C-H stretching in methyl groups was noticed at around 1460 cm^{-1}, while C=O stretching vibration was noticed at 1750 cm^{-1}. C-H, $-CH_2$, and $-CH_3$ resulted in subtle signals between 2800 and 3000cm^{-1} (Wang *et al.*, 2013).

Methylation of chitosan amino groups to acquire TMC was accomplished by using methyl at an elevated temperature and a strong alkaline environment to bind the acid generated during the reaction (Mourya e Inamdar, 2009). Main bands are considered to characterize TMC. One of them, around 3400cm^{-1}, is assigned to the OH groups stretching vibration (De Britto *et al.*, 2012). This region also encompasses amine N-H stretching; thus, tertiary amines are easily differentiated from primary and secondary amines. Since TMC is synthesized by substituting its amino group, when a high degree of substitution is achieved this signal becomes very subtle or may even disappear, as we can observe from the results presented in this study.

The FTIR spectra of PLGA/TMC empty NPs (**Figure 11**D) showed peaks similar to those of PLGA and TMC. For instance, C=O stretching vibration at 1750 cm^{-1}, which occurred in the PLGA spectrum, also appeared for empty NPs. Regardless of the presence or not of CHC, new significant peaks appeared at 2880 cm^{-1} and 1090 cm^{-1}, which indicates that they are associated to the PLGA-TMC interaction. It is well-known that when NPs are produced, chitosan can reacts with the

activated surface carboxyl groups on the PLGA particle suspension to form an amide bond (Chakravarthi; Robinson, 2011).

CHC-loaded PLGA/TMC NPs presented a spectrum similar to the empty NPs. The typical signal for CHC, around 2200 cm^{-1}, is associated to the vibrational CN and does not appear in CHC-loaded NPs spectrum. Therefore, the drug may have been associated into the polymer chains interacting with the polymer matrix by supramolecular forces.

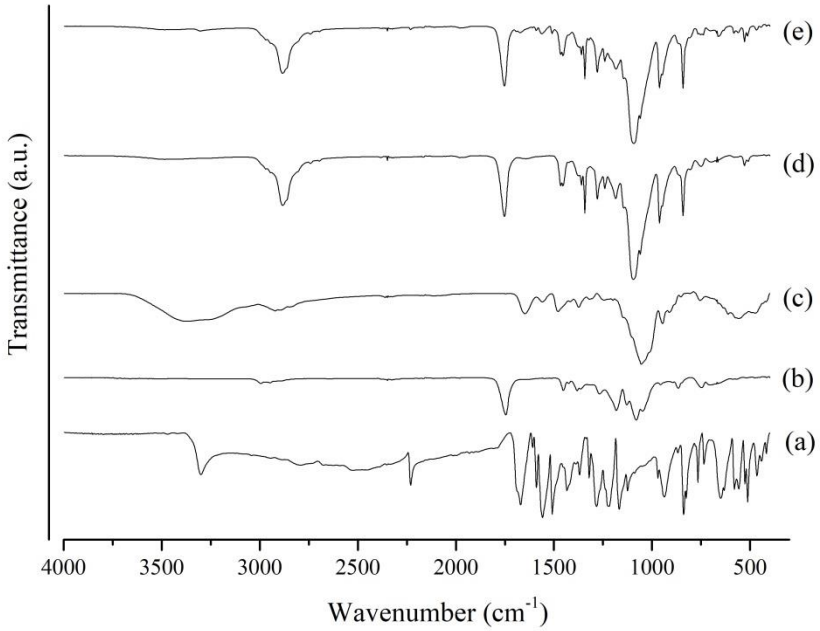

Figure 11: ATR-FTIR spectra of (a) CHC, (b) PLGA, (c) TMC, (d) empty PLGA/TMC NPs, and (e) CHC-loaded PLGA/TMC NPs.

Figure 12 contains the FTIR spectrum of isolated materials and NPs PLGA/OCS for comparative purposes. Chitosan oligosaccharide lactate (**Figure 12C**) exhibited a common band of 3630–3502 cm^{-1} assigned to the N–H stretching vibration overlapped by the O–H stretching vibration. A band at 1240 cm^{-1} is normally assigned to C–O–C vibrations and a peak at 860 cm^{-1} to the aromatic groups in OCS (Linlin; Kyusik, 2018). Once again, PLGA/OCS NPs and CHC-loaded PLGA/OCS NPs spectra were similar to PLGA and OCS spectra. New signs at 2880 cm^{-1} and 1090 cm^{-1} previously observed for PLGA/TMQ NPs formation were also noticeable for PLGA/OCS NPs, reinforcing the idea that they are related to the association between chitosan and PLGA structure.

The vibrational CN sign related to CHC once again disappear for CHC-loaded NPs, an indication that chemical interactions between CHC drug and polymeric network may occur.

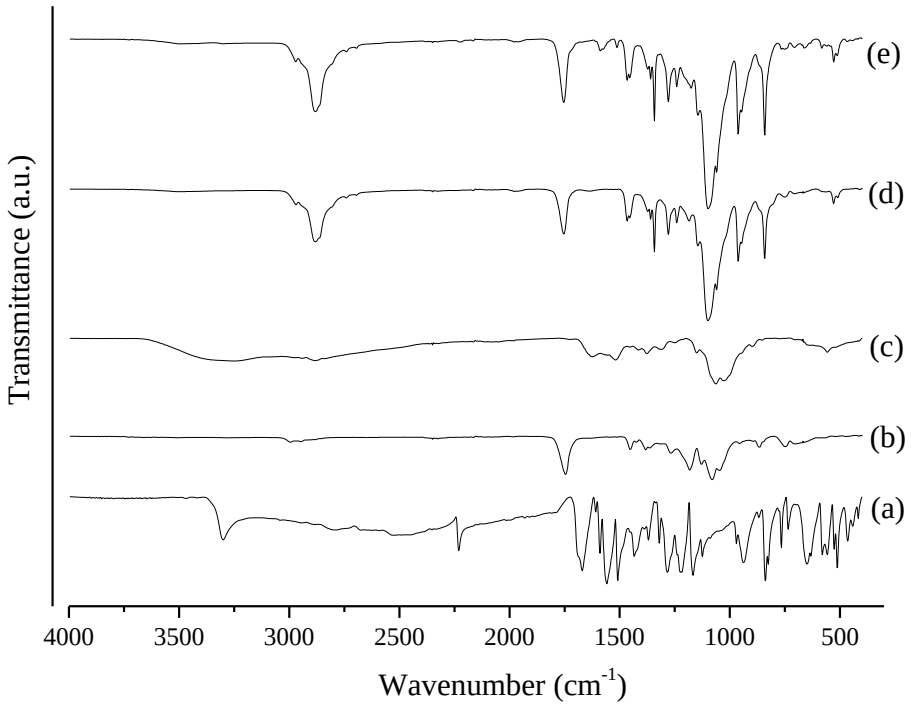

Figure 12: ATR-FTIR spectra of (a) CHC, (b) PLGA, (c) OCS, (d) empty PLGA/OCS NPs, and (e) CHC-loaded PLGA/OCS NPs.

6.3.3. X-ray diffraction (XRD)

In order to comparatively study the crystallinity of CHC, PLGA, TMC, OCS, and developed NPs, XRD analyses were carried out and the patterns observed are presented below. According to **Figure 13**, with the exception of the CHC drug, patterns of all isolated materials showed few peaks and wide halos, indicating typical behavior of amorphous materials. Generally, PLGA is recognized as an amorphous material (Kang *et al.*, 2017). On the other hand, CHC exhibits several intense and well-defined peaks due its crystalline characteristics. Peaks are displayed mainly in low values of 2θ, at about 19.4, 24.6, and 27.95°. However, one peak was noticed at 57.9°. In regard to TMC, a semi-crystalline structure with a very low crystallinity level is expected usually where crystalline regions do not exhibit sufficiently detectable X-ray scattering intensities.

The pattern of empty PLGA/TMC NPs shows two peaks in low values of 2θ, at 19.1 and 23.1°, highlighting the occurrence of structural changes for NP formation, which probably occurred due to the rearrangement of the polymer chains, resulting in the development of structures with higher levels of organization. These results are in agreement with previous discussed FTIR spectra.

For CHC-loaded PLGA/TMC NPs, the XRD pattern clearly shows an intense and well-defined peak at 2θ=27.9°, which indicates the presence of CHC in the polymeric structure.

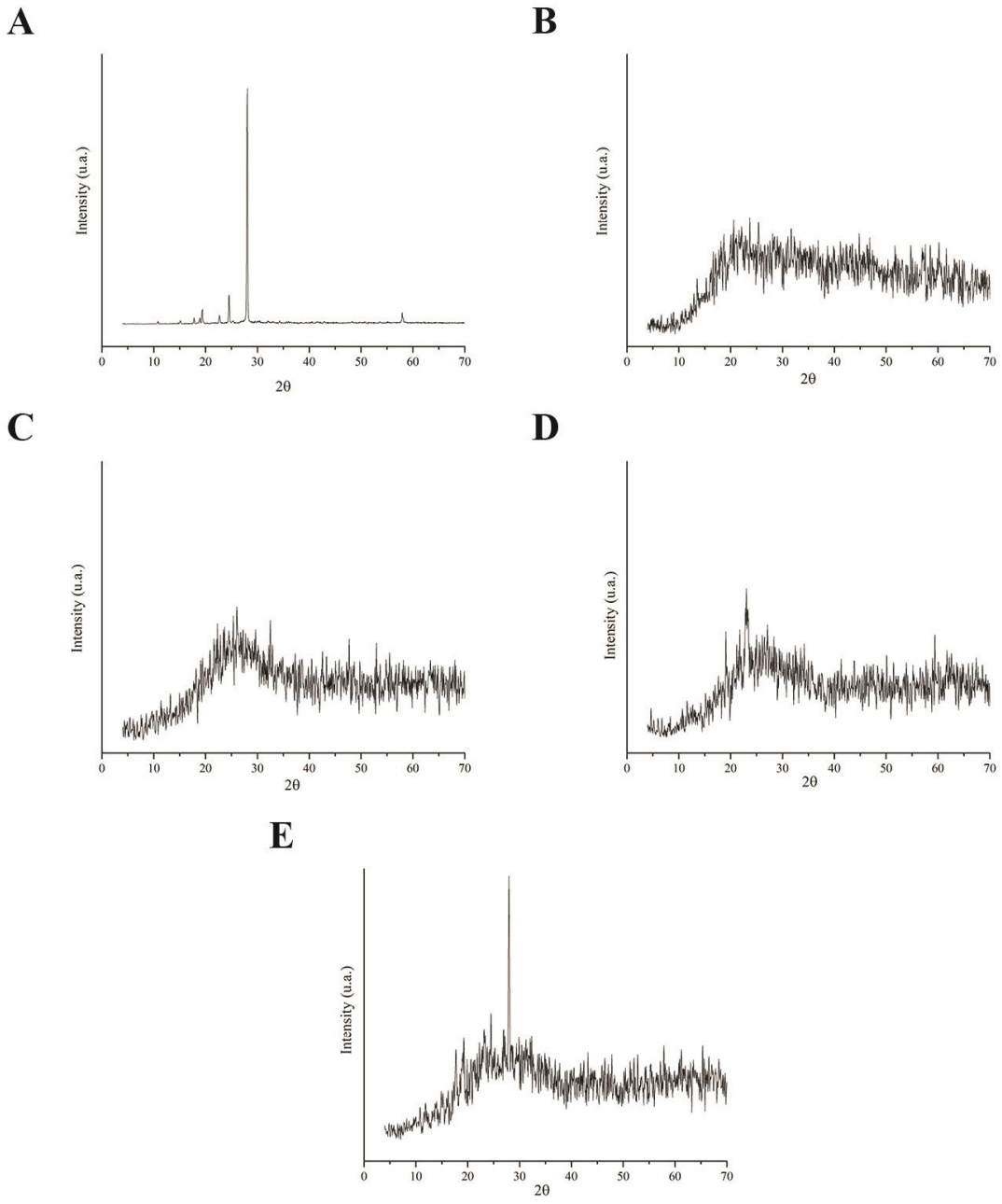

Figure 13: X-ray diffraction patterns of isolated materials. (A) CHC; (B) PLGA; (C) TMC, and (D) empty PLGA/TMC NPs, (E) CHC-loaded PLGA/TMC NPs.

Figure 14 shows PLGA and OCS diffractograms patterns, which exhibited a typical behavior of amorphous materials, where no peak of crystallinity was observed. As we can notice, the formation of empty PLGA/OCS NPs resulted in a diffractogram characteristic of semicrystalline material. This structure showed a wide, amorphous halo and new peaks at 2θ= 18.95 and 23.15°.

This profile indicates that PLGA and OCS association promoted a significant structural rearrangement during NP formation, where a nanostructure with a higher degree of organization was built. Furthermore, the same peaks appeared in greater intensity in CHC-loaded PLGA/OCS NPs, suggesting that CHC may contribute to building more organized structures than empty NPs. Curiously, herein, typical sharp and well-defined peaks of CHC were not noticed. This observation suggests that the interaction between drug and polymer changed the diffraction pattern of CHC. Therefore, it is possible that CHC was molecularly dispersed in the polymer matrix, disrupting crystalline drug patterns.

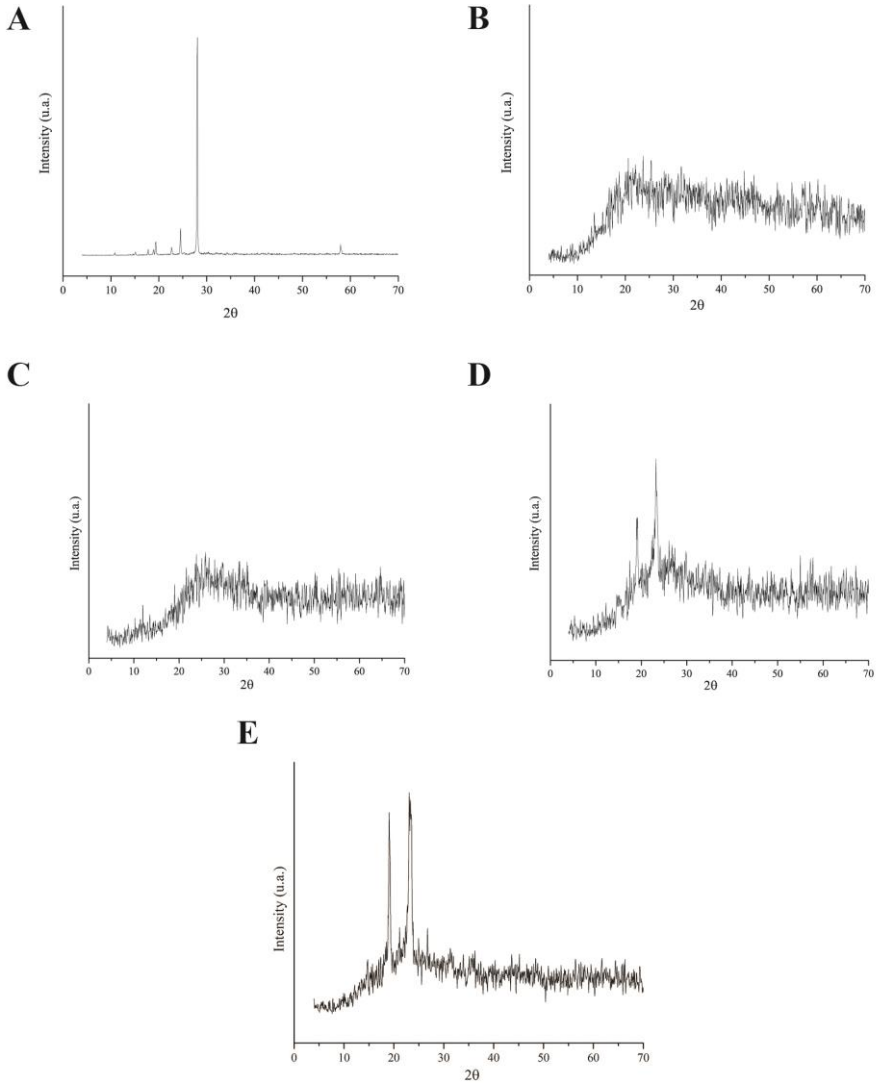

Figure 14: X-ray diffraction patterns of isolated materials. (A) CHC; (B) PLGA; (C) OCS, and (D) empty PLGA/OCS NPs, (E) CHC-loaded PLGA/OCS NPs.

6.3.4. Field emission scanning electron microscopy (FEG-SEM)

Pharmaceutical technology has increasingly innovated the development of nanostructured delivery systems providing new materials together with novel technological processes. Facing this trend, the need for suitable technology able to provide reliable information about the surface morphology with atomic resolution of these systems is unquestionable.

Electron microscopy offers the possibility of deeper visualization on delivery systems engineered in the nanoscale. Scanning electron microscopy, particularly, affords a pronounced focus in combination with a singular method for image acquisition (Klang *et al.*, 2013).

Representative images of empty PLGA/TMC NPs and CHC-loaded PLGA/TMC NPs at different magnifications, shown in Erro! Fonte de referência não encontrada.**,** highlight the formation of spherical and uniformly shaped particles, including a mixed population of sizes. Acquisition of empty NPs through the recorded image was in the range of 150nm. Because of its amphiphilic character, PLGA usually provides formation of core-shell spherical structures due to its micelle-like behavior. Especially for nanoprecipitation technology, nanoparticle assembly is a direct function of block size of employed polymer and phase separation, which can be reasonably predicted *a priori*. Thus, size and morphology of the developed nanoparticles can be controlled by tuning the block lengths (Schubert *et al.*, 2011).

Encapsulation of the CHC drug into the PLGA/TMC NPs (CHC-loaded NPs) resulted in formation of larger particles which, contrarily to the empty NPs, do not exhibit perfect spherical, well-defined shapes (**Figure 15**). These results are in agreement with size and PDI determinations that had been previously recorded using DSL. Interestingly, regardless of CHC presence, size, measured by SEM, was lower than hydrodynamic particle size recorded from DLS. This fact can be explained by the presence of hydrated layers found in NPs evaluated by light scattering, but absent in dry conditions imposed by SEM. Differences in particle-size measured by DLS and SEM were previously reported and attributed to distinctions in measurement conditions for sample preparation (Vu-Quang *et al.*, 2016; Kang *et al.*, 2017).

SEM images of PLGA/OCS NPs are disclosed in **Figure 16**. As we can notice, developed empty NPs or CHC-loaded NPs show a spherical morphology of greater homogeneity when compared to PLGA/TMC NPs. Once again, in fact, the incorporation of CHC into the NPs resulted in increased size.

Taken together, these results reveal that, according to MEV images, particle size and particle surface does not seem to change considerably when NPs were prepared by nanoprecipitation or

single-emulsion solvent evaporation. Notwithstanding, the higher measured PDI for CHC-loaded PLGA/TMC NPs compared with CHC-loaded PLGA/OCS NPs can be clearly reinforced by SEM images. Importantly, PLGA/TMC appears to be more susceptible to NP agglomeration.

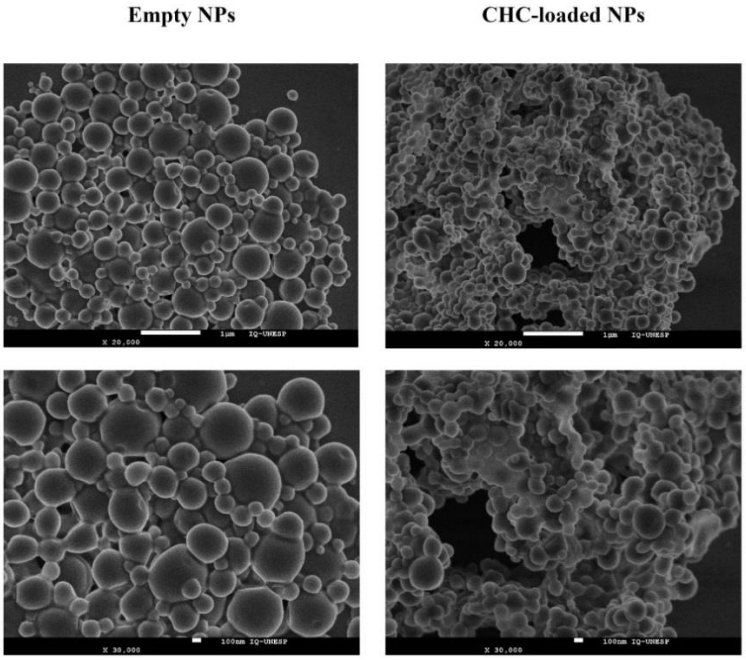

Figure 15: SEM micrographs exhibit surface morphology of both empty and CHC-loaded PLGA/TMC NPs at different magnifications.

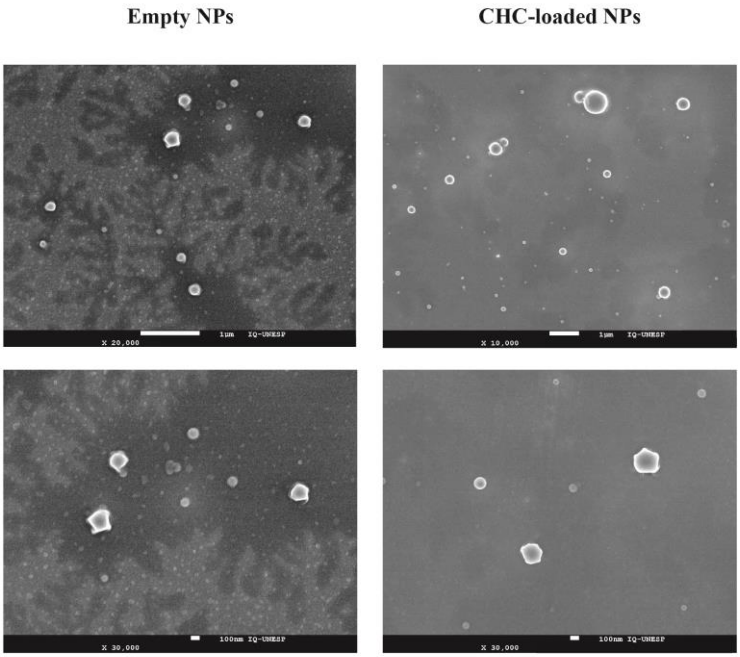

Figure 16: SEM micrographs exhibit surface morphology of both empty and CHC-loaded PLGA/OCS NPs at different magnifications.

6.3.5. Transmission electron microscopy (TEM)

The conventional transmission electron microscope is composed by electron optical instrument analogous to the light microscope where samples are illuminated by an electron beam, condition that requires the operation in vacuum. Thus, images are recorded as a result of interactions between the electrons and evaluated material. The resolution in TEM is rather limited by the properties of the specimens and available instrumentation. Dark regions in a bright field image are regions of higher scattering. Overall, no images of good quality are normally acquired by conventional TEM for polymeric nano-systems (Klang *et al.*, 2012).

Images acquired by this technique are outlined in **Figure 17** and reinforces the spherical shape evidenced in SEM images. Similarities among SEM and TEM should be highlighted such as the acquisition of increased size by the CHC incorporation into the NPs. Indeed, herein, a greater homogeneity of NPs PLGA/OCS compared to NPs PLGA/TMC could also be noticed. On the other hand, unlike the images acquired by SEM, here, the use of solvent emulsion evaporation technique and OCS appears to provide smaller particles.

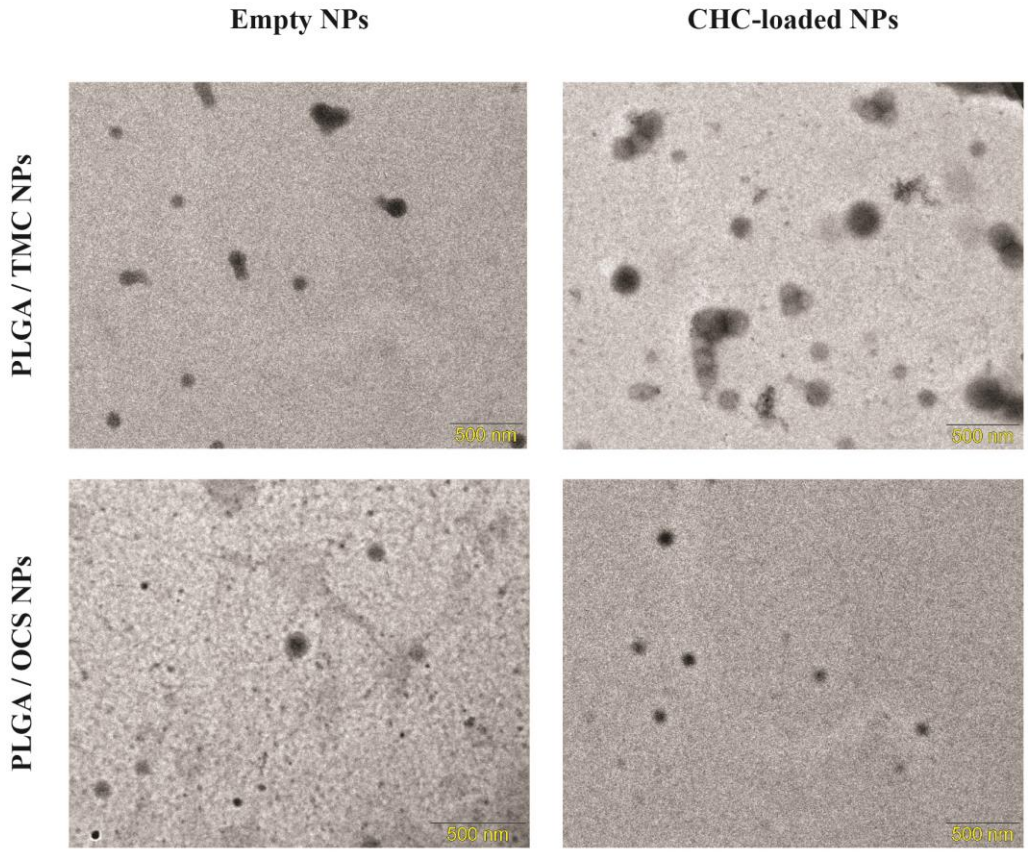

Figure 17: Representative TEM micrographs of developed empty or CHC-loaded NPs.

6.4. NP conjugation with CTX by supramolecular forces and covalent bonds

Over the last few years, substantial efforts have been made to develop delivery systems that contain target molecules attached to their surface. Several studies have focused on antibody conjugates to develop highly specific systems (Manjappa *et al.*, 2011). Since such molecules are naturally polyelectrolytes, supramolecular associations can be considered for the conjugation procedure. Supramolecular interactions are non-covalent forces that, although less energetic than covalent bonds, enables a wide set of advantages to design drug delivery systems and can be responsible for the organization of nanostructured systems at the nanobiointerface (Nel *et al.*, 2009). These interactions are weak by nature and are significantly affected by pH. Therefore, we explore the supramolecular association between CHC-loaded NPs and CTX at pH 4.0 and 6.0.

Results for the different processes applied to CTX conjugation are described in **Table 4**. Supramolecular interactions at pH 4.0 resulted in about 53% of CTX associated to the system. On the other hand, the increase in pH improved these interactions reaching an efficiency of 85% at pH 6.0. The acquired results may be advantageous for the intended application, since tumor microregions and nasal environment tend to show slightly acidic pH values (around 6.0) when compared to most physiological pH (Ferreira *et al.*, 2017). Therefore, we selected this condition of preparation for future studies.

Table 4: Values of efficiency (%) found for conjugation process. They were calculated from 3 independent experiments (n=3) using the average and standard deviation.

System	**Covalent bonds**	**Supramolecular forces**	
	CHC-loaded PLGA/OCS NPs	**CHC-loaded PLGA/TMC NPs**	
		pH 4.0	pH 6.0
Efficiency (%)	58±5%	53±5.2%	85±2.3%

The possibility of covalent bonds applied for PLGA/OCS NPs provided 58% of association. Importantly, considering the applied Amicon® filter to the quantification of free CTX not associated to the NPs, the efficiency found cannot be solely attributed to covalent forces; supramolecular associations may also compose this index.

Importantly, both procedures appear to provide a great conjugation between CTX and NPs. Conjugation of CTX on NPs surface can make available or even hinder their site of interaction with EGFR transmembrane domain. Therefore, we further need to investigate if they could act differently in a biologic environment.

6.5. Biological performance *in vitro*

6.5.1. Evaluation of NP biocompatibility and therapeutic efficacy

Understanding NPs interactions with cells and how those interactions can modulate biological performance is essential to explore NP applications. This assessment can help NP design efficiently and can be used as a starting point to investigate new alternatives for drug administration.

NPs are able to interact with cells and extracellular environments promoting a series of biological effects that depend on physicochemical characteristics, which further determine the efficacy of intended outcomes. Evaluating biocompatibility becomes essential to assure safe use of these intended treatments (Naahidi *et al.*, 2013). As stated by all regulatory agencies, it is important that drug delivery systems, no matter how attractive they seem to be, because of the therapeutic effect they provide, hold no weight unless they are considered adequately biocompatible. Importantly, drug delivery system biocompatibility is considered when cell viability is equal or greater than 80% (Naahidi *et al.*, 2013).

Firstly, we determined cell biocompatibility and cell viability of developed NPs by using increased concentrations (0.5 to 1.5µL of NPs). We have chosen to work with nanoparticles amount since in the future, different drugs and concentrations will be applied. Herein, empty PLGA/TMC NPs as well as CHC-loaded PLGA/TMC NPs were used in an attempt to find a specific dosage where empty NPs would not reduce cell viability and CHC-loaded nanoparticle would result in significant reduction of total biomass (**Figure 18A**). As we can observe, for volumes of up to 5µL of empty PLGA/TMC NPs, there was no significant reduction of cell viability for both U251 and SW1088 cell lines. Notably, 0.5, 1, and 5µL of PLGA/TMC NPs did not promote cell viability reduction for the U251 cell line, suggesting that the reduction observed may be attributed to CHC encapsulation rather than the NPs' components.

For SW1088, the results described above were also noticed. Among all applied concentrations of PLGA/TMC NPs, none was able to promote a significant cell viability decrease, reinforcing system biocompatibility. On the other hand, 5 to 15 µL of CHC-loaded PLGA/TMC NPs resulted in considerable cell viability decrease (50% or more). Importantly, these results reinforce, once again, that SW1088 is less sensitive than U251.

Following the investigation of biological performance, conjugated PLGA/TMC NPs (5µL) were further examined to determine if the therapeutic effect they provide is more or less efficient than CHC-loaded NPs and free drugs, at the same concentration. According to the acquired data (**Figure 18B**), the encapsulation of the CHC compound into developed PLGA/TMC NPs alone

resulted in significant increase of therapeutic activity for both U251 and SW1088 cell lines, higher than that of the free CHC drug at the same concentration. However, the reduction of cell viability was more pronounced for U251 cells. The superiority observed for CHC-loaded NPs can be correlated to the CHC solubility or mechanism of action. According to its hydrophobic nature, obtaining a homogeneous CHC solution can be difficult. Therefore, the developed NP structures, as well as other previously proposed delivery systems, may allow the slow release of CHC, increasing drug bioavailability and so far, increasing potency (Amorim *et al.*, 2012). Another hypothesis consists on the fact that NPs could promote CHC entry into the cell. In this way, CHC probably will compromise the entry of pyruvate into the mitochondria and normal cell respiration at much lower concentrations. A combination of the aforementioned effects is also a possibility that should not be excluded (Halestrap; Denton, 1974).

Comparing both free drugs (CHC and CTX), no significant statistical difference was found for cell viability reduction or for the respective controls. Contrarily, conjugated PLGA/TMC NPs resulted in a considerable decrease of cell viability in both studied cell lines. Interestingly, conjugation with CTX by supramolecular forces seemed to improve therapeutic efficacy for U251, while neither CHC-loaded NPs nor conjugated NPs presented no significant evidence of treatment improvements for SW1088 cells. Once again, the higher sensitivity of U251 to the applied treatments was highlighted.

Concerning the reduction in cellular viability produced by the simultaneous application of free CHC and CTX in the initial studies, two hypotheses can be further investigated. On one hand, encapsulation of CHC may have enhanced its therapeutic activity and, as a result, conjugation with CTX did not provide significant benefits. On the other hand, taking into account that CTX acts in the transmembrane of cell domains, its association with nanoparticles by supramolecular forces did not provide the full site of action availability. In this particular case, an alternative CTX conjugation procedure that ensures a novel antibody assembly into the nanostructure (eg. covalent bonds) may effectively increase therapeutic benefits.

Therefore, biocompatibility and cell viability was analyzed for PLGA/OSC NPs where covalent bond were applied for conjugation with CTX.

Results for cell biocompatibility shown that from the concentration of 1 µL for U251 and 5 µL for SW1088, a reduction on cell viability was noticed (**Figure 19A**). However, only the use of 15 µL of PLGA/OCS NPs in U251 cells should induce cytotoxicity. For CHC-loaded PLGA/OCS NPs, therapeutic activity might be interesting and only related to the CHC substance, when 10 to 15

µL of NPs are used. The use of 5 µL of CHC-loaded NPs does not seem to promote a significant reduction in cell viability, although there is some.

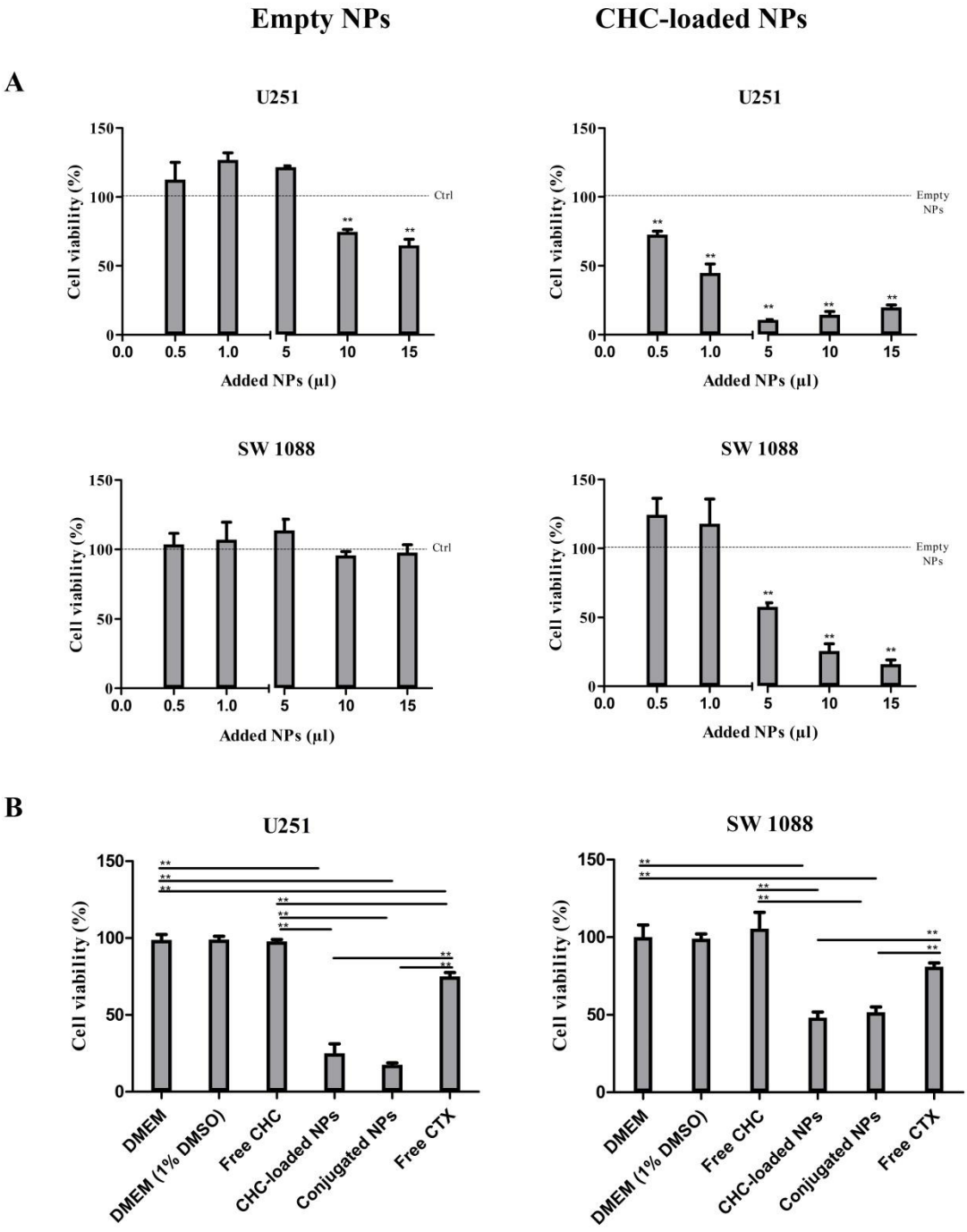

Figure 18: (A) Cell biocompatibility and cell viability results of empty PLGA/TMC NPs and CHC-loaded PLGA/TMC NPs against glioma cell lines U251 and SW1088. (B) Conjugated NPs therapeutic efficacy against glioma cell lines U251 and SW1088 compared to isolated treatments. Results are expressed as mean –SD; n=6. Differences $p<0.05$ between the control and applied treatment were considered statistically significant (**).

Comparing both developed NPs in terms of biocompatibility, in general, when 5µL of PLGA/TMC NPs were added to the U251 and SW1088 cells, no significant reduction in cell

viability was detected. However, the same amount of CHC-loaded NPs, promoted a significant reduction on cell viability. For PLGA/OCS NPs, 5µL of CHC-loaded NPs resulted in about 80% of cell viability for both studied cell lines. Nevertheless, developed systems will be associated with CTX, which should increase its therapeutic capacity. Therefore, the same amount of 5µL of developed NPs was maintained here to future comparisons.

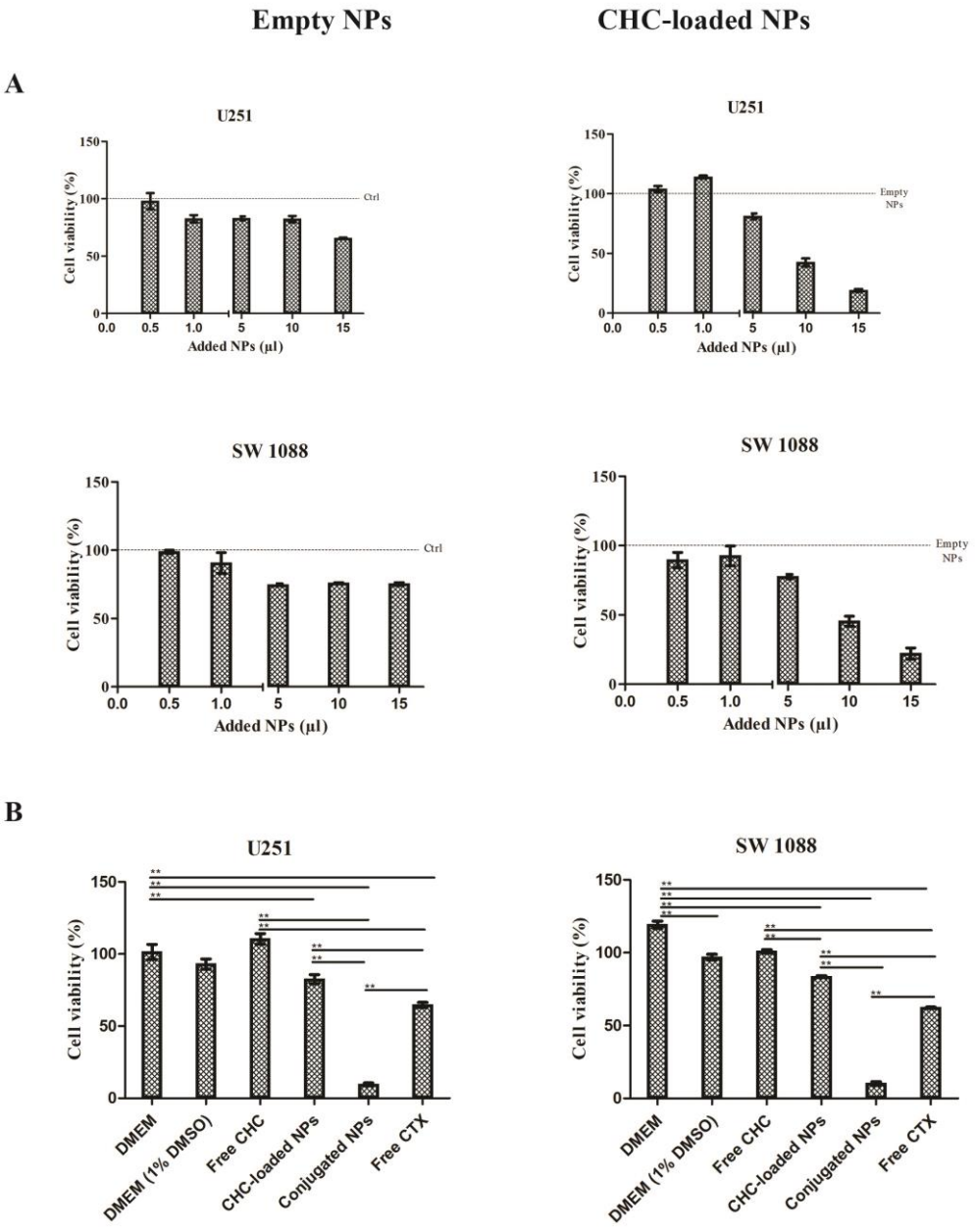

Figure 19: (A) Cell biocompatibility and cell viability results of empty PLGA/OCS NPs and CHC-loaded PLGA/OCS NPs against glioma cell lines U251 and SW1088. (B) Conjugated NPs therapeutic efficacy against glioma cell lines U251 and SW1088 compared to isolated treatments. Results are expressed as mean –SD; n=6. Differences $p<0.05$ between the control and applied treatment were considered statistically significant (**).

Hereafter, therapeutic performance of conjugated PLGA/OCS NPs (**Figure 19B**) had shown that no difference can be attributed for free CHC compared to negative control DMEM (1% DMSO). That is, the amount of encapsulated CHC, as a free applied dosage, does not show therapeutic efficacy against U251 or SW1088.

Comparing both free drugs CHC and CTX, CTX appears to be more effective to induce cell viability reduction and herein, statistical significance can be attributed to this difference. Once again, encapsulation of CHC by itself, reduce cell viability, especially for SW1088 cells.

Importantly, to the PLGA/OCS NPs the use of conjugated systems (acquired through covalent bonds) created a great expectation once cell viability reached almost 5% for both cell lines. Our greatest promise is based on the fact that the developed conjugated NPs appear to have a great therapeutic efficacy exactly for the most resistant cell line SW1088, corroborating the data previously presented for free CHC applied together with CTX.

Observing the acquired results, we must consider that PLGA/OCS NPs were developed with OCS which are proven to show biological activities and potential therapeutic applications especially for cancer treatment (Muanprasat e Chatsudthipong, 2017). Several investigations have demonstrated that OCS can interrupt cancer progression by action in multiple steps such as cell growth, invasion, and metastasis (Park *et al.*, 2011). For instance, Guminska and co-workers have shown that OCS acts on glycolysis and energy production by promoting inhibition of a tumor-specific variant of pyruvate kinase (Gumińska *et al.*, 1996). Although the scientific investigation was conducted in Ehrlich ascites tumor cells, we can hypothesize an association with CHC biologic action. However, if we evaluate cell viability for CHC-loaded PLGA/OCS, the reduction was not significant when compared to CHC-loaded PLGA/TMC.

Therefore based on the hypotheses raised above, probably, CTX organization in the nanostructure provided by covalent bonds, affords greater availability of their action sites improving interaction pattern with the tumor cell. Thus, their biological activity could be evidenced and added to CHC mechanism of action.

Comparing both conjugated NPs, PLGA/OCS NPs seem to have greatly increased therapeutic capacity compared to PLGA/TMC NPs treatments in terms of cell viability. Future studies might investigate their biological activity individually, confirming the therapeutic gain acquired in the proposed innovative association.

6.5.2. Metabolism assay (extracellular glucose and lactate)

One of the striking cancer cells characteristics consists of a marked and uncontrolled proliferation which requires adaptation on cell metabolism linked to energy supply. As a consequence, a common feature well described as "Warburg Effect" reinforces a preference for glucose metabolism where an increased glucose uptake is associated to high rates of glycolysis and production of high amounts of lactic acid independently of the oxygen levels (Gatenby; Gillies, 2004; Hanahan; Weinberg, 2011).

Under these circumstances, high amounts of lactic acid are generated and must be exported to the microenvironment allowing malignant cells survival. Important pH regulators are MCTs, transmembrane proteins belonging to the family of SLC16A plasma membrane transporters (Miranda-Goncalves *et al.*, 2013; Granja, Tavares-Valente, Queirós, *et al.*, 2017). The aromatic compound CHC, proposed as therapeutic strategy in this study, is a classical and broadly described MCT inhibitor which might provide interesting results for glioblastoma treatment (Miranda-Goncalves *et al.*, 2013).

Following the investigation of developed NP therapeutic efficacy, extracellular glucose and lactate levels were analyzed to explore the spectrum of encapsulated CHC activity over cell metabolism. Results expressed for PLGA/TMC NPs are illustrated in **Figure 20**. Regarding U251 cells, at 24 hours, CHC and conjugated PLGA/TMC NPs exhibited higher glucose consumption than their respective negative controls. This behavior can be associated with initial efforts to compensate metabolic pathways (**Figure 20A**). On the other hand, at 24 hours, extracellular lactate was higher for all applied treatments than their respective controls, with the exception of free CHC. Acquired results were expected since as a free drug, CHC acts as a competitive lactate inhibitor outside the cell. However, when encapsulated and also internalized into GBM cells, it may be inhibiting mitochondrial function and stimulating glycolysis (Halestrap; Denton, 1974).

Glucose consumption was higher at 48 hours than at 24 hours for CHC-loaded PLGA/TMC NP and CHC treatments, although this increase is also evident for empty NPs and conjugated NPs. No significant difference was found between 24 and 48 hours for extracellular lactate. Since U251 cells are known to be highly glycolytic, the glucose consumption noticed for CHC-loaded PLGA/TMC NPs and CHC between 24 and 48 hours should be accompanied by higher production of extracellular lactate. As this fact was not observed, the lactate efflux to the extracellular environment was probably effectively hampered by CHC activity, what may be related to drug initially released from NPs.

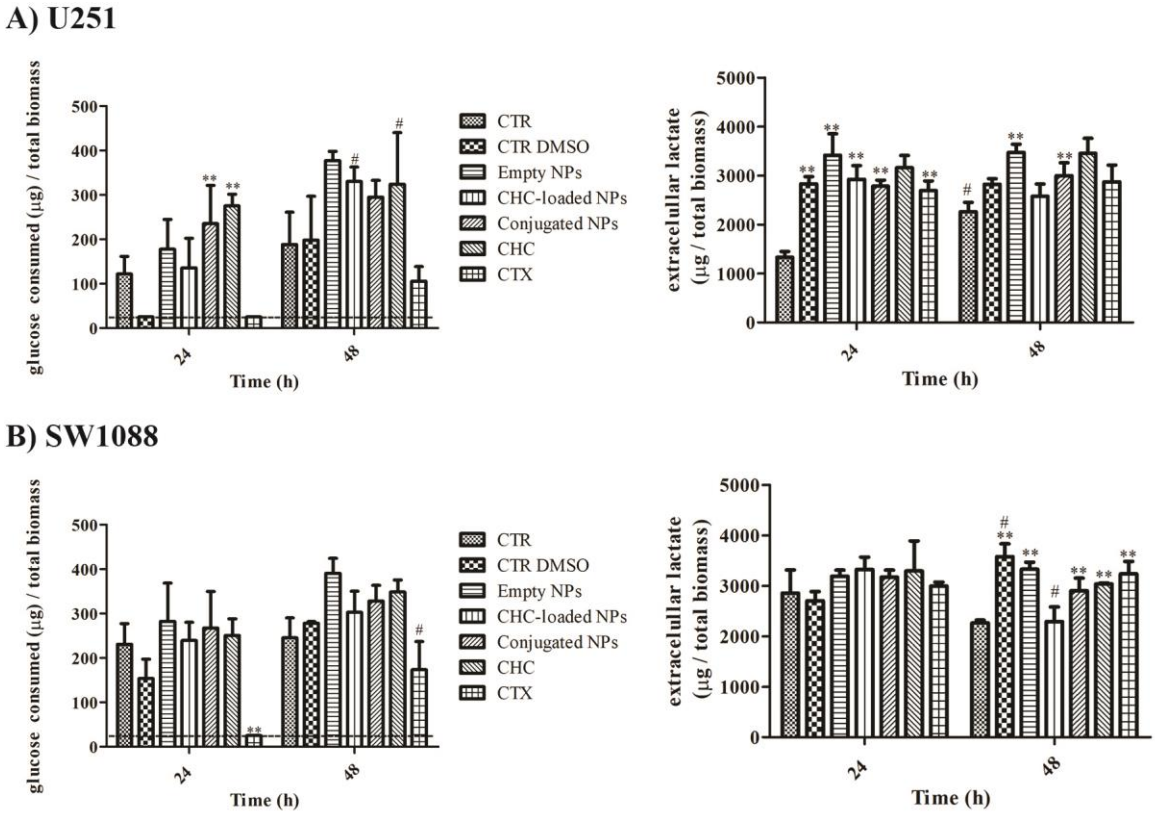

Figure 20: Glucose consumption and extracellular lactate (µg) /total biomass of (A) U251 and (B) SW1088 cells applying different treatments. CTR: negative control (DMEM 10% FBS); CTR DMSO: DMEM 10% FBS + 1% DMSO; NPs: empty PLGA/TMC NPs diluted in DMEM 10% FBS; CHC-loaded NPs: CHC-loaded PLGA/TMC NPs diluted in DMEM 10% FBS; Conjugated NPs: CTX conjugated PLGA/TMC CHC-loaded NPs; CHC: free CHC diluted in DMEM 10% FBS + 1%DMSO; CTX: free CTX diluted in DMEM 10% FBS. Results are representative of the three independent experiments, each one in triplicate; **p<0.05 Treatment *versus* control. # p<0.05 24 and 48 hours. Dotted line represents that glucose concentration was lower than quantification limit.

For the SW1088 cell line (**Figure 20B**), at 24 hours, glucose consumption was notoriously low for CTX treatment, but higher at 48 hours. Concerning extracellular lactate quantification at 24 and 48 hours, while an increase could be noticed for the CTR DMSO, CHC-loaded NPs exhibited reduction of extracellular lactate levels, likely due to CHC action.

Analyzing these results together, the increased glucose consumption between 24 and 48 hours appeared to be more evident for U251 than for SW1088. On the other hand, extracellular lactate for both cell lines remained markedly unchanged between 24 and 48 hours, with the exception of CHC-loaded PLGA/TMC NPs applied to SW1088 cells.

Preceding the metabolism evaluation, conjugated PLGA/OCS NPs and their respective associated treatments were investigated against GBM cell lines (**Figure 21**).

In U251 cells at 24 hours, no differences for glucose consumption were found between applied treatments. In fact, glucose consumption was not properly quantified for many applied

treatments since glucose levels were lower than the quantification limit (**Figure 21A**). Besides, glucose consumption after 48 hours was significative higher than 24 hours for all applied treatment. The increase in glucose consumption for U251 cells is expected by the glycolytic nature of these cells. Regarding extracellular lactate quantification (**Figure 21A**), at 24 hours, levels were significantly higher for NPs, CHC-loaded NPs and conjugated NPs compared with respective negative control. Furthermore, treatment that comprises CHC molecule (CHC-loaded NPs and conjugated NPs) appears to be responsible for the highest levels of extracellular lactate at 24 hours. Concerning PLGA/OCS NPs, the higher lactate levels observed at 24 hours, may be related somehow to the biological action of OCS, what should be further investigated (Gumińska *et al.*, 1996).

After 48 hours, both applied treatments resulted on the same extracellular lactate even glucose consumed was undoubtedly higher.

The analysis of SW1088 cell metabolism (**Figure 21B**) established that no differences were noticed for glucose consumption after 24 hours of applied treatment compared with their respective controls. On the other hand, glucose consumption at 48 hours was higher for PLGA/OCS NP treatment. Comparing different time points (24 and 48 hours) glucose consumption increases for the control (DMEM DMSO) and CHC treatment. It is also noticeable that CTX initially reduces glucose consumption (24 hours). Yang and co-workers have shown increased glucose uptake and lactate production by the activation of EGFR in GBM suggesting that those targets might exhibit a self-regulation relationship (Yang *et al.*, 2012).

For extracellular lactate quantification, at 24 hours, higher amount was noticed for NPs, CHC-loaded NPs and Conjugated NPs. Once again, treatment that comprise CHC molecule (CHC-loaded NPs and conjugated NPs) appears to be responsible for the highest levels of extracellular lactate at 24 hours, in agreement with U251 behavior.

After 48 hours, no differences were evident for extracellular lactate except for CHC treatment. Comparing both 24 and 48 hours, glucose consumed was higher for CHC treatment and, at the same time, a decrease in extracellular lactate was also evident.

A) U251

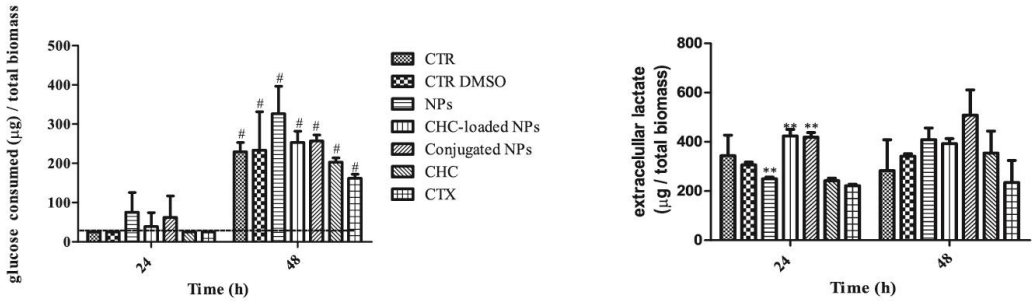

B) SW1088

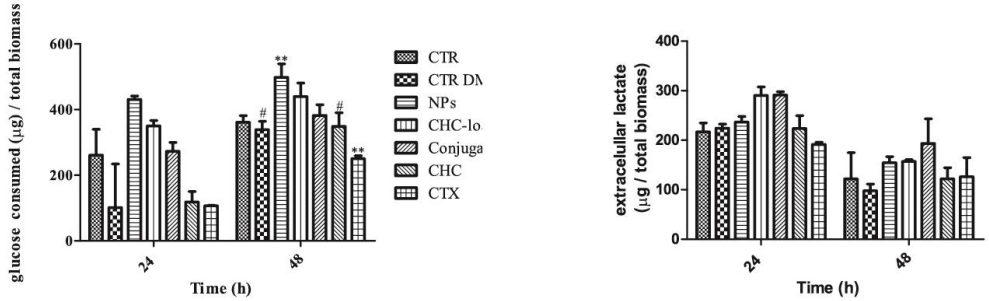

Figure 21: Glucose consumption and extracellular lactate (µg) /total biomass of (A) U251 and (B) SW1088 cells applying different treatments. CTR: negative control (DMEM 10% FBS); CTR DMSO: DMEM 10% FBS + 1% DMSO; NPs: empty PLGA/OCS NPs diluted in DMEM 10% FBS; CHC-loaded NPs: CHC-loaded PLGA/OCS NPs diluted in DMEM 10% FBS; Conjugated NPs: CTX conjugated PLGA/OCS CHC-loaded NPs; CHC: free CHC diluted in DMEM 10% FBS + 1%DMSO; CTX: free CTX diluted in DMEM 10% FBS. Results are representative of the three independent experiments, each one in triplicate; **p<0.05 Treatment *versus* control. # p<0.05 24 and 48 hours. Dotted line represents that glucose concentration was lower than quantification limit.

The analysis of glucose consumption and lactate production of the different cell lines U251 and SW1088 together with applying different developed NPs shows that U251 appears to be more glycolytic than SW1088 especially when PLGA/OCS NPs were employed. For PLGA/OCS NPs, biological action expected for CHC was not evident even when the drug was applied as a free drug. Therefore, based on the acquired cell viability results for conjugated PLGA/OCS NPs, the biological activity of CTX after functionalization must be investigated.

Based on previous results acquired, especially by the cytotoxic potential that NPs have shown against GBM cell lines, we decided to further explore the role of CTX conjugated to NPs using only PLGA/OCS NPs. While conjugation procedure for PLGA/OCS NPs was achieved by covalent bond, the chosen and applied protocol showed critical steps that could compromise CTX therapeutic

efficacy. Therefore, from now on, all data that we will address for biological performance is related to PLGA/OCS NPs.

6.5.3. Western blot analysis

In order to explore the spectrum of conjugated PLGA/OCS NPs on EGFR pathways a western blot analysis was used to investigate total and phosphorylated EGFR. In addition, PARP cleavage, ERK and AKT phosphorylation was also examined to certify the occurrence of apoptosis induction and the effect on intracellular signaling pathways.

Upon EGF stimulation we found that EGFR phosphorylation was totally abolished when conjugated NPs and free CTX were applied to both cell lines U251 and SW1088. These data support that CTX therapeutic efficacy was not compromised from the conjugation process and conjugation efficiency was accurately calculated. The total EGFR expression was also evaluated to corroborate these results (**Figure 22**).

As expected, the analysis of total PARP was confirmed for all applied treatments in both cell lines since all cells might show this active mechanism. However, PARP cleavage measurement revealed no induction of apoptosis. These results can be explained since the chosen time point was three hours and, most of the time, PARP cleavage takes a longer time to be detected.

ERK phosphorylation was confirmed for all applied treatment. It is clear, however, that there is a partial inhibition when conjugated NPs and free CTX were used to both cell lines compared to their respective controls. This result was expected once this signaling pathway was not activated only by phosphorylated EGFR. A similar profile was noticed for phosphorylated AKT in U251 and SW1088 cell lines.

Taken together, the blot analysis confirms that CTX associated to PLGA/OCS NPs by covalent bonds continues to exert its therapeutic efficacy in addition to reinforce that system efficacy was specific and not associated to toxicity. Accordingly, the therapeutic efficacy highlighted for conjugated NPs can be associated with the CHC and CTX biological action.

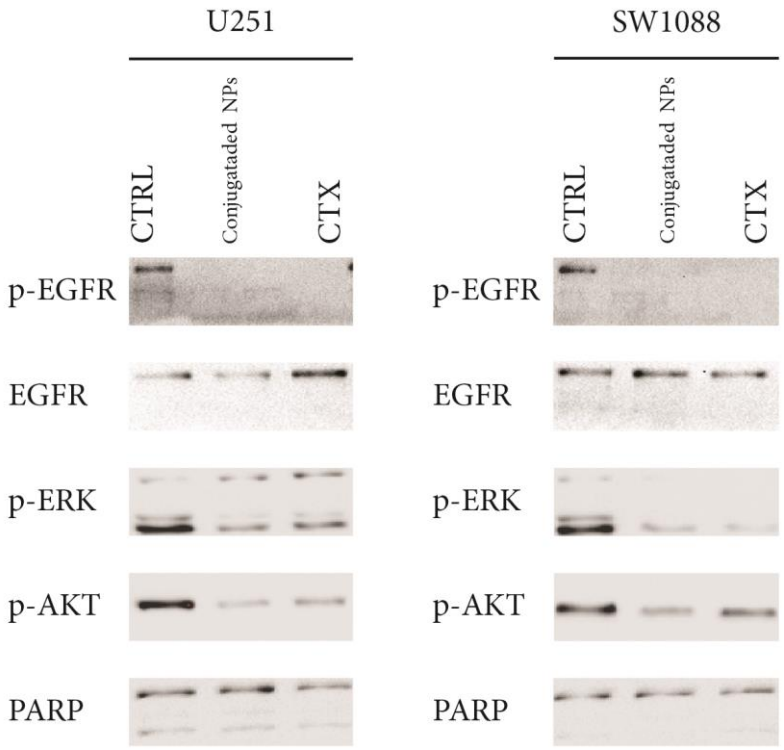

Figure 22: Analysis of EGFR total and phosphorylated, pERK and pAKT in U251 and SW1088 GBM cell lines by Westerns Blot. EGF ligand was used at 10 ng/mL for 15 minutes. CTRL: DMEM 0.5% FBS was used as negative control; conjugated NPs: developed CHC-loaded PLGA/OCS NPs covalently linked to cetuximab; CTX: free cetuximab at the same concentration.

6.6. Evaluation of NP concentration and size distribution using nanoparticle tracking analysis (NTA)

Evaluation of NP concentration and their size distribution can be efficiently determined in real time by the use of nanoparticle tracking analysis (NTA), an alternative nanoparticle characterization technique developed in the mid-2000s. Different from DLS technique, data recorded over time here, enables detection of physical instability which were not assessed by subtle changes in size distribution (Kestens *et al.*, 2017).

Several studies have compared the DLS and NTA methods in terms of accuracy, advantages and drawbacks considering their particularities. While DLS determines particle size from fluctuations in scattered light intensity due to Brownian particle movement, NTA combines laser light scattering microscopy with a charge-coupled device camera, which enables the visualization and recording of nanoparticles in solution. Thus, NTA software can identify and track individual

particles in addition to relate the movement to a particle size by the use of the Stokes-Einstein equation (Filipe *et al.*, 2010; Boyd *et al.*, 2011) .

Determination of size for both monodisperse and polydisperse samples can be accurately measured by NTA. In addition, the technique gives an approximate particle concentration what is outmost important for correlations with biological responses (Filipe *et al.*, 2010; De Morais Ribeiro *et al.*, 2018).

Since NP size and concentration are parameters that show potential to bridge the gap between *in vitro* characterization and biological performance of colloids, NTA was employed for accurate determination of size and concentration into empty PLGA/OCS NPs, CHC-loaded PLGA/OCS NPs and conjugated NPs before evaluation of biological performance using *in vivo* protocols.

NTA analysis has shown that empty NPs exhibited an approximate size of 340 nm. Indeed, CHC-loaded NPs exhibited 425 nm and conjugated NPs 312nm. It is important to point out that the given mode parameter was always lower than the main size registered **Table 5**). Take into account the calculated standard deviation, no statistical differences were found between DLS and NTA measurements for these samples.

Importantly, NTA also allows the particle concentration to be predicted directly, with good linearity. Estimated values for empty NPs, CHC-loaded NPs and conjugated NPs were $4.72x10^{10}$, $2.03x10^{10}$ and $3.56x10^{10}$, and important data that will be considered for future studies.

Table 5: NTA analysis of empty NPs, CHC-loaded NPs and conjugated NPs. Values represent the average of 3 (n=3) determinations and standard deviation.

Sample	**Nanoparticle Tracking Analysis (NTA)**		
	Size (nm)		
	Média	**Mode**	**SD**
Empty NPs	339.4	245.8	137
CHC-loaded NPs	424.9	314.1	179.4
Conjugated NPs	311.8	248.1	125.6

6.7. Biological performance *in vivo*

Following the evaluation of the biological activity applying *in vitro* protocols with cell culture, the next step of this investigation was the evaluation of therapeutic performance using *in vivo* models. The CAM assay represents a suitable model most of the time considered an *in vivo* approach or even a transient model between *in vitro* and *in vivo* (Aristotle *et al.*, 1965). Nevertheless, by its complex environment, they can provide a more reliable drug or NPs performance than *in vitro* testing.

6.7.1. Analysis of tumor development, progression and antiangiogenic activity, using the CAM assay

The CAM model was used to investigate the antitumoral and antiangiogenic activity provided by conjugated CHC-loaded PLGA/OCS NPs against 3D tumor of U251 cell line. The choice of U251 cells instead of SW1088 was based on their greater sensitivity according to all results presented above.

Three days after tumor cell implantation into the CAM using a matrigel support, eggs were divided in different experimental groups (containing at least n=10): DMEM (negative control), NPs (empty PLGA/OCS NPs), CHC-loaded NPs (CHC-loaded PLGA/OCS NPs) and conjugated NPs (CTX conjugated with CHC-loaded PLGA/OCS NPs). Tumor dimensions (area and perimeter) were measured before (Day 0) and four days after treatment (Day 4). Results are depicted in **Figure 23.** The analysis of tumor dimensions before and after treatment showed that when DMEM was applied, no differences on tumor area or dimensions were noticed. However, a tendency to decrease tumor area and perimeter was observed as a result of NPs, CHC-loaded NPs and conjugated NPs treatments.

Regarding NPs group, the mean of calculated tumor area was 56985±11437 cm before applied treatment and 31121±6726 4 days after treatment. The observation of tumor regression by the empty NPs may be related with biological properties of OCS, especially their antitumor effect previously described (Muanprasat; Chatsudthipong, 2017).

For CHC-loaded NPs, tumor area decrease from 64104 cm to 32603 cm, that is, at the end of the experiment, tumor area was 2-fold smaller. Results of cell viability discussed above had already evidenced therapeutic gains by the encapsulation of CHC. Herein, a significative antitumoral activity was highlighted for CHC-loaded NPs compared to the other treatments. This observation is also in agreement with previously published results which highlighted that CHC decreases cell growth and induce cell death against glioma cell lines (Miranda-Goncalves *et al.*, 2013).

Regarding the treatment with conjugated NPs, the trend of tumor reduction was also observed in agreement with acquired data for cell viability. However, it is important to notice that from the beginning of the applied protocol (Day 0), the main tumor dimensions were lower for conjugated NPs group.

Evaluation of tumor dimensions and vascular network can also be considered by the observation of pictures taken *in ovo* before (Day 0) and after (Day 4) the different applied

treatments. Representative images are depicted in **Figure 24** highlighting tumor behavior over the experimental time.

Neoplastic cell populations are powerful and efficient to originate a clinical observable 3D tumor if the host offers a vascular network capable to sustain their growth. Then, the occurrence of angiogenesis, creation of a network of blood vessels that supplies cell needs, is crucial for tumor development (Mauriz; González-Gallego, 2008).

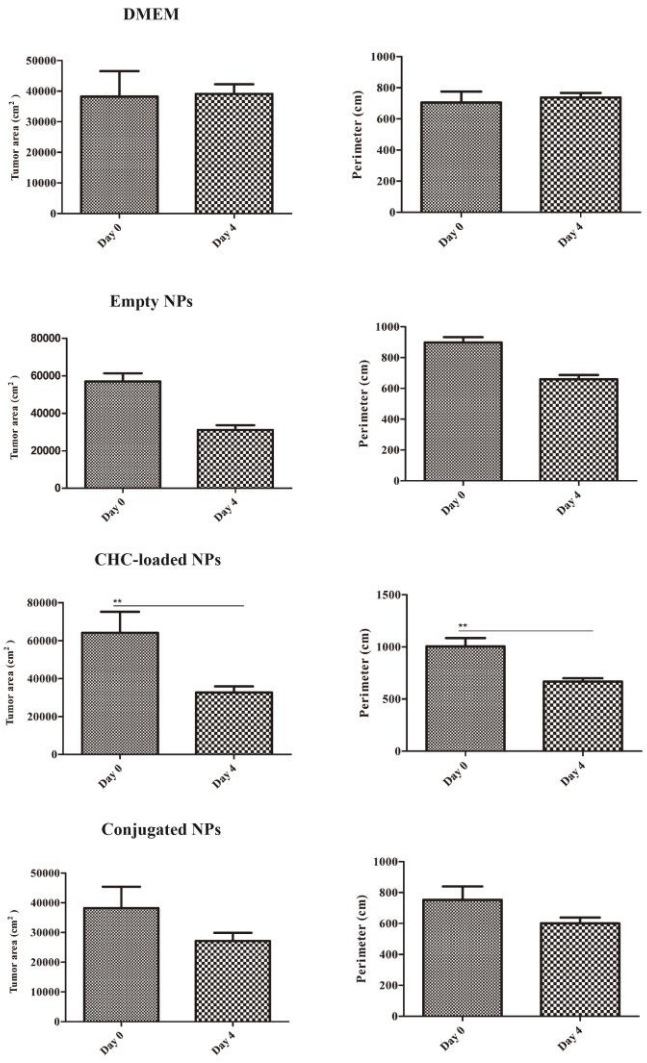

Figure 23: Effect of conjugated PLGA/OSC NPs in U251 glioma cells: area (cm^2) and perimeter (cm) of tumors after different treatments. Day 0 represents tumor dimensions before eggs received respective treatment: A) DMEM, B) Empty NPS, C) CHC-loaded NPs and D) conjugated NPs. Day 4 relates to tumor measurements 4 days post applied therapy. Results are expressed as mean –SD; n=10. One-way analysis of variance followed by Tukey´s multiple comparison was used for statistical analysis **($p<0.005$)

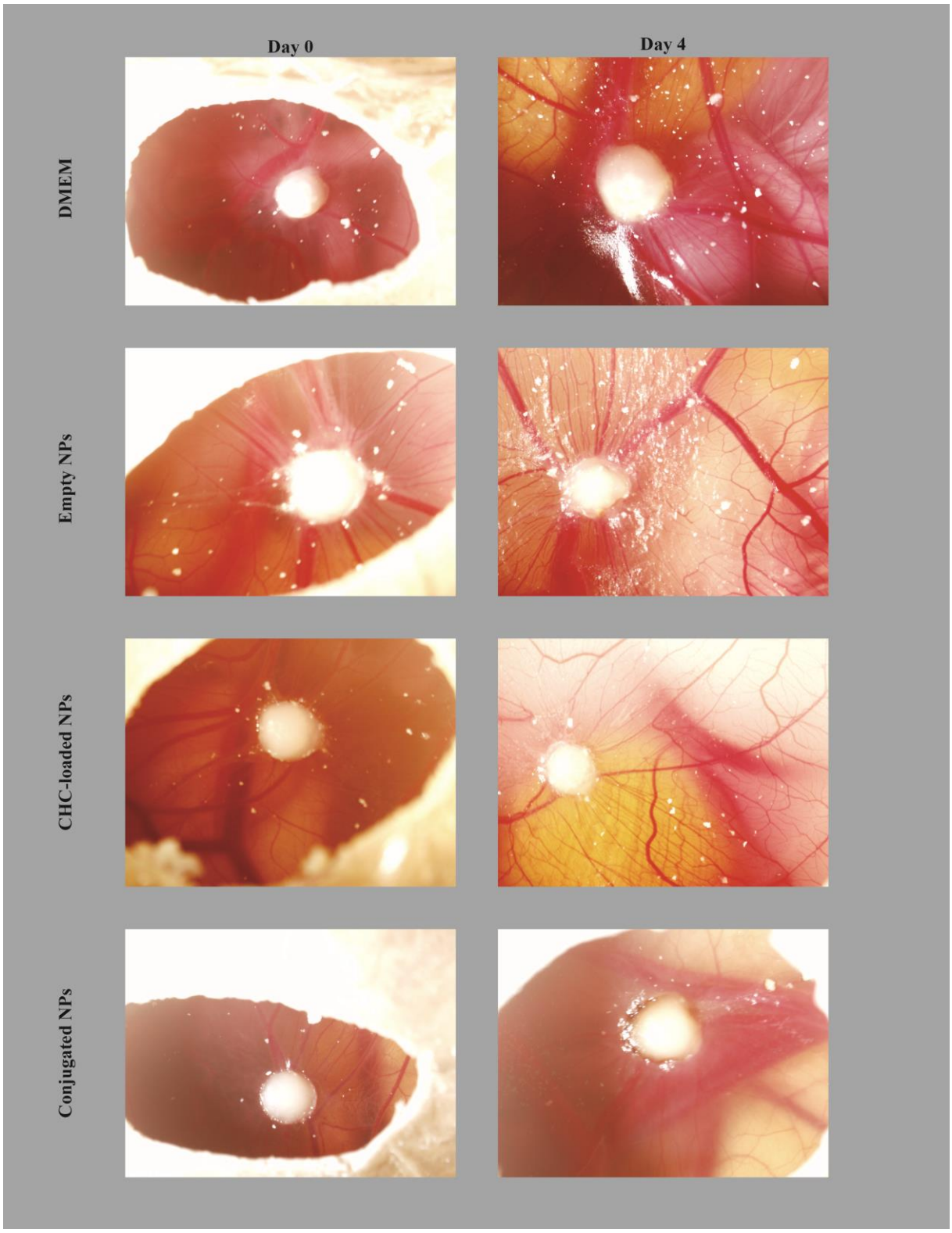

Figure 24: Representative stereomicroscope images acquired *in ovo* before (day 0) and after (day 4) the applied treatments.

Representative images acquired *in ovo* 4 days after applied treatment for blood vessels quantification are shown in **Figure 25**. The macroscopic observation of all experimental groups led us to believe that vascular patterns appear to be more tunable, robust and abundant when DMEM and NPs were employed. Those findings indicate that antitumoral activity observed for empty NPs are not possibly related to an antiangiogenic effect although previous investigation has described this property to OCS (Wang *et al.*, 2007). Moreover, it is observable that when CHC-loaded NPs was applied, the vascular network became deficient with narrower blood vessels. Regarding the conjugated NP treatment, remarkably, blood vessels became weak and the occurrence of necrosis can be also observed at the tumor edge.

Since the mid-2000, when Petit and co-workers were the first to state the antiangiogenic properties of CTX, extensive evidence has shown that this EGFR inhibitor also decrease tumor cell production of angiogenic growth factors such as VEGF, bFGF and interleukin-8 (IL-8) (Petit *et al.*, 1997; Vincenzi *et al.*, 2010). Based on this information, we also investigate the dimension of anti-angiogenic activity provided from developed conjugated NPs.

Macroscopic evaluation of the blood vessels area was carried out using *ex ovo* processed images after 4 days of applied treatment. For this purpose, stereomicroscope images were kept constant and pictures taken "*ex ovo*" were processed as 300x300 pixels around the tumor. Quantification was done by the use of ImageJ 1.48v Software (Ferreira *et al.*, 2017). Counts for each egg were performed by two independent observers to minimize failure.

The analysis of **Figure 25** also revealed modification on vascular patters converging between experimental groups. While vascular network evidently became more generous for DMEM and empty NPs on day 4, a decreased or weaker distribution was noticed for CHC-loaded NPs and conjugated NPs. Once again and now, more evident for conjugated NPs group, tumor cells are partially necrotic as a result of deficient blood and oxygen supply.

The average values of blood vessel count after CAM excision are shown in **Figure 26**. According to the data acquired among different experimental groups for blood vessels quantification, no differences were noticed between our negative control (DMEM) and empty NPs group. However, encapsulation of CHC into developed PLGA/OSC NPs resulted in a significant reduction compared with empty NPs ($p<0.05$). Once again, CHC induced a significant decrease in the number of blood vessels around the tumors compared to negative control; however, presumably, this effect is mediated by the tumor cells and not directed linked to the blood vessels (Miranda-Goncalves *et al.*, 2013). Otherwise, when CTX conjugated with the developed system was applied, the reduction in blood vessel number was significantly higher, in agreement with previous

published studies which highlight the antiangiogenic activity of CTX (Petit *et al.*, 1997; Vincenzi *et al.*, 2008).

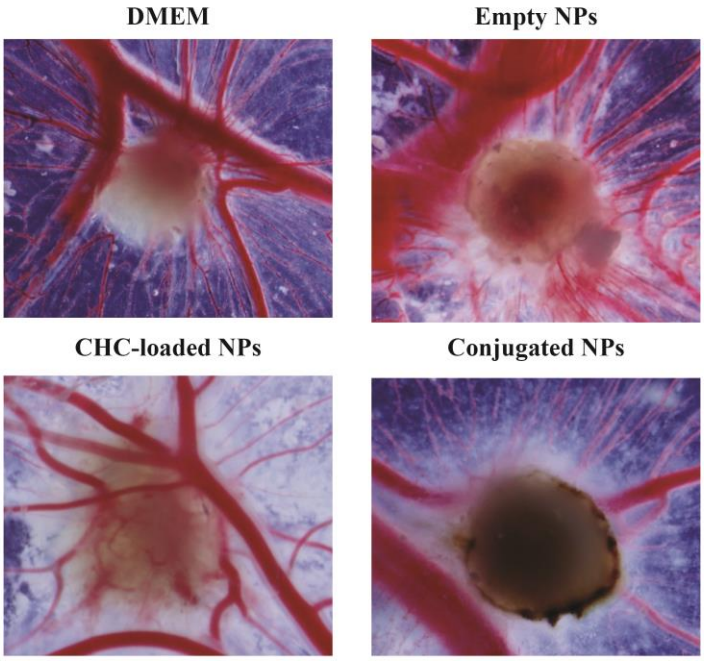

Figure 25: Representative stereomicroscopy images acquired ex ovo 4 days after applied treatment, for blood vessel quantification.

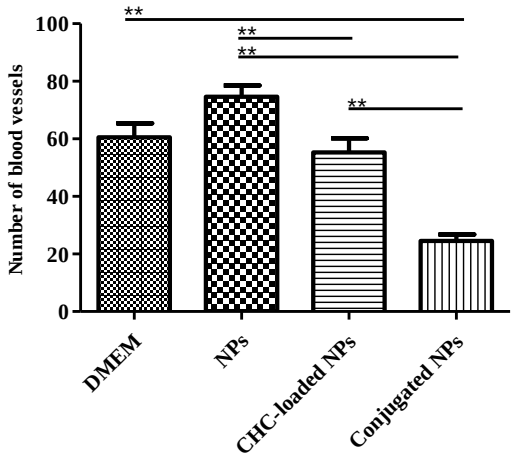

Figure 26: *Ex ovo* quantification of number of blood vessels 4 days after applied treatment using ImageJ Software. Counts for each egg were performed by two independent observers to minimize failure and average values were used. Results are expressed as mean –SD; n=10. One-way analysis of variance followed by Tukey´s multiple comparison was used for statistical analysis ($p<0.05$)

6.8. *In vitro* release study

After administration, drug therapeutic performance is directly related to their release profile from the delivery platform[10]. The ability of CHC-loaded NPs and conjugated NPs to release CHC and CTX was evaluated by *in vitro* dissolution test applying Franz diffusion cells with cellulose membrane. **Figure 27** presents the CHC and CTX release profiles from CHC-loaded NPs and conjugated NPs in a phosphate buffer pH 6.5.

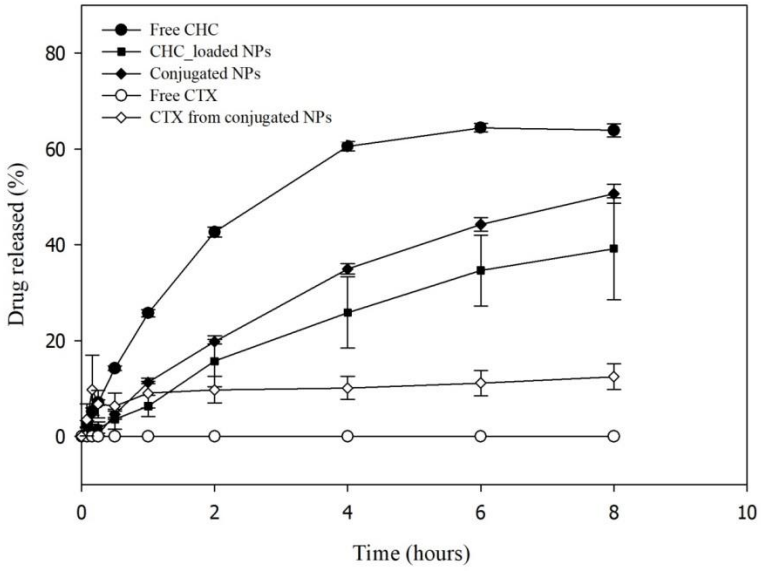

Figure 27: CHC and CTX release profile (%) from NPs and conjugated NPs in a phosphate buffer pH 6.5. Full symbols represent CHC release and empty symbols are related to CTX release. Data show the average of six measurements (n=6) and their standard deviation.

Figure 27 shows that both developed platforms promoted modified release of CHC and CTX compared to the free drug. In fact, as we can notice, CHC loaded NPs, despite the conjugation procedure, exhibited their initial release sustained and decreased compared to the free CHC. Thus, CHC inclusion into the polymeric platform promoted significant reduction on CHC release rates during the assay; so that, after 8 hours, CHC released from NPs was almost 1.5-fold lower; indeed, the amount released from conjugated NPs was also lower when compared to the free CHC drug profile.

Since the release studies were performed following the sink condition and free CHC drug release is direct related to its dissolution, the release profile exhibited can be assigned to the adopted methodology, which includes a unidirectional process and the need to cross a membrane.

Regarding CTX drug, we could notice that as a free drug, the macromolecule was not able to enter the regenerated cellulose membrane during the assay. This fact may be associated with drug - membrane incompatibility. Considering the CTX isoelectric point 8.48 (Tseng *et al.*, 2015), below this value, the macromolecule assumes a positive charge, which can hinder its passage. Previous published work have also demonstrated that the release profile depend on the membrane type (Salamanca; Barrera-Ocampo, 2018). However, when CTX drug was structured in the nanoparticle surface by covalent bonds, the macromolecule was able to cross the membrane and been quantified as a free drug on the receptor compartment. Thereabout 3 to 6% of CTX drug was released in the first half hour reaching 12% after 8 hours. According to those results, two hypotheses can be formulated: in regard to CTX macromolecule, possibly, a deeper investigation on drug-membrane interaction might clarify acquired results; on the other hand, it is likely that conjugated NPs were able to cross the membrane and release part of the conjugated drug. Importantly, the low release rate can be justified by the nature of covalent bonds applied for conjugation.

Quantitative interpretation of release data is greatly facilitated when general mathematical models which describe the entire curve by significative parameters are applied (Langenbucher, 1972). In order to deeper understand the mechanism that drives CHC and CTX release processes from NPs and conjugated NPs, suitable mathematical models were applied to the profiles shown in **Figure 27** (Korsmeyer *et al.*, 1983; Peppas; Narasimhan, 2014). The statistical calculated coefficient of determination (r^2) is the based criteria adopted to assess the data fits into the proposed model equation.

CHC released from CHC-loaded NPs and conjugated NPs correlated better with Weibull model (r^2=0.997 and r^2=0.999, respectively) (**Table 6**). According to this model, originally proposed by Waloddi Weibull in 1951 (Weibull, 1951), the cumulative drug amount to the medium at a certain time can be adjusted to different dissolution profiles, according to **Equation 1** (Adams *et al.*, 2001).

$$m = 1 - \exp\left[\frac{-(t - T_i)^b}{a}\right] \qquad \textbf{Equation 1}$$

Where *m* is the accumulated drug, in solution at time *t*, which *a* defines the time scale of the process. T_i represents the lag time before the onset of the dissolution or release process and *b* characterizes the curve as either exponential. The linearity of Weibull plot requires that data points asymptotically come forward the final plateau as we could observed to those samples (around 4 to 6

hours) (Langenbucher, 1972). For this model, the *b* exponent value indicated the drug transport thought the polymer matrix. In accordance, when values of b higher than 1 is found drug transport follows a complex release mechanism where release rates increases up non linearly to the inflection point and thereafter declines (Papadopoulou *et al.*, 2006).

Table 6: Coefficients of mathematical models applied to release profiles (Higuchi, KorsmeyerPeppas, First order, Hixson-Crowell and Weibull)

Mathematical models		Samples		
		CHC release		CTX release
		CHC-loaded NPs	**Conjugated NPs**	**Conjugated NPs**
Higuchi	k	38.22	49.737	16.165
	r^2	0.930	0.930	0.122
Korsmeyer-Peppas	k	20.734	15.828	25.059
	r^2	0.989	0.985	0.836
	n	2.67	4.018	0.561
First order	k	0.7154	0.727	11.285
	r^2	0.989	0.990	0.0
Hixson-Crowell	k	0.063	0.086	0.020
	r^2	0.989	0.9837	0.0
Weibull	r^2	0.997	0.999	0.736
	b	3.0	3.0	3.0

Release profiles from swellable polymeric matrices as PLGA-chitosan are governed by physical and chemical process which may involve liquid penetration into the polymer network, swelling and polymer hydration, drug diffusion throughout swollen matrix or even matrix erosion. Therefore, values of b=3 highlighted that drug release is related to the matrix swelling plus erosion concomitantly (Carbinatto *et al.*, 2014).

CTX release profile from conjugated NPs was fitted into mathematical models just for comparative purposes. Since drug released reached only 12% during the assay, there is a fundamental difficulty to portray its profile. This fact can be exemplified by the lower r^2 values found. Low k values reveal a late release, what might be related to the strong interaction involved into the covalent bonds.

Taken together, these data have shown that CHC release was sustained and retarded by the drug encapsulation into NPs especially by the need of drug diffusion along the polymeric network. Indeed, the conjugation procedure might increase chain flexibility, slightly accelerating drug release, results evidenced by the higher k values. Additionally, both release profile better correlated with Weibull model following a complex release mechanism. Furthermore, part of the CTX drug structured in NPs by covalent bonds could transpose cellulose membrane and release from the developed system.

6.9. *Ex vivo* permeation study applying nasal porcine mucosa

Permeability studies are essential and of great importance when a nanostructure carrier is designed for mucosal administration. The assay can provide relevant data about drug transport through an epithelium or even about the effect of chosen excipients on drug permeability (Mcmartin *et al.*, 1987; Salade *et al.*, 2019). Permeation studies were carried out using nasal porcine mucosa selected by the similarity with human mucosa on its physiology and anatomic, as well as histological and biochemical aspects (Kumar *et al.*, 2013). The choice of run time of 12 hours is justified by the tissue preservation and viability previously reported by Bechgaard and co-workers based on rabbit nasal mucosa (Bechgaard *et al.*, 1992).

Importantly, drug solubility in the receptor medium solution is essential to maintain the sink condition. In this regard, CHC saturation solubility was determined to be around 8±3.2 mg/mL. CTX is commercially available as a parenteral solution in phosphate buffer 5mg/ mL and therefore, meets the desired specification.

Permeation profile of CHC solution, CHC from NPs and conjugated NPs are shown in **Figure 28**. According to the results, CHC permeation was delayed by the inclusion of system complexity. As a free drug, high amount of CHC could permeate the porcine tissue; the probable reason for acquired profile in comparison to NPs can be the hydrophobic nature of the drug. Importantly, as an experimental anticancer drug with no FDA approval, no information about CHC logP was found to reinforce acquired results.

The encapsulation of CHC into nanostructures based on PLGA/OCS normally provides higher drug permeation due to the greater surface area given by the nanosize and enhancing activity of OCS, which is able to opening tight junctions (Qureshi *et al.*, 2019). However, the positive ZP of NPs can increase the interaction between positively charged amino groups of CS with negatively charged cell membranes, a phenomenon well known as mucoadhesion (Piazzini *et al.*, 2019). Herein, the sites available for interaction between positively OCS and negative biological membrane were used to ensure conjugation with CTX. Therefore, the lowest permeation of conjugated NPs may be related to the presence of CTX macromolecule on its surface.

Figure 29 displays the permeation profile of free CTX and CTX from conjugated NPs. Apparently, the profile tends to be similar despite the covalent link between CTX and NPs. Considering the great variability, thereabout 30% of CTX could permeate the biological membrane. Lesser permeation of free CTX and CTX from conjugated NPs may be related to the complex

macromolecular structure and hydrophilic nature of the drug. The high solubility of polar drugs in the mucus should provide reduced drug permeation (Javia; Thakkar, 2017).

High variability on acquired results was expected since the membrane applied can contemplate different areas of the nasal cavity, a parameter difficult to predict. Previous results have shown how the tissue thickness is a crucial and directly influences the drug diffusion (Salade *et al.*, 2019).

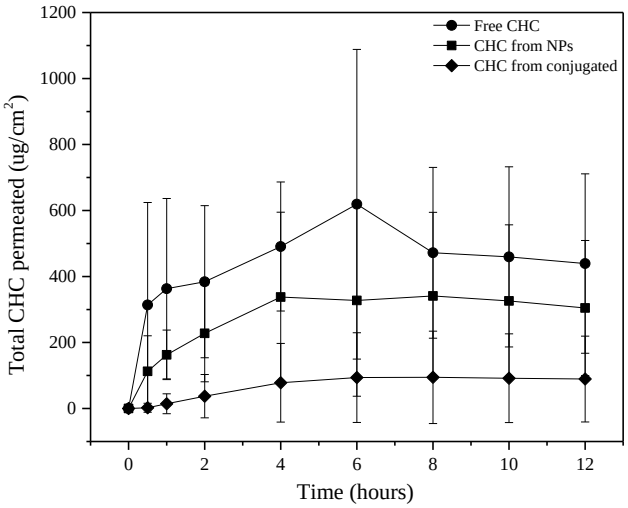

Figure 28: Permeation profile of free CHC, CHC from NPs and CHC from conjugated NPs. Data show the average of six measurements (n=6) and their standard deviation.

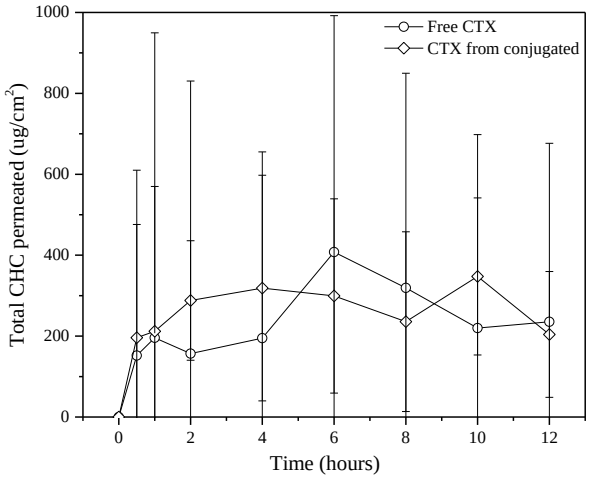

Figure 29: Permeation profile of free CTX and CTX from conjugated NPs. Data show the average of six measurements (n=6) and their standard deviation.

The permeability coefficient (CP) across the mucosa was calculated from the slope of the linear part of the line obtained by plotting the mass transported per unit area against time (Piazzini *et al.*, 2019). The apparent permeability coefficient of free CHC was $1.4x10^{-2}$ while CHC from NPs was $1.06\ x10^{-2}$. Regarding CHC from functionalized NPs, the CP was even lower ($0.8\ x10^{-2}$). A greater CP is expected to correlate with higher absorption (Piazzini *et al.*, 2019). Concerning the acquired results for CTX drug, CP for free CTX was found to be $2.9x10^{-3}$ while CTX from conjugated NPs was $2.079x10^{-3}$.

The steady state flux after 12 hours was found to be 22.5 µg/cm^2/h for free CHC, 21.22 µg/cm^2/h for CHC from NPs and 8.3 µg/cm^2/h for CHC from conjugated NPs. CTX as a free solution exhibited steady state flux of 14.8 µg/cm^2/h whereas CTX from conjugated NPs have shown 10.3 µg/cm^2/h.

Another parameter analyzed in this study was the amount of CHC and CTX retained in the mucosa tissue after 12 h of experiment. CHC has been detected only in small traces in the digested membrane for NPs and conjugated NPs while no quantification of CTX was observed. Considering the amount of permeated drug, especially for CTX, two approaches are hypothesized: the digestion method applied may not be effective in extracting the retained drug or part of CTX remains covalently associated with NPs. Further efforts are needed to define the exact role of this absorption pathway.

6.10. Analysis of nose to brain delivery using fluorescence tomography

CHC-loaded NPs and NPs was developed using the IR-780 marker for image acquisition. Size, PDI and ZP of developed systems were measured using DLS according to the procedure described on section 3.4.1 and 3.4. **Table 7** shows values found for IR780 NPs that will be applied for *in vivo* studies compared with CHC-loaded NPs and conjugated NPs. According to these results, we can observe no statistical differences between NPs and IR780-loaded NPs in terms of size and PDI. Slight alterations were found in ZP values. However, we do not know what this modification can provide in terms of interaction and transport through the brain.

Table 7: Size, PDI and ZP of developed IR780-loaded NPs and IR780-loaded conjugated NPs. Values represent the average of 3 measurements (n=3) and standard deviation.

	Samples			
	CHC-loaded NPs	**IR780-loaded NPs**	**conjugated NPs**	**IR780-loaded conjugated NPs**
Size (nm)	258±32.1	268.1±27.2	297±23	307.1±7.0
PDI	0.44±0.05	0.49±0.03	0.38±0.05	0.36±0.02
ZP (mV)	37±3.8**	15.66±0.5	-14.8±2.5**	8.03±3.05

Differences $p<0.05$ were considered statistically significant (**).

Evidence that nanotechnology can enhance the direct transport to CNS is noticeable and crucial, since it not only allows drug protection, but most importantly, it improves the uptake by the olfactory mucosa (Gao *et al.*, 2007; Migliore *et al.*, 2010; Xia *et al.*, 2011; Mittal *et al.*, 2014; Samaridou; Alonso, 2018). Thus, encapsulation of the drug in a nanostructured delivery vehicle can serve as a very powerful strategic approach for nose-to brain transport (Yadav *et al.*, 2015).

The analysis of brain tomography might provide an indication that NPs are efficient to provide the direct drug transport into the brain via nasal route.

According to the results depicted in **Figure 30** IR780-loaded NPs exhibited intensive signals after 30 min of nasal administration. On the other hand, IR780-loaded conjugated NPs seems to show progressive signs from 0.5 to 3 hours. Take into account NPs concentration (IR780-loaded conjugated NPs are diluted considering the conjugation procedure when compared to IR780-loaded NPs) and also the permeation profile previously demonstrated, it was expected that signals provided from IR780-loaded NPs were quickly detected. Importantly, IR-780 signal remained in the brain for up to 3 hours for both NPs.

The applied assay represent a qualitative response and based on all the results discussed above, especially release and permeation profile, the acquired FMT images can lead to the hypothesis of a rapid translocation and NPs accumulation into the brain for both developed IR-loaded systems.

It is well-known that particle size represents a key factor for nanostructured platforms performance or ability to overcome mucus barriers or well-organized epithelia. A scientific investigation using labeled nanoparticles with different fluorescent probes has shown the translocation profile of different nanoparticle sizes along the passage nose-to-brain. The transport was proven to be effective for 400 nm particles in slower pace, which apparently can be related to the faster mucociliar clearance (Ahmad *et al.*, 2017).

Concerning ZP, herein, a higher positive value seems to have enhanced NPs transport. However, their effect on particle performance has not been clearly elucidated yet, although the use

of positively charged molecules provide stronger adherence to the mucus layer. Interestingly, the potential benefit of this adhesive/retention behavior remains unclear. Nevertheless, both surface charges are proven to provide the transport (Bonaccorso *et al.*, 2017).

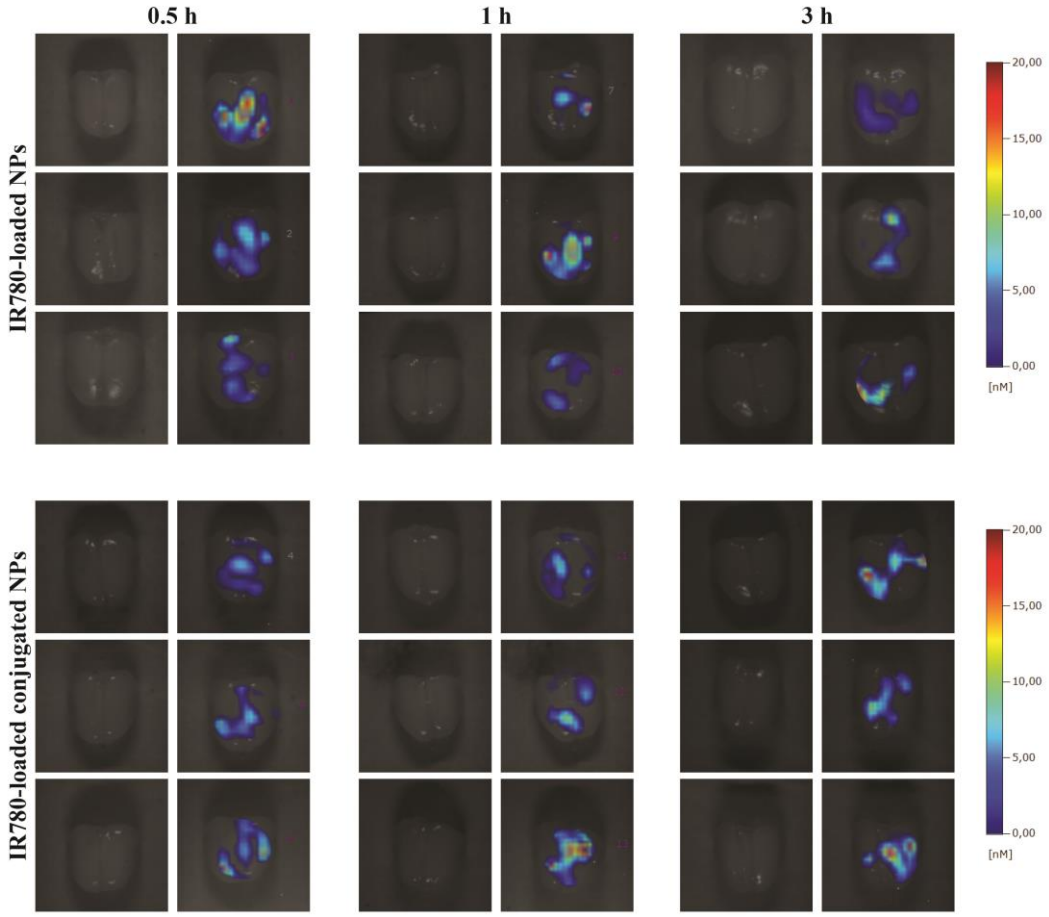

Figure 30: *Ex vivo* brain fluorescence tomography. Pictures were taken 0.5, 1 and 3 hours after intranasal administration of IR780-loaded NPs and IR780-loaded conjugated NPs; (n=3). First column represents the negative controls.

Taken together, these data provides evidence that developed nanoparticles of PLGA/OCS in the range of 250 to 310 nm of size, were effective to provide nose-to-brain transport, independent of the conjugated procedure. Futures studies are needed to quantify the dimension of transport provided by these systems.

7. CONCLUSIONS

The present study has provided the first investigation of a dual therapeutic strategy combining CHC and CTX against GBM, using the SW1088 and U251 glioma cell lines. Besides, nanotechnology has brought important features to the proposed strategy, considering that

nanostructured systems are able to optimize the therapeutic effect, especially for complex pathological processes.

In this work, we have successfully rationally developed innovative delivery systems based on PLGA and chitosan (PLGA/TMC and PLGA/OCS) polymeric nanoparticles for CHC encapsulation. Both developed platforms resulted in a nanostructured organization at about 300 to 400 nm of size containing chitosan on its outermost surface, what led to a positive ZP, and a high percentage of CHC encapsulation.

Complete physicochemical characterizations have shown that CHC drug could modify the kinetic aspects of NPs stabilization. In addition, interaction between CHC drug and PLGA/OCS NPs follows different patterns than PLGA/TMC NPs. Therefore, conjugation between CTX and developed NPs was optimally obtained by supramolecular forces (PLGA/TMC NPs) at pH 6.5 and covalent bonds (PLGA/OCS NPs), resulting in 85 and 58% of efficacy, respectively.

Comparing both developed systems in terms of cell viability and metabolism assay, PLGA/OCS NPs showed more promising results than those obtained with PLGA/TMC NPs. For that reason, this system was chosen to proceed the scientific investigation.

In vitro release profile showed that CHC release was modified by the drug encapsulation into NPs. Additionally, both release profile correlated better with the Weibull model following a complex release mechanism. The *ex vivo* permeation study using nasal porcine mucosa has shown that CHC permeation was delayed by the inclusion of system complexity.

Blot analysis confirmed that CTX associated to PLGA/OCS NPs by covalent bonds were biologically active in addition to reinforce that system efficacy was specific and not associated to toxicity. Analysis of antiangiogenic activity, tumor development and progression using the CAM assay disclose a trend for tumor reduction when conjugated NPs were employed as therapeutic strategy, in addition to provide a significative reduction in the blood vessel number compared with all other applied treatment.

Analysis of nose-to-brain delivery using fluorescence tomography provided evidence that developed NPs, regardless of the CTX conjugation procedure, were effectively transported from nose to the brain.

Taking into consideration all of the aforementioned results, we anticipate that the developed CHC-loaded PLGA/OCS NPs conjugated with CTX by covalent bonds, exhibited a set of favorable attributes that make them promising alternatives to be further explored and considered in GBM treatment.

8. REFERENCES

ADAMS, E. et al. Evaluation of dissolution profiles using principal component analysis. **International Journal of Pharmaceutics,** v. 212, n. 1, p. 41-53, 2001/01/05/ 2001. ISSN 0378-5173. Disponível em: < http://www.sciencedirect.com/science/article/pii/S0378517300005810 >.

AFONSO, J. et al. Clinical significance of metabolism-related biomarkers in non-Hodgkin lymphoma - MCT1 as potential target in diffuse large B cell lymphoma. **Cell Oncol (Dordr),** v. 42, n. 3, p. 303-318, Jun 2019. ISSN 2211-3428.

AGNIHOTRI, S.; ZADEH, G. Metabolic reprogramming in glioblastoma: the influence of cancer metabolism on epigenetics and unanswered questions. **Neuro Oncol,** v. 18, n. 2, p. 160-172, 2016. ISSN 1522-8517.

AHMAD, E. et al. Evidence of nose-to-brain delivery of nanoemulsions: cargoes but not vehicles. **Nanoscale,** v. 9, n. 3, p. 1174-1183, Jan 19 2017. ISSN 2040-3364.

ALEX, A. T. et al. Development and evaluation of carboplatin-loaded PCL nanoparticles for intranasal delivery. **Drug delivery**, p. 1-10, 2015. ISSN 1071-7544.

ALEXANDER, A. et al. Recent expansions of novel strategies towards the drug targeting into the brain. **Int J Nanomedicine,** v. 14, p. 5895-5909, 2019. ISSN 1176-9114.

ALSHAMSAN, A. Nanoprecipitation is more efficient than emulsion solvent evaporation method to encapsulate cucurbitacin I in PLGA nanoparticles. **Saudi Pharmaceutical Journal,** v. 22, n. 3, p. 219-222, 2014/07/01/ 2014. ISSN 1319-0164. Disponível em: < http://www.sciencedirect.com/science/article/pii/S1319016413001138 >.

AMORIM, R. et al. Monocarboxylate transport inhibition potentiates the cytotoxic effect of 5-fluorouracil in colorectal cancer cells. **Cancer Letters,** v. 365, n. 1, p. 68-78, 2015. ISSN 0304-3835. Disponível em: < http://www.sciencedirect.com/science/article/pii/S0304383515003559 >.

AMORIM, R. et al. Zeolite structures loading with an anticancer compound as drug delivery systems. **The Journal of Physical Chemistry C,** v. 116, n. 48, p. 25642-25650, 2012. ISSN 1932-7447.

ARISTOTLE et al. **Historia animalium**. London; Cambridge, Mass.: Heinemann ; Harvard University Press, 1965. ISBN 0674994817 9780674994812 0674994825 9780674994829 0674994833 9780674994836.

BALTAZAR, F. et al. Monocarboxylate transporters as targets and mediators in cancer therapy response. **Histol Histopathol,** v. 29, n. 12, p. 1511-24, Dec 2014. ISSN 0213-3911.

BANNISTER, T. D. Inhibitors of Lactate Transport: A Promising Approach in Cancer Drug Discovery. 2014. ISSN 0128012382.

BARBI, M. D. S. et al. Preparation and characterization of chitosan nanoparticles for zidovudine nasal delivery. **Journal of nanoscience and nanotechnology,** v. 15, n. 1, p. 865-874, 2015. ISSN 1533-4880.

BARNHOLTZ-SLOAN, J. S.; OSTROM, Q. T.; COTE, D. Epidemiology of Brain Tumors. **Neurologic Clinics**, 2018. ISSN 0733-8619. Disponível em: < http://www.sciencedirect.com/science/article/pii/S0733861918311988 >.

BASSO, J. et al. Repurposing drugs for glioblastoma: From bench to bedside. **Cancer Letters,** v. 428, p. 173-183, 2018. ISSN 0304-3835. Disponível em: < http://www.sciencedirect.com/science/article/pii/S0304383518303124 >.

BEAM, A.; MOTSINGER-REIF, A. Beyond IC50s: towards robust statistical methods for in vitro association studies. **Journal of pharmacogenomics & pharmacoproteomics,** v. 5, n. 1, p. 1000121, 2014.

BECHGAARD, E. et al. The viability of isolated rabbit nasal mucosa in the Ussing chamber, and the permeability of insulin across the membrane. **International Journal of Pharmaceutics,** v. 87, n. 1, p. 125-132, 1992/11/10/ 1992. ISSN 0378-5173. Disponível em: < http://www.sciencedirect.com/science/article/pii/037851739290235T >.

BEGLEY, D. J. Delivery of therapeutic agents to the central nervous system: the problems and the possibilities. **Pharmacology & therapeutics,** v. 104, n. 1, p. 29-45, 2004. ISSN 0163-7258.

BELDA-INIESTA, C. et al. Long term responses with cetuximab therapy in glioblastoma multiforme. **Cancer Biol Ther,** v. 5, n. 8, p. 912-914, 2006. ISSN 1538-4047 (Print) 1538-4047.

BENOIT, J. P. et al. Development of microspheres for neurological disorders: from basics to clinical applications. **J Control Release,** v. 65, n. 1-2, p. 285-296, 2000. ISSN 0168-3659 (Print) 0168-3659.

BHATTACHARJEE, S. DLS and zeta potential–what they are and what they are not? **Journal of Controlled Release,** v. 235, p. 337-351, 2016. ISSN 0168-3659.

BILATI, U.; ALLÉMANN, E.; DOELKER, E. Nanoprecipitation versus emulsion-based techniques for the encapsulation of proteins into biodegradable nanoparticles and process-related stability issues. **Aaps Pharmscitech,** v. 6, n. 4, p. E594-E604, 2005. ISSN 1530-9932.

BINDER, Z. A. et al. Epidermal growth factor receptor extracellular domain mutations in glioblastoma present opportunities for clinical imaging and therapeutic development. **Cancer cell,** v. 34, n. 1, p. 163-177. e7, 2018. ISSN 1535-6108.

BONACCORSO, A. et al. Nose to brain delivery in rats: Effect of surface charge of rhodamine B labeled nanocarriers on brain subregion localization. **Colloids Surf B Biointerfaces,** v. 154, p. 297-306, Mar 18 2017. ISSN 0927-7765.

BOYD, R. D.; PICHAIMUTHU, S. K.; CUENAT, A. New approach to inter-technique comparisons for nanoparticle size measurements; using atomic force microscopy, nanoparticle tracking analysis and dynamic light scattering. **Colloids and Surfaces A: Physicochemical and Engineering Aspects,** v. 387, n. 1-3, p. 35-42, 2011. ISSN 0927-7757.

BRANNON-PEPPAS, L. Recent advances on the use of biodegradable microparticles and nanoparticles in controlled drug delivery. **International Journal of Pharmaceutics,** v. 116, n. 1, p. 1-9, 1995. ISSN 0378-5173. Disponível em: < http://www.sciencedirect.com/science/article/pii/037851739400324X >.

BRAY, F. et al. Global cancer statistics 2018: GLOBOCAN estimates of incidence and mortality worldwide for 36 cancers in 185 countries. **CA: a cancer journal for clinicians,** v. 68, n. 6, p. 394-424, 2018. ISSN 0007-9235.

CAHILL, J. et al. Brain tumor symptoms as antecedents to uncertainty: an integrative review. **J Nurs Scholarsh,** v. 44, n. 2, p. 145-55, Jun 2012. ISSN 1527-6546.

CALDWELL, G. W. et al. The IC(50) concept revisited. **Curr Top Med Chem,** v. 12, n. 11, p. 1282-1290, 2012. ISSN 1568-0266.

CARBINATTO, F. M. et al. Insights into the swelling process and drug release mechanisms from cross-linked pectin/high amylose starch matrices. **Asian Journal of Pharmaceutical Sciences,** v. 9, n. 1, p. 27-34, 2014/02/01/ 2014. ISSN 1818-0876. Disponível em: < http://www.sciencedirect.com/science/article/pii/S1818087613000780 >.

CASETTARI, L.; ILLUM, L. Chitosan in nasal delivery systems for therapeutic drugs. **Journal of Controlled Release,** v. 190, p. 189-200, 2014. ISSN 0168-3659. Disponível em: < http://www.sciencedirect.com/science/article/pii/S0168365914002946 >.

CHAKRAVARTHI, S. S.; ROBINSON, D. H. Enhanced cellular association of paclitaxel delivered in chitosan-PLGA particles. **International Journal of Pharmaceutics,** v. 409, n. 1, p. 111-120, 2011/05/16/ 2011. ISSN 0378-5173. Disponível em: < http://www.sciencedirect.com/science/article/pii/S0378517311001694 >.

CHEN, T. C.; DA FONSECA, C. O. Intranasal Perillyl Alcohol for Glioma Therapy: Molecular Mechanisms and Clinical Development. v. 19, n. 12, Dec 6 2018. ISSN 1422-0067.

CHENG, C. et al. Alterations of monocarboxylate transporter densities during hypoxia in brain and breast tumour cells. **Cellular oncology,** v. 35, n. 3, p. 217-227, 2012. ISSN 2211-3428.

CHENG, Y.; PRUSOFF, W. H. Relationship between the inhibition constant (K1) and the concentration of inhibitor which causes 50 per cent inhibition (I50) of an enzymatic reaction. **Biochem Pharmacol,** v. 22, n. 23, p. 3099-3108, 1973. ISSN 0006-2952 (Print)
0006-2952.

CHU, L. et al. Nose-to-brain delivery of temozolomide-loaded PLGA nanoparticles functionalized with anti-EPHA3 for glioblastoma targeting. **Drug delivery,** v. 25, n. 1, p. 1634-1641, 2018. ISSN 1071-7544.

COELHO, J. F. et al. Drug delivery systems: Advanced technologies potentially applicable in personalized treatments. **EPMA journal,** v. 1, n. 1, p. 164-209, 2010. ISSN 1878-5077.

COLEN, C. B. et al. Metabolic remodeling of malignant gliomas for enhanced sensitization during radiotherapy: an in vitro study. **Neurosurgery,** v. 59, n. 6, p. 1313-1323, 2006. ISSN 0148-396x.

COLEN, C. B. et al. Metabolic targeting of lactate efflux by malignant glioma inhibits invasiveness and induces necrosis: an in vivo study. **Neoplasia,** v. 13, n. 7, p. 620-632, Jul 2011. ISSN 1476-5586.

COMBS, S. E. et al. In Vitro Responsiveness of Glioma Cell Lines to Multimodality Treatment With Radiotherapy, Temozolomide, and Epidermal Growth Factor Receptor Inhibition With Cetuximab. **International Journal of Radiation Oncology • Biology • Physics,** v. 68, n. 3, p. 873-882, 2007. ISSN 0360-3016. Disponível em: < https://doi.org/10.1016/j.ijrobp.2007.03.002 >. Acesso em: 2018/11/30.

COSTANTINO, H. R. et al. Intranasal delivery: physicochemical and therapeutic aspects. **Int J Pharm,** v. 337, n. 1-2, p. 1-24, 2007. ISSN 0378-5173 (Print)
0378-5173.

COUVREUR, P. Polyalkylcyanoacrylates as colloidal drug carriers. **Crit Rev Ther Drug Carrier Syst,** v. 5, n. 1, p. 1-20, 1988. ISSN 0743-4863 (Print)
0743-4863.

CRESPO, I. et al. Molecular and genomic alterations in glioblastoma multiforme. **The American journal of pathology,** v. 185, n. 7, p. 1820-1833, 2015. ISSN 0002-9440.

CROWE, T. P. et al. Mechanism of intranasal drug delivery directly to the brain. **Life sciences,** v. 195, p. 44-52, 2018. ISSN 0024-3205.

CRUCHO, C. I. C.; BARROS, M. T. Polymeric nanoparticles: A study on the preparation variables and characterization methods. **Materials Science and Engineering: C**, 2017. ISSN 0928-4931. Disponível em: < http://www.sciencedirect.com/science/article/pii/S092849311732163X >.

DA FONSECA, C. O. et al. Efficacy of monoterpene perillyl alcohol upon survival rate of patients with recurrent glioblastoma. **Journal of cancer research and clinical oncology,** v. 137, n. 2, p. 287-293, 2011. ISSN 0171-5216.

DAHLMANN, H. A. efficacy of cancer drugs: looking beyond the IC50. **Chem. Res. Toxicol,** v. 26, p. 1776−1777, 2013.

DANHIER, F. et al. PLGA-based nanoparticles: An overview of biomedical applications. **Journal of Controlled Release,** v. 161, n. 2, p. 505-522, 2012. ISSN 0168-3659. Disponível em: < http://www.sciencedirect.com/science/article/pii/S0168365912000752 >.

DE BRITTO, D.; ASSIS, O. B. G. A novel method for obtaining a quaternary salt of chitosan. **Carbohydrate Polymers,** v. 69, n. 2, p. 305-310, 2007. ISSN 0144-8617. Disponível em: < http://www.sciencedirect.com/science/article/pii/S0144861706004851 >.

DE BRITTO, D. et al. N, N, N-trimethyl chitosan nanoparticles as a vitamin carrier system. **Food hydrocolloids,** v. 27, n. 2, p. 487-493, 2012. ISSN 0268-005X.

DE MORAIS RIBEIRO, L. N. et al. Use of nanoparticle concentration as a tool to understand the structural properties of colloids. **Scientific reports,** v. 8, n. 1, p. 1-8, 2018. ISSN 2045-2322.

DE OLIVEIRA JUNIOR, E. R. et al. Increased Nose-to-Brain Delivery of Melatonin Mediated by Polycaprolactone Nanoparticles for the Treatment of Glioblastoma. v. 36, n. 9, p. 131, Jul 1 2019. ISSN 0724-8741.

DEMBERELDORJ, U.; JOO, S.-W. Infrared Spectroscopic Study of α-Cyano-4-hydroxycinnamic Acid on Nanocrystalline TiO 2 Surfaces: Anchoring of Metal-Free Organic Dyes at Photoanodes in Dye-Sensitized Solar Cells. **Bulletin of the Korean Chemical Society,** v. 31, n. 1, p. 116-119, 2010. ISSN 0253-2964.

DERRINGER, G.; SUICH, R. Simultaneous optimization of several response variables. **J Qual Technol** v. 12, n. 4, p. 214–219, 1980.

DES RIEUX, A. et al. Nanoparticles as potential oral delivery systems of proteins and vaccines: a mechanistic approach. **Journal of controlled release,** v. 116, n. 1, p. 1-27, 2006. ISSN 0168-3659.

DIERS, A. R. et al. Pyruvate fuels mitochondrial respiration and proliferation of breast cancer cells: effect of monocarboxylate transporter inhibition. **Biochemical Journal,** v. 444, n. 3, p. 561-571, 2012. ISSN 0264-6021.

DITTMANN, K.; MAYER, C.; RODEMANN, H.-P. Inhibition of radiation-induced EGFR nuclear import by C225 (Cetuximab) suppresses DNA-PK activity. **Radiotherapy and Oncology,** v. 76, n. 2, p. 157-161, 2005. ISSN 0167-8140.

DJUPESLAND, P. G. Nasal drug delivery devices: characteristics and performance in a clinical perspective—a review. **Drug delivery and translational research,** v. 3, n. 1, p. 42-62, 2013. ISSN 2190-393X.

DJUPESLAND, P. G.; MESSINA, J. C.; MAHMOUD, R. A. The nasal approach to delivering treatment for brain diseases: an anatomic, physiologic, and delivery technology overview. **Therapeutic Delivery,** v. 5, n. 6, p. 709-733, 2014. Disponível em: < https://www.future-science.com/doi/abs/10.4155/tde.14.41 >.

DOWNWARD, J.; PARKER, P.; WATERFIELD, M. D. Autophosphorylation sites on the epidermal growth factor receptor. **Nature,** v. 311, p. 483-485, 1984. Disponível em: < https://doi.org/10.1038/311483a0 >.

EDER, K.; KALMAN, B. Molecular heterogeneity of glioblastoma and its clinical relevance. **Pathol Oncol Res,** v. 20, n. 4, p. 777-787, 2014. ISSN 1219-4956.

EL-SAY, K. M.; EL-SAWY, H. S. Polymeric nanoparticles: Promising platform for drug delivery. **International Journal of Pharmaceutics,** v. 528, n. 1, p. 675-691, 2017. ISSN 0378-5173. Disponível em: < http://www.sciencedirect.com/science/article/pii/S0378517317305604 >.

ELLER, J. L. et al. Anti-epidermal growth factor receptor monoclonal antibody cetuximab augments radiation effects in glioblastoma multiforme in vitro and in vivo. **Neurosurgery,** v. 56, n. 1, p. 155-162, 2005. ISSN 0148-396x.

Enzyme inhibitors as drugs / edited by Merton Sandler. Baltimore: University Park Press, 1980. ISBN 0839141300.

FABER, W. M. The nasal mucosa and the subarachnoid space. **American Journal of Anatomy,** v. 62, n. 1, p. 121-148, 1937. ISSN 0002-9106. Disponível em: < https://onlinelibrary.wiley.com/doi/abs/10.1002/aja.1000620106 >.

FERREIRA, L. M. B. et al. Exploiting supramolecular interactions to produce bevacizumab-loaded nanoparticles for potential mucosal delivery. **European Polymer Journal,** v. 103, p. 238-250, 2018/06/01/ 2018. ISSN 0014-3057. Disponível em: < http://www.sciencedirect.com/science/article/pii/S0014305718304683 >.

FERREIRA, N. N. et al. Alginate hydrogel improves anti-angiogenic bevacizumab activity in cancer therapy. **European Journal of Pharmaceutics and Biopharmaceutics,** v. 119, p. 271-282, 2017. ISSN 0939-6411. Disponível em: < http://www.sciencedirect.com/science/article/pii/S0939641116305628 >.

FILIPE, V.; HAWE, A.; JISKOOT, W. Critical evaluation of Nanoparticle Tracking Analysis (NTA) by NanoSight for the measurement of nanoparticles and protein aggregates. **Pharmaceutical research,** v. 27, n. 5, p. 796-810, 2010. ISSN 0724-8741.

FINE, H. A. New strategies in glioblastoma: exploiting the new biology. **Clinical Cancer Research**, p. 1984-1988, 2015. ISSN 1078-0432.

FRIEDMAN, H. S.; KERBY, T.; CALVERT, H. Temozolomide and treatment of malignant glioma. **Clinical cancer research,** v. 6, n. 7, p. 2585-2597, 2000. ISSN 1078-0432.

FU, J. et al. Overcoming cetuximab resistance in Ewing's sarcoma by inhibiting lactate dehydrogenase-A. **Mol Med Rep,** v. 14, n. 1, p. 995-1001, 2016. ISSN 1791-2997.

FUKAI, J. et al. Antitumor activity of cetuximab against malignant glioma cells overexpressing EGFR deletion mutant variant III. **Cancer Sci,** v. 99, n. 10, p. 2062-9, Oct 2008. ISSN 1347-9032.

G NAVA-ARZALUZ, M. et al. Single emulsion-solvent evaporation technique and modifications for the preparation of pharmaceutical polymeric nanoparticles. **Recent patents on drug delivery & formulation,** v. 6, n. 3, p. 209-223, 2012. ISSN 1872-2113.

GAO, X. et al. Brain delivery of vasoactive intestinal peptide enhanced with the nanoparticles conjugated with wheat germ agglutinin following intranasal administration. **J Control Release,** v. 121, n. 3, p. 156-167, 2007. ISSN 0168-3659.

GARTZIANDIA, O. et al. Nanoparticle transport across in vitro olfactory cell monolayers. **International journal of pharmaceutics,** v. 499, n. 1-2, p. 81-89, 2016. ISSN 0378-5173.

GATELY, L. et al. Long-term survivors of glioblastoma: a closer look. **J Neurooncol,** v. 136, n. 1, p. 155-162, 2018. ISSN 0167-594x.

GATENBY, R. A.; GILLIES, R. J. Why do cancers have high aerobic glycolysis? **Nature reviews Cancer,** v. 4, n. 11, p. 891-899, 2004. ISSN 1474-175X (Print)1474-175x.

GAUMET, M. et al. Nanoparticles for drug delivery: the need for precision in reporting particle size parameters. **European journal of pharmaceutics and biopharmaceutics,** v. 69, n. 1, p. 1-9, 2008. ISSN 0939-6411.

GILLIES, R. J.; ROBEY, I.; GATENBY, R. A. Causes and consequences of increased glucose metabolism of cancers. **J Nucl Med,** v. 49 Suppl 2, p. 24s-42s, 2008. ISSN 0161-5505 (Print) 0161-5505.

GOLAY, J.; INTRONA, M. Mechanism of action of therapeutic monoclonal antibodies: Promises and pitfalls of in vitro and in vivo assays. **Archives of Biochemistry and Biophysics,** v. 526, n. 2, p. 146-153, 2012/10/15/ 2012. ISSN 0003-9861. Disponível em: < http://www.sciencedirect.com/science/article/pii/S0003986112000628 >.

GONÇALVES, V. M.; BALTAZAR, F.; REIS, R. M. Brain Tumor Metabolism—Unraveling Its Role in Finding New Therapeutic Targets. In: (Ed.). **Molecular considerations and evolving surgical management issues in the treatment of patients with a brain tumor**: InTech, 2015.

GRANJA, S. et al. Value of pH regulators in the diagnosis, prognosis and treatment of cancer. **Seminars in Cancer Biology,** v. 43, p. 17-34, 2017. ISSN 1044-579X. Disponível em: < http://www.sciencedirect.com/science/article/pii/S1044579X16300815 >.

GREENING, D. W. et al. Molecular profiling of cetuximab and bevacizumab treatment of colorectal tumours reveals perturbations in metabolic and hypoxic response pathways. **Oncotarget,** v. 6, n. 35, p. 38166-38180, 2015. ISSN 1949-2553.

GUILE, S. D. et al. Potent blockers of the monocarboxylate transporter MCT1: Novel immunomodulatory compounds. **Bioorganic & Medicinal Chemistry Letters,** v. 16, n. 8, p. 2260-2265, 2006. ISSN 0960-894X. Disponível em: < http://www.sciencedirect.com/science/article/pii/S0960894X06000448 >.

GUMIŃSKA, M.; IGNACAK, J.; WOJCIK, E. In vitro inhibitory effect of chitosan and its degradation products on energy metabolism in Ehrlich ascites tumour cells (EAT). **Polish journal of pharmacology,** v. 48, n. 5, p. 495-501, 1996. ISSN 1230-6002.

GURRAPU, S. et al. Monocarboxylate transporter 1 inhibitors as potential anticancer agents. **ACS Med Chem Lett,** v. 6, n. 5, p. 558-561, 2015. ISSN 1948-5875.

GURRAPU, S. et al. Coumarin carboxylic acids as monocarboxylate transporter 1 inhibitors: In vitro and in vivo studies as potential anticancer agents. **Bioorganic & medicinal chemistry letters,** v. 26, n. 14, p. 3282-3286, 2016. ISSN 0960-894X.

HALATSCH, M.-E.et al. Epidermal growth factor receptor inhibition for the treatment of glioblastoma multiforme and other malignant brain tumours. **Cancer Treatment Reviews,** v. 32, n. 2, p. 74-89, 2006. ISSN 0305-7372. Disponível em: < http://www.sciencedirect.com/science/article/pii/S0305737206000090 >.

HALESTRAP, A. P.; DENTON, R. M. Specific inhibition of pyruvate transport in rat liver mitochondria and human erythrocytes by alpha-cyano-4-hydroxycinnamate. **Biochem J,** v. 138, n. 2, p. 313-6, Feb 1974. ISSN 0264-6021 (Print) 0264-6021.

HALESTRAP, A. P.; PRICE, N. T. The proton-linked monocarboxylate transporter (MCT) family: structure, function and regulation. **The Biochemical journal,** v. 343 Pt 2, p. 281-299, 1999. ISSN 0264-6021 (Print)
0264-6021.

HANAHAN, D.; WEINBERG, R. A. Hallmarks of cancer: the next generation. **Cell,** v. 144, n. 5, p. 646-674, 2011. ISSN 0092-8674.

HAQUE, S. et al. Development and evaluation of brain targeted intranasal alginate nanoparticles for treatment of depression. **J Psychiatr Res,** v. 48, n. 1, p. 1-12, 2014. ISSN 0022-3956.

HELFAND, W. H.; COWEN, D. L. Evolution of pharmaceutical oral dosage forms. **Pharmacy in history,** v. 25, n. 1, p. 3-18, 1983. ISSN 0031-7047.

HICKS, M. J. et al. Anti-Epidermal Growth Factor Receptor Gene Therapy for Glioblastoma. **PLoS One,** v. 11, n. 10, p. e0162978, 2016. ISSN 1932-6203.

HOFFMAN, A. S. The origins and evolution of "controlled" drug delivery systems. **Journal of Controlled Release,** v. 132, n. 3, p. 153-163, 2008. ISSN 0168-3659. Disponível em: < http://www.sciencedirect.com/science/article/pii/S0168365908004690 >.

HSU, S. P. C. et al. Temozolomide, sirolimus and chloroquine is a new therapeutic combination that synergizes to disrupt lysosomal function and cholesterol homeostasis in GBM cells. **Oncotarget,** v. 9, n. 6, p. 6883-6896, Jan 23 2018. ISSN 1949-2553.

HUMBLET, Y. Cetuximab: an IgG(1) monoclonal antibody for the treatment of epidermal growth factor receptor-expressing tumours. **Expert Opin Pharmacother,** v. 5, n. 7, p. 1621-1633, 2004. ISSN 1465-6566 (Print)
1465-6566.

IZUMI, H. et al. Cellular pH regulators: potentially promising molecular targets for cancer chemotherapy. **Cancer treatment reviews,** v. 29, n. 6, p. 541-549, 2003. ISSN 0305-7372 (Print)
0305-7372.

JACOB, J. et al. Biopolymer based nanomaterials in drug delivery systems: A review. **Materials Today Chemistry,** v. 9, p. 43-55, 2018. ISSN 2468-5194. Disponível em: < http://www.sciencedirect.com/science/article/pii/S2468519418300880 >.

JAVIA, A.; THAKKAR, H. Intranasal delivery of tapentadol hydrochloride-loaded chitosan nanoparticles: formulation, characterisation and its in vivo evaluation. **J Microencapsul,** v. 34, n. 7, p. 644-658, Nov 2017. ISSN 0265-2048.

KAMIYA-MATSUOKA, C.; GILBERT, M. R. Treating recurrent glioblastoma: an update. **CNS Oncol,** v. 4, n. 2, p. 91-104, 2015. ISSN 2045-0907.

KANG, B.-S. et al. Enhancing the in vitro anticancer activity of albendazole incorporated into chitosan-coated PLGA nanoparticles. **Carbohydrate polymers,** v. 159, p. 39-47, 2017. ISSN 0144-8617.

KARSY, M. et al. Surgical treatment of glioblastoma in the elderly: the impact of complications. **Journal of Neuro-Oncology**, 2018. ISSN 1573-7373. Disponível em: < https://doi.org/10.1007/s11060-018-2777-9 >.

KARSY, M. et al. Surgical treatment of glioblastoma in the elderly: the impact of complications. v. 138, n. 1, p. 123-132, 2018. ISSN 0167-594x.

KASZUBA, M. et al. High-concentration zeta potential measurements using light-scattering techniques. **Philos Trans A Math Phys Eng Sci,** v. 368, n. 1927, p. 4439-4451, 2010. ISSN 1364-503X (Print)
1364-503x.

KELLER, S.; SCHMIDT, M. H. H. EGFR and EGFRvIII Promote Angiogenesis and Cell Invasion in Glioblastoma: Combination Therapies for an Effective Treatment. **Int J Mol Sci,** v. 18, n. 6, 2017. ISSN 1422-0067.

KESTENS, V. et al. Validation of a particle tracking analysis method for the size determination of nano- and microparticles. **Journal of Nanoparticle Research,** v. 19, n. 8, p. 271, 2017/08/04 2017. ISSN 1572-896X. Disponível em: < https://doi.org/10.1007/s11051-017-3966-8 >.

KIM, H. S. et al. Carbohydrate restriction and lactate transporter inhibition in a mouse xenograft model of human prostate cancer. **BJU international,** v. 110, n. 7, p. 1062-1069, 2012. ISSN 1464-4096.

KLANG, V. et al. Electron microscopy of nanoemulsions: An essential tool for characterisation and stability assessment. **Micron,** v. 43, n. 2, p. 85-103, 2012. ISSN 0968-4328. Disponível em: < http://www.sciencedirect.com/science/article/pii/S0968432811001235 >.

KLANG, V.; VALENTA, C.; MATSKO, N. B. Electron microscopy of pharmaceutical systems. **Micron,** v. 44, p. 45-74, 2013. ISSN 0968-4328. Disponível em: < http://www.sciencedirect.com/science/article/pii/S0968432812002156 >.

KORSMEYER, R. W. et al. Mechanisms of solute release from porous hydrophilic polymers. **International Journal of Pharmaceutics,** v. 15, n. 1, p. 25-35, 1983. ISSN 0378-5173. Disponível em: < http://www.sciencedirect.com/science/article/pii/0378517383900649 >.

KOST, J.; LANGER, R. Responsive polymeric delivery systems. **Advanced drug delivery reviews,** v. 64, p. 327-341, 2012. ISSN 0169-409X.

KULKARNI, A. D. et al. N,N,N-Trimethyl chitosan: An advanced polymer with myriad of opportunities in nanomedicine. **Carbohydrate Polymers,** v. 157, p. 875-902, 2017. ISSN 0144-8617. Disponível em: < http://www.sciencedirect.com/science/article/pii/S0144861716312036 >.

KUMAR, M. et al. Evaluation of neuropeptide loaded trimethyl chitosan nanoparticles for nose to brain delivery. **International Journal of Biological Macromolecules,** v. 61, p. 189-195, 2013/10/01/ 2013. ISSN 0141-8130. Disponível em: < http://www.sciencedirect.com/science/article/pii/S0141813013003693 >.

LALATSA, A.; BARBU, E. Carbohydrate Nanoparticles for Brain Delivery. **Int Rev Neurobiol,** v. 130, p. 115-153, 2016. ISSN 0074-7742 (Print)
0074-7742.

LANGENBUCHER, F. Linearization of dissolution rate curves by the Weibull distribution. **J Pharm Pharmacol,** v. 24, n. 12, p. 979-81, Dec 1972. ISSN 0022-3573 (Print)
0022-3573.

LAPOINTE, S.; PERRY, A.; BUTOWSKI, N. A. Primary brain tumours in adults. **The Lancet,** v. 392, n. 10145, p. 432-446, 2018/08/04/ 2018. ISSN 0140-6736. Disponível em: < http://www.sciencedirect.com/science/article/pii/S0140673618309905 >.

LEE, C. Y.; OOI, I. H. Preparation of Temozolomide-Loaded Nanoparticles for Glioblastoma Multiforme Targeting-Ideal Versus Reality. **Pharmaceuticals (Basel),** v. 9, n. 3, Sep 8 2016. ISSN 1424-8247 (Print)
1424-8247.

LI, H. et al. Resveratrol sensitizes glioblastoma-initiating cells to temozolomide by inducing cell apoptosis and promoting differentiation. **Oncology reports,** v. 35, n. 1, p. 343-351, 2016. ISSN 1021-335X.

LINLIN, Z.; KYUSIK, Y. Fluorometric 'switch-on' detection of heparin based on a system composed of rhodamine-labeled chitosan oligosaccharide lactate, and graphene oxide. **Methods and Applications in Fluorescence,** v. 6, n. 3, p. 035011, 2018. ISSN 2050-6120. Disponível em: < http://stacks.iop.org/2050-6120/6/i=3/a=035011 >.

LIU, J. et al. Synthesis, characterization, bioactivity and potential application of phenolic acid grafted chitosan: A review. **Carbohydrate polymers,** v. 174, p. 999-1017, 2017. ISSN 0144-8617.

LIU, Q.; ZHANG, Q. 10 - Nanoparticle systems for nose-to-brain delivery. In: GAO, H. e GAO, X. (Ed.). **Brain Targeted Drug Delivery System**: Academic Press, 2019. p.219-239. ISBN 978-0-12-814001-7.

LIU, Y.-J. et al. Combination therapy with micellarized cyclopamine and temozolomide attenuate glioblastoma growth through Gli1 down-regulation. **Oncotarget,** v. 8, n. 26, p. 42495-42509, 2017.

LU, H. et al. Cetuximab reverses the Warburg effect by inhibiting HIF-1-regulated LDH-A. **Mol Cancer Ther,** v. 12, n. 10, p. 2187-2199, 2013. ISSN 1535-7163.

LUO, J. et al. Acetyl-CoA carboxylase rewires cancer metabolism to allow cancer cells to survive inhibition of the Warburg effect by cetuximab. **Cancer Lett,** v. 384, p. 39-49, 2017. ISSN 0304-3835.

LUWOR, R. B. et al. The antiepidermal growth factor receptor monoclonal antibody cetuximab/C225 reduces hypoxia-inducible factor-1 alpha, leading to transcriptional inhibition of vascular endothelial growth factor expression. **Oncogene,** v. 24, n. 27, p. 4433, 2005. ISSN 1476-5594.

LV, S. et al. Correlation of EGFR, IDH1 and PTEN status with the outcome of patients with recurrent glioblastoma treated in a phase II clinical trial with the EGFR-blocking monoclonal antibody cetuximab. **International journal of oncology,** v. 41, n. 3, p. 1029-1035, 2012. ISSN 1019-6439.

MA, D. J. et al. A phase II trial of everolimus, temozolomide, and radiotherapy in patients with newly diagnosed glioblastoma: NCCTG N057K. **Neuro Oncol,** v. 17, n. 9, p. 1261-1269, Sep 2015. ISSN 1522-8517.

MAHER, E. A. et al. Malignant glioma: genetics and biology of a grave matter. **Genes & development,** v. 15, n. 11, p. 1311-1333, 2001. ISSN 0890-9369 (Print)
0890-9369.

MAINARDES, R. M.; SILVA, L. P. Drug delivery systems: past, present, and future. **Current drug targets,** v. 5, n. 5, p. 449-455, 2004. ISSN 1389-4501.

MALHOTRA, M. et al. Development and characterization of chitosan-PEG-TAT nanoparticles for the intracellular delivery of siRNA. **Int J Nanomedicine,** v. 8, p. 2041-2052, 2013. ISSN 1176-9114.

MANJAPPA, A. S. et al. Antibody derivatization and conjugation strategies: Application in preparation of stealth immunoliposome to target chemotherapeutics to tumor. **Journal of Controlled Release,** v. 150, n. 1, p. 2-22, 2011. ISSN 0168-3659. Disponível em: < http://www.sciencedirect.com/science/article/pii/S016836591000903X >.

MARTÍNEZ RIVAS, C. J. et al. Nanoprecipitation process: From encapsulation to drug delivery. **International Journal of Pharmaceutics,** v. 532, n. 1, p. 66-81, 2017/10/30/ 2017. ISSN 0378-5173. Disponível em: < http://www.sciencedirect.com/science/article/pii/S0378517317307718 >.

MARTINHO, O. et al. Downregulation of RKIP Is Associated with Poor Outcome and Malignant Progression in Gliomas. **PLoS ONE,** v. 7, n. 1, p. e30769, 2012. Disponível em: < http://dx.doi.org/10.1371%2Fjournal.pone.0030769 >.

MARTINHO, O. et al. HER Family Receptors are Important Theranostic Biomarkers for Cervical Cancer: Blocking Glucose Metabolism Enhances the Therapeutic Effect of HER Inhibitors. **Theranostics**, Sydney**,** v. 7, n. 3, p. 717-732, 2017. ISSN 1838-7640. Disponível em: < http://www.ncbi.nlm.nih.gov/pmc/articles/PMC5327645/ >.

MARTINHO, O. et al. In Vitro and In Vivo Analysis of RTK Inhibitor Efficacy and Identification of Its Novel Targets in Glioblastomas. **Translational oncology,** v. 6, n. 2, p. 187-196, 2013. ISSN 1936-5233.

MATHUPALA, S. P.; PARAJULI, P.; SLOAN, A. E. Silencing of monocarboxylate transporters via small interfering ribonucleic acid inhibits glycolysis and induces cell death in malignant glioma: an in vitro study. **Neurosurgery,** v. 55, n. 6, p. 1410-1419, 2004. ISSN 0148-396x.

MAURIZ, J. L.; GONZÁLEZ-GALLEGO, J. Antiangiogenic Drugs: Current Knowledge and New Approaches to Cancer Therapy. **Journal of Pharmaceutical Sciences,** v. 97, n. 10, p. 4129-4154,

2008. ISSN 0022-3549. Disponível em: < http://www.sciencedirect.com/science/article/pii/S0022354916327290 >.

MCMARTIN, C. et al. Analysis of Structural Requirements for the Absorption of Drugs and Macromolecules from the Nasal Cavity. **Journal of Pharmaceutical Sciences,** v. 76, n. 7, p. 535-540, 1987/07/01/ 1987. ISSN 0022-3549. Disponível em: < http://www.sciencedirect.com/science/article/pii/S0022354915474659 >.

MENG, Q. et al. Intranasal delivery of Huperzine A to the brain using lactoferrin-conjugated N-trimethylated chitosan surface-modified PLGA nanoparticles for treatment of Alzheimer's disease. **International journal of nanomedicine,** v. 13, p. 705-718, 2018. ISSN 1178-2013 1176-9114. Disponível em: < https://pubmed.ncbi.nlm.nih.gov/29440896 https://www.ncbi.nlm.nih.gov/pmc/articles/PMC5798568/ >.

MESSAOUDI, K.; CLAVREUL, A.; LAGARCE, F. Toward an effective strategy in glioblastoma treatment. Part I: resistance mechanisms and strategies to overcome resistance of glioblastoma to temozolomide. **Drug Discovery Today,** v. 20, n. 7, p. 899-905, 2015. ISSN 1359-6446. Disponível em: < http://www.sciencedirect.com/science/article/pii/S135964461500080X >.

MIGLIORE, M. M. et al. Brain delivery of proteins by the intranasal route of administration: a comparison of cationic liposomes versus aqueous solution formulations. **Journal of pharmaceutical sciences,** v. 99, n. 4, p. 1745-1761, 2010. ISSN 0022-3549.

MIR, M.; AHMED, N.; REHMAN, A. U. Recent applications of PLGA based nanostructures in drug delivery. **Colloids and Surfaces B: Biointerfaces,** v. 159, p. 217-231, 2017. ISSN 0927-7765. Disponível em: < http://www.sciencedirect.com/science/article/pii/S0927776517304502 >.

MIRANDA-GONCALVES, V. et al. Metabolic alterations underlying Bevacizumab therapy in glioblastoma cells. **Oncotarget,** v. 8, n. 61, p. 103657-103670, 2017. ISSN 1949-2553.

MIRANDA-GONCALVES, V. et al. Monocarboxylate transporters (MCTs) in gliomas: expression and exploitation as therapeutic targets. **Neuro-oncology,** v. 15, n. 2, p. 172-188, 2013. ISSN 1522-8517.

MITTAL, D. et al. Insights into direct nose to brain delivery: current status and future perspective. **Drug Deliv,** v. 21, n. 2, p. 75-86, Mar 2014. ISSN 1071-7544.

MOJICA, E.-R. E.; VEDAD, J.; DESAMERO, R. Z. B. Vibrational analysis of α-cyanohydroxycinnamic acid. **Journal of Molecular Structure,** v. 1094, p. 203-209, 2015. ISSN 0022-2860. Disponível em: < http://www.sciencedirect.com/science/article/pii/S0022286015002914 >.

MORA-HUERTAS, C. E. et al. Nanocapsules prepared via nanoprecipitation and emulsification–diffusion methods: Comparative study. **European Journal of Pharmaceutics and Biopharmaceutics,** v. 80, n. 1, p. 235-239, 2012. ISSN 0939-6411.

MORTENSEN, J. H. et al. Targeted antiepidermal growth factor receptor (cetuximab) immunoliposomes enhance cellular uptake in vitro and exhibit increased accumulation in an

intracranial model of glioblastoma multiforme. **Journal of drug delivery,** v. 2013, p. 205-209, 2013. ISSN 2090-3014 (Print)
2090-3022.

MOSMANN, T. Rapid colorimetric assay for cellular growth and survival: Application to proliferation and cytotoxicity assays. **Journal of Immunological Methods,** v. 65, n. 1, p. 55-63, 1983 1983. ISSN 0022-1759. Disponível em: < http://www.sciencedirect.com/science/article/pii/0022175983903034 >.

MOURYA, V.; INAMDAR, N. N. Trimethyl chitosan and its applications in drug delivery. **Journal of Materials Science: Materials in Medicine,** v. 20, n. 5, p. 1057, 2009. ISSN 0957-4530.

MUANPRASAT, C.; CHATSUDTHIPONG, V. Chitosan oligosaccharide: Biological activities and potential therapeutic applications. **Pharmacology & Therapeutics,** v. 170, n. Supplement C, p. 80-97, 2017/02/01/ 2017. ISSN 0163-7258. Disponível em: < http://www.sciencedirect.com/science/article/pii/S0163725816301929 >.

NAAHIDI, S. et al. Biocompatibility of engineered nanoparticles for drug delivery. **Journal of Controlled Release,** v. 166, n. 2, p. 182-194, 2013. ISSN 0168-3659. Disponível em: < http://www.sciencedirect.com/science/article/pii/S0168365912008553 >.

NAGAVARMA, B. et al. Different techniques for preparation of polymeric nanoparticles-a review. **Asian J. Pharm. Clin. Res,** v. 5, n. 3, p. 16-23, 2012.

NASKAR, S.; SHARMA, S.; KUOTSU, K. Chitosan-based nanoparticles: An overview of biomedical applications and its preparation. **Journal of Drug Delivery Science and Technology,** v. 49, p. 66-81, 2019. ISSN 1773-2247. Disponível em: < http://www.sciencedirect.com/science/article/pii/S1773224718306026 >.

NAVEED, M. et al. Chitosan oligosaccharide (COS): An overview. **International Journal of Biological Macromolecules**, 2019/01/29/ 2019. ISSN 0141-8130. Disponível em: < http://www.sciencedirect.com/science/article/pii/S0141813018354527 >.

NEL, A. E. et al. Understanding biophysicochemical interactions at the nano-bio interface. **Nature Materials,** v. 8, n. 7, p. 543-557, 2009. Disponível em: < http://dx.doi.org/10.1038/nmat2442 >.

NIGAM, K. et al. Nose-to-brain delivery of lamotrigine-loaded PLGA nanoparticles. **Drug delivery and translational research**, p. 1-12, 2019. ISSN 2190-393X.

OMURO, A.; DEANGELIS, L. M. Glioblastoma and other malignant gliomas: a clinical review. **Jama,** v. 310, n. 17, p. 1842-1850, 2013. ISSN 0098-7484.

ORELLANA, E. A.; KASINSKI, A. L. Sulforhodamine B (SRB) Assay in Cell Culture to Investigate Cell Proliferation. **Bio-protocol,** v. 6, n. 21, p. e1984, 2016. ISSN 2331-8325. Disponível em: < http://www.ncbi.nlm.nih.gov/pmc/articles/PMC5448418/ >.

OSTROM, Q. T. et al. CBTRUS Statistical Report: Primary brain and other central nervous system tumors diagnosed in the United States in 2010–2014. **Neuro-Oncology,** v. 19, n. suppl_5, p. v1-

v88, 2017. ISSN 1522-8517. Disponível em: < https://doi.org/10.1093/neuonc/nox158 >. Acesso em: 6/3/2019.

PAPADOPOULOU, V. et al. On the use of the Weibull function for the discernment of drug release mechanisms. **International Journal of Pharmaceutics,** v. 309, n. 1, p. 44-50, 2006/02/17/ 2006. ISSN 0378-5173. Disponível em: < http://www.sciencedirect.com/science/article/pii/S0378517305007672 >.

PARK, A. K. et al. Constitutive asymmetric dimerization drives oncogenic activation of epidermal growth factor receptor carboxyl-terminal deletion mutants. **Oncotarget,** v. 6, n. 11, p. 8839-8850, 2015. ISSN 1949-2553.

PARK, J. K. et al. Effects of the molecular weight and the degree of deacetylation of chitosan oligosaccharides on antitumor activity. **Int J Mol Sci,** v. 12, n. 1, p. 266-77, Jan 6 2011. ISSN 1422-0067.

PARK, K. Facing the truth about nanotechnology in drug delivery. **ACS nano,** v. 7, n. 9, p. 7442-7447, 2013. ISSN 1936-0851.

PARK K.. Controlled drug delivery systems: Past forward and future back. **Journal of Controlled Release,** v. 190, p. 3-8, 2014. ISSN 0168-3659. Disponível em: < http://www.sciencedirect.com/science/article/pii/S0168365914002508 >.

PEPPAS, N. A. Historical perspective on advanced drug delivery: How engineering design and mathematical modeling helped the field mature. **Advanced Drug Delivery Reviews,** v. 65, n. 1, p. 5-9, 2013. ISSN 0169-409X. Disponível em: < http://www.sciencedirect.com/science/article/pii/S0169409X12003018 >.

PEPPAS, N. A.; NARASIMHAN, B. Mathematical models in drug delivery: how modeling has shaped the way we design new drug delivery systems. **J Control Release,** v. 190, p. 75-81, 2014. ISSN 0168-3659.

PÉREZ-ESCUREDO, J. et al. Monocarboxylate transporters in the brain and in cancer. **Biochimica et Biophysica Acta (BBA)-Molecular Cell Research,** v. 1863, n. 10, p. 2481-2497, 2016. ISSN 0167-4889.

PÉRTEGA-GOMES, N.; BALTAZAR, F. Lactate transporters in the context of prostate cancer metabolism: what do we know? **International journal of molecular sciences,** v. 15, n. 10, p. 18333-18348, 2014.

PETIT, A. M. et al. Neutralizing antibodies against epidermal growth factor and ErbB-2/neu receptor tyrosine kinases down-regulate vascular endothelial growth factor production by tumor cells in vitro and in vivo: angiogenic implications for signal transduction therapy of solid tumors. **Am J Pathol,** v. 151, n. 6, p. 1523-1530, 1997. ISSN 0002-9440 (Print)
0002-9440.

PIAZZINI, V. et al. Chitosan coated human serum albumin nanoparticles: A promising strategy for nose-to-brain drug delivery. **International Journal of Biological Macromolecules,** v. 129, p. 267-

280, 2019/05/15/ 2019. ISSN 0141-8130. Disponível em: < http://www.sciencedirect.com/science/article/pii/S014181301836923X >.

PIERRE, K.; PELLERIN, L. Monocarboxylate transporters in the central nervous system: distribution, regulation and function. **Journal of neurochemistry,** v. 94, n. 1, p. 1-14, 2005. ISSN 0022-3042.

PINTO REIS, C. et al. Nanoencapsulation I. Methods for preparation of drug-loaded polymeric nanoparticles. **Nanomedicine: Nanotechnology, Biology and Medicine,** v. 2, n. 1, p. 8-21, 2006. ISSN 1549-9634. Disponível em: < http://www.sciencedirect.com/science/article/pii/S1549963406000050 >.

PORTNOW, J. et al. The neuropharmacokinetics of temozolomide in patients with resectable brain tumors: potential implications for the current approach to chemoradiation. **Clin Cancer Res,** v. 15, n. 22, p. 7092-8, Nov 15 2009. ISSN 1078-0432 (Print)
1078-0432.

POURGHOLI, F. et al. Nanoparticles: Novel vehicles in treatment of Glioblastoma. **Biomed Pharmacother,** v. 77, p. 98-107, Feb 2016. ISSN 0753-3322.

QUINTANA, D. S.; WESTLYE, L. T. Low-dose intranasal oxytocin delivered with Breath Powered device modulates pupil diameter and amygdala activity: a randomized controlled pupillometry and fMRI study. v. 44, n. 2, p. 306-313, Jan 2019. ISSN 0893-133x.

QURESHI, M. et al. Formulation and Evaluation of Neuroactive Drug Loaded Chitosan Nanoparticle for Nose to Brain Delivery: In-vitro Characterization and In-vivo Behavior Study. **Curr Drug Deliv,** v. 16, n. 2, p. 123-135, 2019. ISSN 1567-2018.

RANA, V.; SHARMA, R. Chapter 5 - Recent Advances in Development of Nano Drug Delivery. In: MOHAPATRA, S. S.;RANJAN, S., *et al* (Ed.). **Applications of Targeted Nano Drugs and Delivery Systems**: Elsevier, 2019. p.93-131. ISBN 978-0-12-814029-1.

RAO, J. P.; GECKELER, K. E. Polymer nanoparticles: Preparation techniques and size-control parameters. **Progress in Polymer Science,** v. 36, n. 7, p. 887-913, 2011. ISSN 0079-6700. Disponível em: < http://www.sciencedirect.com/science/article/pii/S0079670011000232 >.

REILLY, E. B. et al. Characterization of ABT-806, a Humanized Tumor-Specific Anti-EGFR Monoclonal Antibody. **Molecular cancer therapeutics,** v. 14, n. 5, p. 1141-1151, 2015. ISSN 1535-7163.

RINAUDO, M. Chitin and chitosan: Properties and applications. **Progress in Polymer Science,** v. 31, n. 7, p. 603-632, 2006. ISSN 0079-6700. Disponível em: < http://www.sciencedirect.com/science/article/pii/S0079670006000530 >.

RINAUDO, M. Main properties and current applications of some polysaccharides as biomaterials. **Polymer International,** v. 57, n. 3, p. 397-430, 2008. ISSN 1097-0126. Disponível em: < http://dx.doi.org/10.1002/pi.2378 >.

RODERO, C. F. et al. Curcumin-Loaded Liquid Crystalline Systems for Controlled Drug Release and Improved Treatment of Vulvovaginal Candidiasis. v. 15, n. 10, p. 4491-4504, Oct 1 2018. ISSN 1543-8384.

ROMEO, V. D. et al. Effects of physicochemical properties and other factors on systemic nasal drug delivery. **Adv Drug Deliv Rev,** v. 29, n. 1-2, p. 89-116, 1998. ISSN 0169-409x.

ROSKOSKI, R. The ErbB/HER family of protein-tyrosine kinases and cancer. **Pharmacological Research,** v. 79, p. 34-74, 2014. ISSN 1043-6618. Disponível em: < http://www.sciencedirect.com/science/article/pii/S1043661813001771 >.

SAFDAR, R. et al. Potential of Chitosan and its derivatives for controlled drug release applications – A review. **Journal of Drug Delivery Science and Technology,** v. 49, p. 642-659, 2019. ISSN 1773-2247. Disponível em: < http://www.sciencedirect.com/science/article/pii/S1773224718307901 >.

SAKANE, T. et al. Transport of cephalexin to the cerebrospinal fluid directly from the nasal cavity. **Journal of Pharmacy and Pharmacology,** v. 43, n. 6, p. 449-451, 1991. ISSN 0022-3573. Disponível em: < https://onlinelibrary.wiley.com/doi/abs/10.1111/j.2042-7158.1991.tb03510.x >.

SALADE, L. et al. How to characterize a nasal product. The state of the art of in vitro and ex vivo specific methods. **International Journal of Pharmaceutics,** v. 561, p. 47-65, 2019/04/20/ 2019. ISSN 0378-5173. Disponível em: < http://www.sciencedirect.com/science/article/pii/S0378517319301498 >.

SALAMANCA, C. H.; BARRERA-OCAMPO, A. Franz Diffusion Cell Approach for Pre-Formulation Characterisation of Ketoprofen Semi-Solid Dosage Forms. v. 10, n. 3, Sep 5 2018. ISSN 1999-4923 (Print)
1999-4923.

SAMARIDOU, E.; ALONSO, M. J. Nose-to-brain peptide delivery – The potential of nanotechnology. **Bioorganic & Medicinal Chemistry,** v. 26, n. 10, p. 2888-2905, 2018. ISSN 0968-0896. Disponível em: < http://www.sciencedirect.com/science/article/pii/S0968089617317273 >.

SANNA, V. et al. Development of novel cationic chitosan-and anionic alginate-coated poly(D,L-lactide-co-glycolide) nanoparticles for controlled release and light protection of resveratrol. **Int J Nanomedicine,** v. 7, p. 5501-5516, 2012. ISSN 1176-9114.

SCHUBERT, S.; DELANEY JR, J. T.; SCHUBERT, U. S. Nanoprecipitation and nanoformulation of polymers: from history to powerful possibilities beyond poly (lactic acid). **Soft Matter,** v. 7, n. 5, p. 1581-1588, 2011.

SEMENZA, G. L. Tumor metabolism: cancer cells give and take lactate. **The Journal of clinical investigation,** v. 118, n. 12, p. 3835-3837, 2008. ISSN 0021-9738.

SHAH, A. H. et al. Recognizing and correcting failures in glioblastoma treatment. **Cancer Invest,** v. 32, n. 6, p. 299-302, 2014. ISSN 0735-7907.

SHARMA, S. et al. PLGA-based nanoparticles: A new paradigm in biomedical applications. **TrAC Trends in Analytical Chemistry,** v. 80, p. 30-40, 2016. ISSN 0165-9936.

SHEN, K.-T. et al. Inhibitory effects of chitooligosaccharides on tumor growth and metastasis. **Food and chemical toxicology,** v. 47, n. 8, p. 1864-1871, 2009. ISSN 0278-6915.

SILVA-CORREIA, J. et al. Angiogenic potential of gellan-gum-based hydrogels for application in nucleus pulposus regeneration: in vivo study. **Tissue engineering. Part A,** v. 18, n. 11-12, p. 1203-1212, 2012. ISSN 1937-3341.

SILVA-OLIVEIRA, R. J. et al. AKT can modulate the in vitro response of HNSCC cells to irreversible EGFR inhibitors. **Oncotarget,** v. 8, n. 32, p. 53288-53301, 2017. ISSN 1949-2553.

SKEHAN, P. et al. New Colorimetric Cytotoxicity Assay for Anticancer-Drug Screening. **JNCI: Journal of the National Cancer Institute,** v. 82, n. 13, p. 1107-1112, 1990. ISSN 0027-8874. Disponível em: < http://dx.doi.org/10.1093/jnci/82.13.1107 >.

SONVEAUX, P. et al. Targeting lactate-fueled respiration selectively kills hypoxic tumor cells in mice. **The Journal of Clinical Investigation,** v. 118, n. 12, p. 3930-3942, 2008. ISSN 0021-9738 1558-8238. Disponível em: < http://www.ncbi.nlm.nih.gov/pmc/articles/PMC2582933/ >.

STUPP, R. et al. Current and future developments in the use of temozolomide for the treatment of brain tumours. **Lancet Oncol,** v. 2, n. 9, p. 552-560, Sep 2001. ISSN 1470-2045 (Print) 1470-2045.

STUPP , R. et al. Radiotherapy plus Concomitant and Adjuvant Temozolomide for Glioblastoma. **New England Journal of Medicine,** v. 352, n. 10, p. 987-996, 2005. Disponível em: < http://www.nejm.org/doi/full/10.1056/NEJMoa043330 >.

SU, Y. et al. Selective CD4+ lymphopenia in melanoma patients treated with temozolomide: a toxicity with therapeutic implications. **Journal of Clinical Oncology,** v. 22, n. 4, p. 610-616, 2004. ISSN 0732-183X.

SUKUMAR, U. K. et al. Intranasal delivery of targeted polyfunctional gold-iron oxide nanoparticles loaded with therapeutic microRNAs for combined theranostic multimodality imaging and presensitization of glioblastoma to temozolomide. **Biomaterials,** v. 218, p. 119342, Oct 2019. ISSN 0142-9612.

TABATABAEI, P. et al. Glucose metabolites, glutamate and glycerol in malignant glioma tumours during radiotherapy. **Journal of neuro-oncology,** v. 90, n. 1, p. 35-39, 2008. ISSN 0167-594X.

TAMIMI, A. F.; JUWEID, M. Epidemiology and Outcome of Glioblastoma. In: VLEESCHOUWER, S. D. (Ed.). **Glioblastoma**. Department of Neurosurgery, University Hospitals Leuven, Leuven, Belgium: Codon Publications, 2017.

TAYLOR, T. E.; FURNARI, F. B.; CAVENEE, W. K. Targeting EGFR for treatment of glioblastoma: molecular basis to overcome resistance. **Curr Cancer Drug Targets,** v. 12, n. 3, p. 197-209, 2012. ISSN 1568-0096.

THANOU, M. M. et al. Effects of N-trimethyl chitosan chloride, a novel absorption enhancer, on Caco-2 intestinal epithelia and the ciliary beat frequency of chicken embryo trachea. **International journal of pharmaceutics,** v. 185, n. 1, p. 73-82, 1999. ISSN 0378-5173.

TOLOCHKO, N. History of nanotechnology. Nanoscience and nanotechnology. Encyclopaedia of life Support Systems (EOLSS), Developed under the auspices of the UNESCO, **SEolss Published, oxford**, p. 3-4, 2009.

TONG, G.-F.; QIN, N.; SUN, L.-W. Development and evaluation ofDesvenlafaxine loaded PLGA-chitosan nanoparticles for brain delivery. **Saudi Pharmaceutical Journal,** v. 25, n. 6, p. 844-851, 2017/09/01/ 2017. ISSN 1319-0164. Disponível em: < http://www.sciencedirect.com/science/article/pii/S1319016416301372 >.

TRINH, V. A.; PATEL, S. P.; HWU, W.-J. The safety of temozolomide in the treatment of malignancies. **Expert opinion on drug safety,** v. 8, n. 4, p. 493-499, 2009. ISSN 1474-0338.

TSENG, S.-H.; CHOU, M.-Y.; CHU, I. M. Cetuximab-conjugated iron oxide nanoparticles for cancer imaging and therapy. **International Journal of Nanomedicine,** v. 10, p. 3663-3685, 2015. ISSN 1176-9114
1178-2013. Disponível em: < http://www.ncbi.nlm.nih.gov/pmc/articles/PMC4445874/ >.

TZENG, S. Y.; GREEN, J. J. Therapeutic nanomedicine for brain cancer. **Therapeutic delivery,** v. 4, n. 6, p. 687-704, 2013. ISSN 2041-5990.

VAN DEN EYNDE, M. et al. Epidermal growth factor receptor targeted therapies for solid tumours. **Acta clinica Belgica,** v. 66, n. 1, p. 10-17, 2011. ISSN 1784-3286 (Print)
1784-3286.

VAZ, G. R. et al. Development of Nasal Lipid Nanocarriers Containing Curcumin for Brain Targeting. **J Alzheimers Dis,** v. 59, n. 3, p. 961-974, 2017. ISSN 1387-2877.

VELIZ, I. et al. Advances and challenges in the molecular biology and treatment of glioblastoma—is there any hope for the future? **Annals of Translational Medicine,** v. 3, n. 1, p. 7, 2015. ISSN 2305-5839
2305-5847. Disponível em: < http://www.ncbi.nlm.nih.gov/pmc/articles/PMC4293478/ >.

VELPULA, K. K. et al. Combined targeting of PDK1 and EGFR triggers regression of glioblastoma by reversing the Warburg effect. **Cancer Res,** v. 73, n. 24, p. 7277-7289, 2013. ISSN 0008-5472.

VILAÇA, N. et al. Encapsulation of α-cyano-4-hydroxycinnamic acid into a NaY zeolite. **Journal of Materials Science,** v. 46, n. 23, p. 7511-7516, 2011. ISSN 1573-4803. Disponível em: < http://dx.doi.org/10.1007/s10853-011-5722-2 >.

VINCENZI, B. et al. The biological properties of cetuximab. **Critical Reviews in Oncology/Hematology,** v. 68, n. 2, p. 93-106, 2008. ISSN 1040-8428. Disponível em: < http://www.sciencedirect.com/science/article/pii/S1040842808001467 >.

VINCENZI, B. et al. Cetuximab: from bench to bedside. **Curr Cancer Drug Targets,** v. 10, n. 1, p. 80-95, 2010. ISSN 1568-0096.

VOJNOVIC, D. et al. Simultaneaus Optimization of Several Response Variables in a Granulation Process. **Drug Development and Industrial Pharmacy,** v. 19, n. 12, p. 1479-1496, 1993. ISSN 0363-9045. Disponível em: < http://dx.doi.org/10.3109/03639049309047186 >.

VU-QUANG, H. et al. Chitosan-coated poly (lactic-co-glycolic acid) perfluorooctyl bromide nanoparticles for cell labeling in 19F magnetic resonance imaging. **Carbohydrate polymers,** v. 136, p. 936-944, 2016. ISSN 0144-8617.

WAHL, M. L. et al. Regulation of Intracellular pH in Human Melanoma: Potential Therapeutic Implications 1 Supported by NIH Grant P01 CA56690 (to MLW, RB, CSO, DBL); Grant R25CA48010 from National Cancer Institute, NIH, and Department of Health and Human Services, National Science Foundation MCB RUI Grant 9057010 (to JAO, SSN, RAH); and NIH Grant CA39248 (to DB). 1. **Molecular Cancer Therapeutics,** v. 1, n. 8, p. 617-628, 2002. ISSN 1535-7163.

WANG, Y.; LI, P.; KONG, L. Chitosan-modified PLGA nanoparticles with versatile surface for improved drug delivery. **AAPS PharmSciTech,** v. 14, n. 2, p. 585-592, 2013. ISSN 1530-9932.

WANG, Z. et al. N-acetylchitooligosaccharide is a potent angiogenic inhibitor both in vivo and in vitro. **Biochem Biophys Res Commun,** v. 357, n. 1, p. 26-31, May 25 2007. ISSN 0006-291X (Print)
0006-291x.

WARBURG, O. The Metabolism of Tumours: Investigations from the Kaiser Wilhelm Institute for Biology, translated by Frank Dickens. **Constable & Co Ltd**, 1930.

WARBURG, O. On the origin of cancer cells. **Science,** v. 123, n. 3191, p. 309-314, 1956. ISSN 0036-8075 (Print)0036-8075.

WEIBULL, W. Wide applicability. **Journal of applied mechanics,** v. 103, n. 730, p. 293-297, 1951.

WEINANDY, A. et al. Cetuximab induces eme1-mediated DNA repair: a novel mechanism for cetuximab resistance. **Neoplasia,** v. 16, n. 3, p. 207-220, 2014. ISSN 1476-5586.

WESSELING, P.; CAPPER, D. WHO 2016 classification of gliomas. **Neuropathology and applied neurobiology,** v. 44, n. 2, p. 139-150, 2018. ISSN 0305-1846.

WIN, K. Y. et al. Evaluation of polymeric nanoparticle formulations by effective imaging and quantitation of cellular uptake for controlled delivery of doxorubicin. **Small,** v. 11, n. 9-10, p. 1197-204, 2015. ISSN 1613-6810.

WISE, D. L. **Handbook of pharmaceutical controlled release technology**. CRC Press, 2000. ISBN 0824703693.

WU, H.; HU, K.; JIANG, X. From nose to brain: understanding transport capacity and transport rate of drugs. **Expert Opin Drug Deliv,** v. 5, n. 10, p. 1159-1168, 2008. ISSN 1742-5247 (Print) 1742-5247.

WU, H. et al. Anti-angiogenic activities of chitooligosaccharides. **Carbohydrate Polymers,** v. 73, n. 1, p. 105-110, 2008. ISSN 0144-8617. Disponível em: < http://www.sciencedirect.com/science/article/pii/S0144861707005577 >.

WU, M. et al. Recent research progress on preparation and application of N, N, N-trimethyl chitosan. **Carbohydrate Research,** v. 434, p. 27-32, 2016. ISSN 0008-6215. Disponível em: < http://www.sciencedirect.com/science/article/pii/S0008621516302816 >.

XIA, H. et al. Low molecular weight protamine-functionalized nanoparticles for drug delivery to the brain after intranasal administration. **Biomaterials,** v. 32, n. 36, p. 9888-9898, 2011/12/01/ 2011. ISSN 0142-9612. Disponível em: < http://www.sciencedirect.com/science/article/pii/S0142961211010441 >.

YADAV, S. et al. Comparative Biodistribution and Pharmacokinetic Analysis of Cyclosporine-A in the Brain upon Intranasal or Intravenous Administration in an Oil-in-Water Nanoemulsion Formulation. **Molecular Pharmaceutics,** v. 12, n. 5, p. 1523-1533, 2015/05/04 2015. ISSN 1543-8384. Disponível em: < https://doi.org/10.1021/mp5008376 >.

YANG, W. et al. ERK1/2-dependent phosphorylation and nuclear translocation of PKM2 promotes the Warburg effect. **Nat Cell Biol,** v. 14, n. 12, p. 1295-1304, Dec 2012. ISSN 1465-7392.

YIN, Y. et al. Itaconic acid grafted carboxymethyl chitosan and its nanoparticles: Preparation, characterization and evaluation. **International Journal of Biological Macromolecules,** v. 102, n. Supplement C, p. 10-18, 2017/09/01/ 2017. ISSN 0141-8130. Disponível em: < http://www.sciencedirect.com/science/article/pii/S0141813016328318 >.

YUEN, C. A. et al. Cancer stem cell molecular reprogramming of the Warburg effect in glioblastomas: a new target gleaned from an old concept. **CNS oncology,** v. 5, n. 2, p. 101-108, 2016. ISSN 2045-0907.

YUN, Y. H.; LEE, B. K.; PARK, K. Controlled Drug Delivery: Historical perspective for the next generation. **Journal of Controlled Release,** v. 219, p. 2-7, 2015. ISSN 0168-3659. Disponível em: < http://www.sciencedirect.com/science/article/pii/S0168365915301747 >.

ZAHONERO, C.; SANCHEZ-GOMEZ, P. EGFR-dependent mechanisms in glioblastoma: towards a better therapeutic strategy. **Cell Mol Life Sci,** v. 71, n. 18, p. 3465-3488, 2014. ISSN 1420-682x.

ZANOTTO-FILHO, A. et al. Autophagy inhibition improves the efficacy of curcumin/temozolomide combination therapy in glioblastomas. **Cancer Letters,** v. 358, n. 2, p. 220-231, 2015/03/28/ 2015. ISSN 0304-3835. Disponível em: < http://www.sciencedirect.com/science/article/pii/S0304383514008027 >.

ZHANG, J.; STEVENS, M. F.; BRADSHAW, T. D. Temozolomide: mechanisms of action, repair and resistance. **Curr Mol Pharmacol,** v. 5, n. 1, p. 102-114, 2012. ISSN 1874-4672.

ZHU, J.-Y. et al. Preferential cancer cell self-recognition and tumor self-targeting by coating nanoparticles with homotypic cancer cell membranes. **Nano letters,** v. 16, n. 9, p. 5895-5901, 2016. ISSN 1530-6984.

ZORZAN, M. et al. Molecular targets in glioblastoma. **Future Oncol,** v. 11, n. 9, p. 1407-1420, 2015. ISSN 1479-6694.

ZOU, P. et al. Advances in characterisation and biological activities of chitosan and chitosan oligosaccharides. **Food Chemistry,** v. 190, p. 1174-1181, 2016. ISSN 0308-8146. Disponível em: < http://www.sciencedirect.com/science/article/pii/S0308814615009681 >.